The Adherens Junction Interactome and the Role of Vinculin in Cytoskeletal Integration at the Cardiomyocyte ICD

by

Chelsea DeAnn Merkel

B.S., Eastern University, 2013

Submitted to the Graduate Faculty of the

School of Medicine in partial fulfillment

of the requirements for the degree of

Doctor of Philosophy

University of Pittsburgh

2019

UNIVERSITY OF PITTSBURGH

SCHOOL OF MEDICINE

This dissertation was presented

by

Chelsea DeAnn Merkel

It was defended on

June 21, 2019

and approved by

Ora A. Weisz, Professor, Dept. of Medicine, Renal-Electrolyte Division; Department of Cell Biology

Bernhard Kühn, Associate Professor, Department of Pediatrics

Simon C. Watkins, Distinguished Professor, Department of Cell Biology

Gerald R. Hammond, Assistant Professor, Department of Cell Biology

Dissertation Director: Adam V. Kwiatkowski, Assistant Professor, Department of Cell Biology

The Adherens Junction Interactome and the Role of Vinculin in Cytoskeletal Integration at the Cardiomyocyte ICD

Chelsea DeAnn Merkel, PhD

University of Pittsburgh, 2019

The primary function of the heart is to contract and pump oxygenated blood throughout the body. Coordinated contraction between individual cardiomyocytes requires mechanical and electrical coupling through a specialized adhesive structure called the intercalated disc (ICD). The ICD joins cardiomyocytes and is comprised of adherens junctions (AJ), desmosomes, and gap junctions. The core of the AJ is the cadherin-catenin complex and it links the myofibrils of neighboring cells. Much work has been performed in epithelial cells to study the role of force in regulating complex formation and ligand recruitment. However, the range and scale of forces experienced in epithelial cells is far less than what is produced in the heart, yet the same molecules are responsible to maintain adhesion and tissue integrity. Our studies sought to understand the specialization of the AJ in cardiomyocytes to uncover mechanisms of resilience in tissues. Our group used proximity based proteomics and mass spectrometry to investigate the N-cadherin interactome in primary neonatal mouse cardiomyocytes. We found that cardiomyocytes share core molecular components compared to epithelial cells, however, they recruit a host of unique adapter proteins. Additionally, we demonstrated cross-talk between the ICD and the Z-disk that was previously unreported. From our proximity proteomics data set, I chose to investigate two characterized AJ ligands previously studied in epithelial cells for their roles in mechanotransduction. I found that both vinculin

and afadin are localized at the ICD and can be selectively enriched through the introduction of N-cadherin:αE-catenin fusion constructs. With these constructs, I determined that vinculin enhances the stability of AJs and is necessary and sufficient to link the AJ to the myofibril network. Lastly, I demonstrated that vinculin recruitment is necessary to drive the maturation of the ICD by recruiting desmosomes. Our work demonstrates that tissue-specific differences in the AJ interactome give rise to its specialization and that the known αE-catenin ligand, vinculin, plays an integral role in bridging the AJ-myofibril interface. Together, these data provide a repository for future work into novel ICD proteins and a novel function for vinculin, providing insight for declining cardiomyocyte function and remodeling in disease states.

Table of Contents

List of Tables

List of Figures

Preface

I would first like to thank all the members of the Kwiatkowski lab family, both past and present, for all their support, insight, input, and friendship throughout this process. Graduate school is daunting and intimidating in the beginning, eternal in the middle, and scary at the end, but you have all been there for me both professionally and personally. I would like to especially thank Dr. Adam Kwiatkowski for both his scientific guidance and his mentorship in life beyond experimentation. I would like to extend the warmest gratitude to Ian, Roisin, Jon, Qanber, and Yang for their care and laughter, and for creating a work space that felt more like a home. I owe a sincere thank you to my thesis committee, Drs. Ora Weisz, Gerry Hammond, Simon Watkins, and Bernhard Kühn, for their scientific input and guidance. My project would not have developed into the story it became without their support, advice, and critiques.

Thank you to all the scientific mentors along the way, through AP Chemistry in high school, summer research projects during college, and my college thesis advisor and research instructor, Dr. Lawton. All of these experiences, both good and bad, helped shape me into the scientist that I am as well as the role model that I want to be for others. Thank you also to the Templeton Honors College and the Biochemistry Department at Eastern University. Both of these small, close-knit communities helped mold me into the person I am today and I would not be here without either institution. Thanks is also due to the various funding agencies that have facilitated my education: the Cell Biology Teaching Fellowship through the University of Pittsburgh School of Medicine, and the Ruth L. Kirschstein Pre-doctoral Fellowship from HLBI.

Thank you to all my friends in Pittsburgh who knew the struggles of graduate school and often allowed me to commiserate with them. Our adventures and experiences together have forged life-long friendships that know no geographical bounds. Thank you to Fourth River Solutions, without which I would have missed out on amazing professional development opportunities, leadership opportunities, and friendship from across disciplines. A deep thank you to all my Philly friends. My defense year marks 10 years of friendship with all of you, and you have become family to me and an essential escape and refuge when things became difficult. I can always rely on you all for conversations that have absolutely nothing to do with science. A special callout to my best friend, Holly, who, besides being my Majestic Wildebeest, also served as my constant virtual coworker for these past (almost) seven years. Love and thanks to my partner, Rachel, for understanding the process, giving me space to rant, and showering me with love and encouragement and ice cream when I felt like I was drowning. Lastly, and most importantly, thank you to my parents and family. Together, we have grown so much throughout this experience. You have supported me and listened to me and drove hours to visit at the drop of a hat. To my dad who has moved me into every (6) apartment and hung my peg board. To my mom who has advised on professional clothing choices from afar. To my brother who calls to explain the dietary protein needs of dairy cattle. I love you all and I am proud to be your daughter and sister.

Thank you, thank you, thank you.

List of Abbreviations

ABD: Actin Binding Domain

ACTN2: α-actinin

AFDN: Afadin

AJ: Adherens Junction

ARVC: Arrhythmogenic Right Ventricular Cardiomyopathy

BioID: Biotin Identification

CDH1: E-cadherin

CDH2: N-cadherin

CTNNA1: αE-catenin

CTNNA3: αT-catenin

CTNNB1: β-catenin

CTNND1: p120-catenin

Cx43/GJA1: Connexin 43

DSC2: Desmocollin 2

DSG2: Desmoglein 2

GJ: Gap Junction

EC1, 2, etc: Extracellular cadherin domain (in reference to the 5 EC repeats in the extracellular domain of N-cadherin)

ECM: Extracellular Matrix

ESC: Embyronic Stem Cells

F-actin: Filamentous actin

FA: Focal Adhesion

FRAP: Fluorescence Recovery After Photobleaching

FRET: Förester Resonance Energy Transfer

ICD: Intercalated Disc

IPA: Ingenuity Pathway Analysis

(h)iPSC: (human) induced Pluripotenet Stem Cells

JUP: Plaoglobin

MI: Myocardial Infarction

MOI: Multiplicity Of Infection

MS: Mass Apectrometry

nN: nanoNewtons

P0/P2: Post-natal day 0, 1, 2 in reference to the age of mice

PKP2: Plakophilin 2

pN: Piconewtons

TEM: Transmission Electron Microscopy

VBS: Vinculin Binding Domain

VCL: Vinculin

YAP: Yes Associated Protein 1

ZO-1: Zona Occludens protein 1/TJP1 Tight Junction Protein 1

1.0 Introduction

Understanding how multicellular organisms remain intact has fascinated scientists for hundreds of years. While we have made great strides in our understanding since the discovery of cellular junctions, there are still areas of research that have remained elusive. This certainly applies to the field of mechanobiology, for which we have only recently developed the tools necessary to address questions of force and their impact on cellular and molecular biology. These questions have almost exclusively been investigated in epithelial cells, which provide an easily manipulated system to address areas of force-induced conformational changes, signaling events, and cell movements. Epithelial cells experience forces between 50-100 nN when in a non-motile state (1, 2). Cardiomyocytes are estimated to experience forces in excess of 1000 nN, 10-20 times greater than that measured in epithelial cells (3). This force bearing and transmission is essential for life in multicellular organisms. It is not known how the adherens junction maintains adhesion under extreme and cyclical amounts of force. The work presented here describes our efforts to define the molecular composition of the cardiomyocyte adherens junction and determine how it is coupled to the actin cytoskeleton.

1.1 Cardiomyocytes and the ICD

Cardiomyocytes, the force producing muscle cells of the heart, are responsible for providing the contractile forces necessary to pump oxygenated blood throughout the entire organism. Proper heart function requires individual cardiomyocytes to be coupled together to form a mechanical cardiac syncytium. Cardiomyocytes accomplish mechanical and electrical transduction through a complex adhesive structure known as the intercalated disc (ICD) (4–8). The ICD allows for individual cardiomyocytes to function as a syncytium. In skeletal muscle, individual myoblasts fuse to form large, multinucleated muscle fibers (9). This developmental process is necessary to allow for rapid signal transmission and response of skeletal muscle (10). In cardiac tissue, fusion of individual cells to form a true syncytium would be disastrous should a cell fail. In contrast, a functional syncytium would retain the properties of rapid signal transmission and response without the dangers of whole organ failure (11). The ICD contains three major junctional components: the adherens junction (AJ), desmosome, and gap junction (**Figure 1.1**, (11)). The AJ and desmosome provide mechanical linkage by integrating the actin and intermediate filaments, respectively, of neighboring cells. Gap junctions provide electrical continuity with the free flow of ions (12).

Myofibrils are the force-generating structures within cardiomyocytes, and these massive actin-myosin complexes are integrated at the ICD through AJs (3, 13, 14). The AJ core is comprised of the cadherin/catenin complex (15, 16). N-cadherin, the sole classical (AJ) cadherin expressed in cardiomyocytes, forms homotypic interactions with cadherins on neighboring cells through its extracellular domain (17). The N-cadherin cytoplasmic domain interacts with a pool of catenins: p120- catenin, β-catenin, and α-

catenin. p120-catenin functions to regulate the trafficking of N-cadherin (18–20), while β-catenin binds to α-catenin and α-catenin serves as the primary link to the actin cytoskeleton (21). In the amniotic heart, there are two different isoforms of α-catenin expressed, αE and αT-catenin (22). αE-catenin has been studied extensively in epithelial cells, but less so in cardiomyocytes.

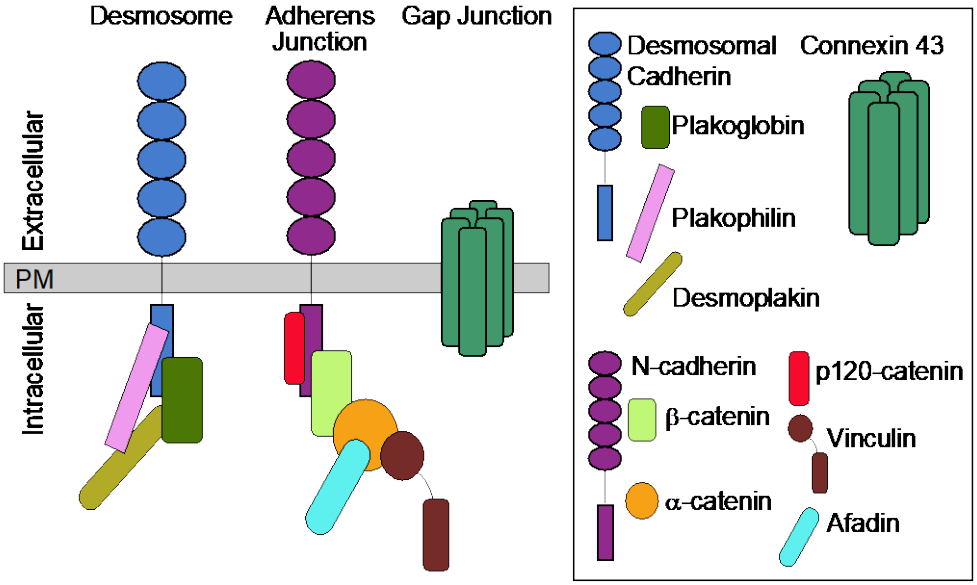

Figure 1-1 Junctional Complexes at the ICD

Cartoon schematic of a desmosome, adherens junction, and gap junction.

1.2 Components of the ICD

1.2.1 The Adherens Junction

The core of the AJ is the cadherin-catenin complex (15, 16). N-cadherin is a member of the classical cadherin family and is the sole classical cadherin expressed in

the heart (11). The extracellular domain forms calcium-dependent homotypic interactions with cadherins on neighboring membranes (23, 24). The N-cadherin intracellular domain is unstructured and binds two different catenins: p120-catenin and β-catenin/plakoglobin (discussed below) (25). N-cadherin is critical for heart development. Loss of N-cadherin is embryonically lethal, in part due to a lack of proper heart formation (26). Adult conditional knock-out of N-cadherin demonstrates that this molecule is the master regulator of the ICD. N-cadherin excision results in the loss of all AJ, desmosome, and gap junctional proteins from the ICD (17). Replacement of N-cadherin with E-cadherin in N-cadherin null hearts during development allows the animals to develop normally, but adult mice developed dilated cardiomyopathy earlier than wild-type mice and with increased mortality (27, 28).

β-catenin plays a dual role in cells; it is a core member of the AJ and a key factor in the Wnt signaling pathway (29). The signaling component of β-catenin is crucial for proper development and plays a role in regulating hypertrophic growth in the adult myocardium (30, 31). β-catenin and the desmosomal protein, plakoglobin, are both members of the armadillo family of proteins. Armadillo proteins contain these 42 amino acid repeat structures first seen in the *Drosophila* protein, Armadillo. In mammals, the Armadillo homologue is β-catenin, and β-catenin underwent a duplication event in its evolution, giving rise to plakoglobin (32). Conditional loss of β-catenin in adult myocardium results in an upregulation of plakoglobin to compensate (33). However, the converse is not true; a loss of plakoglobin is not rescued by β-catenin (34). This is most likely due to the inability of β-catenin to function within the desmosome, whereas plakoglobin can bind α-catenin and ultimately complete the AJ linkage to actin (32, 35).

p120-catenin is another member of the Armadillo family of proteins and binds to the juxtamembrane portion of the cadherin tail, whereas β-catenin binds the distal end (32). p120-catenin does not have a role in joining the AJ to the actin cytoskeleton, however, it plays integral roles in cadherin trafficking and turnover (36). During N-cadherin biogenesis, p120-catenin binds N-cadherin, which is unique amongst all classical cadherins (19, 37). p120-catenin can interact with the microtubule motor, kinesin, to transport N-cadherin to the plasma membrane (38). Once there, p120-catenin remains bound to block internalization of classical cadherins (39). For N-cadherin, the precise mechanism of regulation is unknown, but other classical cadherin studies have demonstrated that the binding site for p120-catenin on the classical cadherin tail also contains a binding motif for AP-2, a necessary member of the clathrin endocytosis machinery (40). Dissociation of p120-catenin reveals the AP-2 site and allows for internalization of classical cadherins.

αE-catenin serves as the primary link between the AJ and actin (21, 41–45). It has an N-terminal domain that can bind β-catenin/plakoglobin or dimerize, a middle/modulatory (M) domain that can bind a host of ligands, including vinculin, afadin, α-actinin, ZO-1, and a C-terminal actin binding domain (46–49). αE-catenin is a force sensitive protein and functions as a mechanosensor at the AJ (discussed below) (50). As a homodimer, αE-catenin binds to actin filaments to prevent branched networks from forming and promotes stable actin bundles in epithelial cells (42, 51, 52) The role of the homodimer pool in cardiomyocytes has yet to be investigated. However, given that the homodimer promotes linear actin bundles and prevents branching, it could play a role in the genesis of myofibrils, which are dependent upon linear actin stress fibers (13).

Conditional loss of αE-catenin in the heart leads to gross morphological changes in the left and right ventricles and increased susceptibility to cardiac wall rupture after a myocardial infarction (53).

αT-catenin was identified over fifteen years ago in the testes (T) and found to localize to the ICD of cardiomyocytes (22). Subsequent work has demonstrated properties of αT-catenin unique among the α-catenin family. It can interact with plakophilin (54), resulting in a hypothesis that αT-catenin can link the AJ and the desmosome in the heart creating a hybrid junction known as the *area composita* (55). αT-catenin is dispensable in the heart and is incapable of rescuing αE-catenin loss in cardiomyocytes (53, 56). Mutations in αT-catenin have been directly linked to arrhythmogenic ventricular cardiomyopathy in patients (57). αT-catenin constitutively binds actin with high affinity as a monomer and in complex with β-catenin (58). The function of αT-catenin in the heart remains unclear, but it is interesting that αT-catenin appears to have arisen with the 4-chambered heart, suggesting that the physical demands of organisms with 4-chambered hearts required an additional AJ catenin. On-going work in our lab and others seeks to determine the role of αT-catenin at the AJ, specifically its response to force and its ability to bind known αE-catenin ligands, like plakoglobin and vinculin.

1.2.2 The Desmosome

Desmosomes are another mechanical linkage complex found specifically in tissues under high levels of mechanical stress: the skin and heart. The desmosome is

composed of three gene family members: cadherins, armadillo proteins, and plakins (59). The desmosomal cadherins, like classical cadherins, are single pass transmembrane proteins that interact through the extracellular domains to form *trans* dimers (60). There are two desmosomal cadherins, desmocollin (DSC2) and desmoglein (DSG2), and they can form hetero-or-homotypic interactions (61, 62). Desmosomal cadherin binding is calcium-dependent, but they can change to a hyper-adhesive state once calcium is removed (63). Intracellularly, the desmosome cadherin tail binds plakoglobin (a homologue of β-catenin) and plakophilin (related to p120-catenin) (64, 65). Plakoglobin is responsible for clustering the cadherins and binding to desmoplakin, which then binds the intermediate filament cytoskeleton (66, 67). Plakophilin is necessary for proper cadherin trafficking to the plasma membrane (68).

Desmosomes and AJs are intimately connected, especially in the heart. First, data in epithelial cells demonstrate that the formation of desmosomes is dependent upon the formation of AJs (69, 70). In the heart, a loss of N-cadherin results in a loss of all desmosomal components (17). Cellular data has suggested that desmosomal and AJ cadherins can interact (71, 72). Recent biophysical data showed that the DSG2 can interact directly with the extracellular domain of E-cadherin to provide stability for DSG2 and promote desmosome formation (73). In the heart, the desmosome and AJ intermingle to form the *area composita* (55, 74). N-cadherin can bind plakoglobin in place of β-catenin, or αT-catenin can bind plakophilin and integrate the actin cytoskeleton with desmosomes (54, 75). The formation of these hybrid junctions is thought to increase mechanical stability and cross-talk between the junctional components (76).

Mutations in desmosomes are the primary cause of a genetic form of cardiomyopathy: arrhythmogenic right ventricular cardiomyopathy (ARVC). ARVC affects 1 in 5,000 individuals and is marked by progressive cardiac decline, increased fibrotic and fatty deposits in the right ventricle, and has an increased prevalence in sudden cardiac death (77–79). All components of the desmosome contain mutations that have been linked to ARVC cases from around the world, varying in their severity. Desmoplakin was the first protein associated with ARVC, with mutations resulting in classical ARVC or increased left ventricular defects (11, 80, 81). Plakophilin 2 mutations account for the highest number of ARVC cases, with estimates of approximately 70% of patients (82).

Both of the desmosomal cadherins, DSG2 and DSC2, have documented mutations, with the DSC2 mutations showing an advanced stage of ARVC (77, 83). Plakoglobin is responsible for a subset of ARVC called Naxos Disease, which includes a cardiac phenotype along with skin and hair phenotypes (84). All ARVC mutations result in a disrupted ICD organization and are accompanied by a loss of gap junctions, indicating that part of the arrhythmia is due to poor electrical communication between individual cardiomyocytes (11).

1.2.3 The Gap Junction

While AJs and desmosomes are responsible for mechanical continuity across cardiomyocytes, gap junctions (GJs) are responsible for electrical communication (85). GJs are made of connexin proteins which are four-pass transmembrane proteins. 21 connexins have been identified in the human genome (86). All connexin names are based on their approximate molecular weight and Connexin 43 (Cx43) is both the most

ubiquitously expressed and the most important isoform in the heart (87, 88). Connexins oligomerize, where six of them interact to form a connexon. Connexons form hemichannels, whereas a full gap junction forms when hemichannels on neighboring cells interact (89, 90). These channels allow for the passage of small metabolites, ions, and water between cells (91). GJs allow for electrical propagation between individual cells (92).

GJs are targeted to the ICD in an AJ-dependent, ZO-1 dependent manner (93, 94). Microtubules can directly target GJs to AJs, where GJs interact with ZO-1 for stability (95). Indeed, when N-cadherin is knocked out during development or conditionally in the adult heart, GJs fail to remain at the ICD (17, 26, 96). Desmosomal mutations resulting in ARVC also cause a loss of GJ localization (97, 98). Mutations in Cx43 itself are linked to oculodentodigital dysplasia, and a subset of these patients exhibit cardiac development or rhythm disturbances (99). The relocalization of GJ proteins does not appear to be a direct result of a disease, but is instead a cellular response to improper mechanical protein localization, or a response post-myocardial infarction (11, 88, 100, 101). In most of these cases, expression of GJs disappear altogether, or GJs are relocalized to the lateral (long) membrane of cardiomyocytes, ultimately resulting in a decrease in electrical coupling.

1.3 The Roles of Force in Adherens Junction Biology

1.3.1 Force and Adhesive Homeostasis

The cadherin molecule is the portion of the AJ furthest removed from the actin cytoskeleton; it requires intracellular tension to be transmitted through two catenins before it could be experienced by the cytoplasmic tail. However, the extracellular domain of the cadherin would be the first portion of the AJ to experience extracellular tension (102). The cadherin extracellular domain is comprised of five extracellular (EC) repeats that form calcium dependent homotypic interactions in *trans* through the most distal EC1 (23). Cadherin molecules on the same cell can form *cis* interactions through an EC1-EC2 binding interface, and this is thought to provide intracellular organization to AJs to create a lattice-like structure (24).

Extracellular interactions of the cadherin *trans* homodimer require two steps for the dimer to form. Initial interaction is through a transitional X-dimer that is short lived before it transitions into a stable strand-swap dimer (103, 104). Structural studies have demonstrated that the X-dimer is a catch bond, which is strengthened under tension. The X-dimer transitions to a slip-bond strand-swap dimer that is weakened under force, but the binding affinity is overall higher than that seen in the X-dimer (102). These steps are thought to allow cadherin molecules to withstand force changes through the X-dimer and then mature to strand-swap dimers as tissues mature and undergo less tensile forces. These studies have been performed across multiple cadherin types, and the most interesting aspect to cardiomyocyte biology is that the X-dimer of N-cadherin is as strong as the strand-swap dimer, which is not seen in E (epithelial)-cadherin (104). The unique

extracellular structure of N-cadherin could make it specifically poised to handle the increased force demands of the AJ in the heart. When N-cadherin is genetically replaced by E-cadherin in transgenic mice, these mice develop early onset dilated cardiomyopathy, indicating that the individual cardiomyocytes were incapable of producing or transmitting the force necessary for proper heart function (27). These results could be explained, in part, by the differences in the biophysical structures between cadherin molecules.

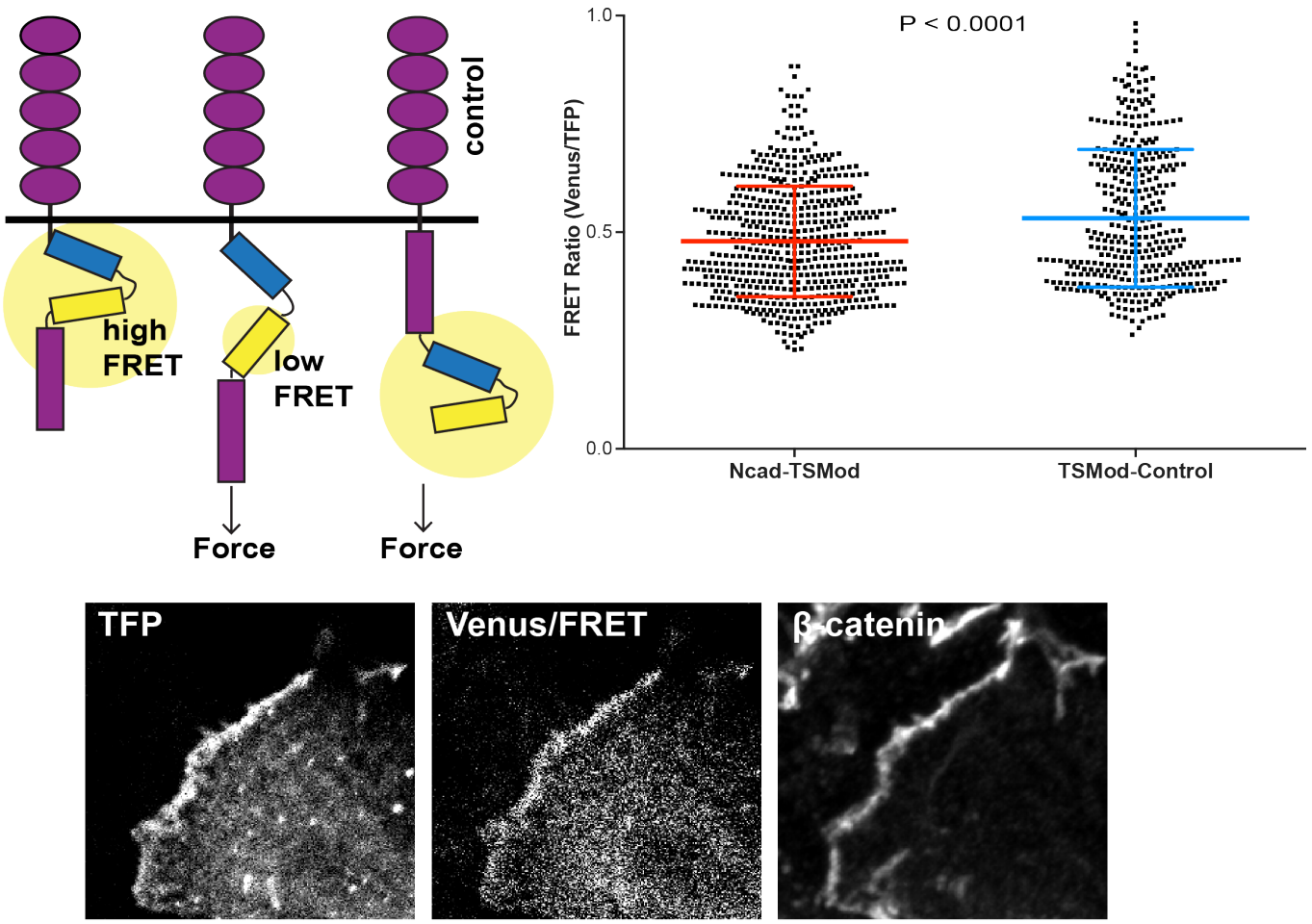

Figure 1-2 N-cadherin is under tension at cardiomyocyte cell-cell contacts

A. Schematic of the N-cadherin tension sensor (left, middle) and the N-cadherin control sensor that cannot experience force (right). B. Ratio of FRET intensities between N-cadTSMod and TSMod-Control. Student's *t* test, $p<0.0001$, error bars represent standard deviation. C. Representative images of the donor channel (TFP), acceptor channel (Venus/FRET), and β-catenin to demonstrate proper construct localization.

The intracellular tails of classical cadherins are also capable of experiencing force. This was demonstrated by the use of a FRET-based tension sensor placed between the transmembrane and cytoplasmic domains of E-cadherin. Changes in the activity of the actomyosin network resulted in changes in the amount of force experienced on the

cadherin molecule, demonstrating that the force was being transduced through the catenin molecules, ultimately resulting in increased tension across E-cadherin. While this did not result in any demonstrable changes in the conformation of the cadherin molecule, it was shown that E-cadherin inserted into a free membrane of the cell (i.e. not localized to a cell-cell contact) was still under tension (105). This indicates that the catenins are still localized to a cadherin molecule not undergoing *trans* interactions and remain connected to the cortical network. This could provide additional anchoring points for the actin cytoskeleton and increase overall cellular structure and rigidity. We utilized this strategy to create an N-cadherin FRET based tension sensor with a similar methodology used for the E-cadherin sensors. In cardiomyocytes, we demonstrated that N-cadherin is also under tension at cell-cell contacts (**Figure 1-2)**.

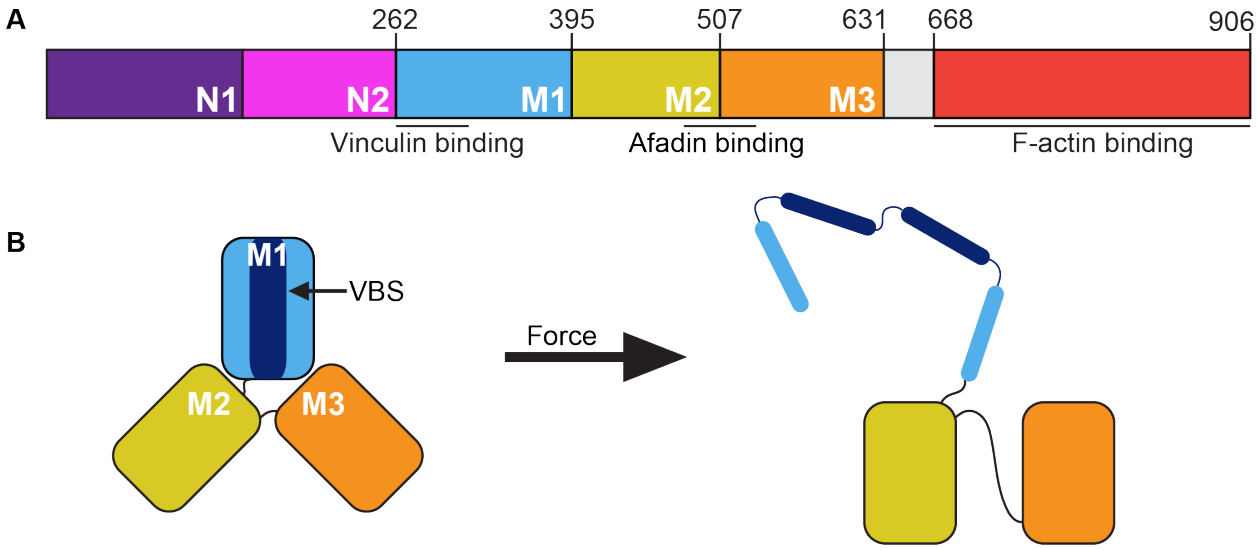

Figure 1-3 Domains and force unfolding of αE-catenin

A) Cartoon schematic of αE-catenin domains, including the approximate location of vinculin and afadin binding domains and amino acid locations. B) Conformational change of αE-catenin with the

application of force. 5pN of force opens αE-catenin, resulting in the unfurling of M1 and revealing the vinculin binding site.

To this date, there is no data suggesting that the cadherin molecule is the main mechanotransducer in the AJ. That role appears to belong to α-catenin, the link between the AJ and actin. The bond between α-catenin and actin is a catch bond where, under low tension, the affinity of α-catenin for actin is relatively low (42, 43). However, when force is applied to actin, the affinity and bond strength increase, resulting in a stable AJ (21). Not only is the α-catenin-actin bond strengthened upon force, but the whole conformation of α-catenin changes in response to it. α-Catenin has three domains: the N-terminal head domain that binds β-catenin, the C-terminal actin binding domain, and the M (middle/modulatory) domain that contains multiple binding sites for various different actin-binding ligands (**Figure 1-3A**) (106). The M-domain is comprised of three 4-helix bundles held in a closed conformation through a series of salt bridges (107). Upon the application of force, the salt bridges are broken, and the M-domain opens to reveal a cryptic binding site for the α-catenin ligand, vinculin (**Figure 1-3B**) (108–110). The amount of force required to open α-catenin, 5pN, is approximately the amount of force produced by a myosin motor, and the calculated amount of force that E-cadherin experiences (105, 111). Vinculin binding stabilizes the conformational change of α-catenin and is thought to provide additional stability for the AJ under tension (109, 112). Notably, the α-catenin-vinculin interaction persists after tension is released from α-catenin (110). In the heart, this phenomenon would prove useful as the heart undergoes cyclical contraction, presumably stretching and relaxing α-catenin with every beat. The ability for vinculin to

maintain engagement for several minutes beyond the loss of tension indicates that vinculin would maintain association with the AJ at all times in the heart, perpetually providing reinforcement with the myofibril network.

1.3.2 Force and the Cytoskeletal Linkage

The textbook drawings of AJs demonstrate a very simple interaction between three proteins and the actin cytoskeleton; but the path to get there included many struggles. *In vivo* data demonstrated that the cadherin and catenins were in close proximity to each other (42). Biochemical data demonstrated that each component could individually bind the suggested partner (43, 44). However, the proposed model came into question when it was demonstrated that αE-catenin binding to β-catenin decreased its affinity for actin, suggesting that αE-catenin did not bind actin when part of the cadherin-catenin complex (42, 43). Increasing the complexity was a demonstration that the homodimer of αE-catenin had the highest actin-binding affinity, but the homodimer could not exist within the AJ (42, 43, 51). This problem remained unsolved for nearly a decade until it was demonstrated that the low-affinity αE-catenin-actin interaction is strengthened under the application of force, describing this binding event as a catch bond (21). The catch bond properties of αE-catenin make it an ideal mechanotransduction candidate, where increased force strengthens its interaction with the cytoskeleton and can prime it for signaling transduction, such as vinculin recruitment (46).

The AJ interacts with the cell cortex, a network of actin-myosin underlying the cell surface that provides rigidity to cells (113). Ligation of cadherin molecules triggers time

and/or force-dependent junctional strengthening (114, 115). This takes the form of increased actin polymerization through the branched actin network nucleator Arp2/3 (116). These branched networks then transition into linear F-actin bundles through the recruitment of the nucleating formin mDia1 and the branched actin destabilizer Coronin 1B (117, 118). Tension continues to increase with the recruitment of nonmuscle myosin II (119). Vinculin is recruited in a nonmuscle myosin dependent manner, and this in turn recruits Ena/VASP proteins to vinculin (120, 121). Ena/VASP proteins promote actin assembly at the junctions (122). Recent biophysical data also showed that the vinculin-actin linkage has asymmetric binding properties; vinculin binds stronger to actin under force directed towards the plus-end (i.e. force *against* the AJ, (123)). This would result in a self-amplifying loop where increased AJ stabilization through force increases the recruitment of stabilizing factors and actin polymerization machinery.

Using cadherin/catenin fusion constructs has been a popular method to elucidate roles of αE-catenin-actin linkages and larger, morphological roles of the AJ with a static system (124–128). The majority of fusion constructs were modeled from a structure developed in 1994 and included a truncated cadherin lacking the cytoplasmic domain fused to full-length α-catenin. However, nearly two decades worth of research was thrown into question when it was demonstrated that these constructs were able to homodimerize intracellularly through the α-catenin full length N-terminal domains (20). Earlier that year, work was published using an alternative fusion construct structure, this one lacking the N-terminal domain of αE-catenin. With these fusion and αE-catenin mutation constructs, they showed that ablating vinculin recruitment resulted in short-lived, dynamic junctions. A construct that removed the αE-catenin actin binding domain (ABD) but constitutively

recruited vinculin resulted in highly stabilized constructs. Additionally, constitutive vinculin recruitment in the absence of the αE-catenin ABD dictated the kind of actin structures these adhesions were localized to; vinculin-null adhesions were associating with the cortical cytoskeleton, vinculin rich adhesions were localizing to stress-fiber actin structures (129). However, this work failed to address the role of force in altering the types of actin structures with which these αE-catenin constructs could interact. Also, this work did not investigate any additional ligands mediating this interaction.

1.3.3 Force and Signaling

An integral signaling platform in organisms is the Hippo pathway. This kinase cascade regulates the transcriptional activity of Yorkie (in *Drosophila)* or YAP/TAZ in mammals. Translocation to the nucleus of YAP/TAZ causes proliferation and organ growth, and tight control of this pathway regulates organ size (130). A loss of YAP results in severe undergrowth of the heart and is embryonically lethal, while constitutively active YAP or loss of its regulatory kinases results in cardiac overgrowth (131, 132). The AJ has been identified as playing a key role in regulating Hippo signaling, either through the canonical kinase cascade or by non-canonical pathways (133).

The first indication that the AJ was involved in Hippo signaling was a study noting that YAP was excluded from the nucleus in confluent, non-proliferative monolayers of cells (134). Known as contact inhibition, this phenomenon describes the cell's ability to cease proliferation once confluency is reached and is regulated by E-cadherin in epithelia cells (133, 135). Since then, two major methods of YAP/TAZ localization have been attributed to αE-catenin in both epithelial cells and the heart. The first method describes

αE-catenin negatively regulating YAP localization, working in concert with the canonical Hippo kinase cascade (136, 137). These studies describe a mechanism whereby phosphorylation of YAP by a canonical kinase creates a binding site for the scaffolding molecule, 14-3-3. This interaction promotes the junctional localization of YAP mediated by 14-3-3 binding αE-catenin (136). This localization could be altered by either 1) low-cell density, or 2) calcium chelation and disruption of the AJ (136, 137).

However, recent studies have demonstrated a mechanical regulation of YAP/TAZ signaling, where increased cellular tension, through actin/myosin or ECM perturbations, caused an upregulation in YAP translocation and cellular proliferation. The main effectors of tension mediated YAP activation appear to be YAP itself and the Ajuba LIM proteins. Ajuba, and its two additional mammalian homologs, can bind and sequester LATS/Warts, kinases that are required to prohibit YAP/TAZ from entering the nucleus (138). In mammalian cells, the Ajuba homologue, LIMD-1, is recruited to the AJ in a tension-dependent manner, and this localization sequesters LATS, preventing it from phosphorylating YAP (139). In flies, it was determined that Ajuba localization is mediated through the tension-dependent conformational change of αE-catenin, where the Ajuba binding site becomes accessible when αE-catenin is under tension, similar to αE-catenin:vinculin binding (109, 140, 141). Additionally, the *Drosophila* YAP homologue, Yorkie, was shown to activate myosin contractility at contacts outside of its well-known transcriptional activity. This result suggests that Yorkie/YAP/TAZ could create a self-amplifying loop where Yorkie-initiated myosin contractility increases cellular tension, thereby promoting Yorkie nuclear translocation (142). In line with tension-dependent activation, changes in ECM substrate stiffness also play a role in YAP activation where

more nuclear localization and proliferation is seen on stiffer ECM surfaces, which are known to increase intracellular tension (143, 144).

How do these two signaling pathways, mediated through αE-catenin, and resulting in juxtaposed outputs, play a role in cardiomyocytes? While the YAP/TAZ pathway is critical in cardiac development, it plays little to no role in normal heart function postnatally, as cardiomyocytes exit the cell cycle and retain extremely limited regenerative capabilities (145). However, several studies have looked at methods to reintroduce the YAP/TAZ pathway in adult rodent hearts following myocardial infarction (MI) to attempt to restart the proliferative pathway. Mice expressing a constitutively active YAP driven in the heart in the latter stages of embryonic development showed an increased proliferative capacity post-MI, as well as rescued cardiac output up to three weeks post-MI (146). Additionally, adeno-associated virus delivery of YAP to adult mice post-MI also improved survival, cardiac function and proliferation. Cardiomyocytes that had re-entered the cell-cycle through YAP signaling activated fetal cardiomyocyte genes, indicating that forced regeneration undergoes fetal reprogramming (147). Lastly, loss of αE and αT-catenin in rodent hearts leads to upregulation of YAP/TAZ signaling and increased proliferative capacity, indicating that α-catenin functions as a negative regulator of YAP/TAZ in cardiomyocytes (148). These changes in α-catenin expression resulted in increased intracellular tension and an increased translocation of YAP to the nucleus, consistent with previous epithelial reports (143, 149). While the mechanism appears unclear, it is likely that increased proliferation and YAP nuclear localization could be explained by a loss of contact-inhibition control. With regards to the Ajuba/αE-catenin/tension pathway, this has yet to be investigated in cardiomyocytes. There is very little data on the existence of the

Ajuba LIM proteins in the heart, and what is known is restricted to early cardiac development and the retinoic acid signaling pathway (150). In a recent proteomics screen of AJ interactome in cardiomyocytes, Ajuba LIM proteins were not identified as AJ interactors (151). These limited data suggest that Ajuba LIM signaling is not present in cardiomyocytes, but this should be an area of future investigation as increased ECM stiffening and increased cardiomyocyte tension are a direct result of MI (152–154).

1.3.4 Force and Polarity

Cardiomyocytes lack the apical-basal polarity of epithelial cells; however, they do possess strong bipolar morphology. Myofibrils run from end to end along the length of a rod-shaped cardiomyocyte (12). The ICD is concentrated at the short end of cardiomyocytes where myofibrils terminate between cells (11), whereas the lateral membrane is the site of cell-ECM integration through costameres (155). During development, cardiomyocytes are more rounded and AJs, desmosomes, and gap junctions are found along all points of cell-cell contact (lateral membranes). In both rodents and humans, the AJ complex is the first to migrate to the bipolar ends, establishing the sites of the ICDs. AJs are quickly followed by desmosomes, and finally gap junctions, which take the longest time to localize. This process extends beyond fetal heart development and into postnatal cardiac remodeling (12, 156, 157).

At the same time that junctions are remodeling and migrating to the polar ends, the cardiomyocytes are also beating and actively maturing their myofibril network (158). The primitive heart tube begins beating in the first month of human embryonic development and the first ten days of mouse embryonic development. The rate of

contraction increases throughout development, pointing to the increased electrical signaling, as well as myofibril maturation (159). Contraction is thought to self-correct poorly aligned myofibrils and drive either their reorganization or disassembly (158). Loss of contraction in developing cells results in poorly formed myofibrils (160). Indeed, during development, the myofibrils lack their linear organization in early stages and increase in their polarity throughout development (157). Similar observations were made in cardiomyocytes derived from stem cells. Cardiomyocyte-driven human pluripotent stem cells have a fetal cardiomyocyte phenotype, which can be matured by promoting contraction (161, 162). Myofibril development is postulated to begin at cell-ECM contacts and arise near the cell edges (13). At some undetermined time, it is hypothesized that myofibrils are then “handed off” to the AJ within the ICD, linking the myofibril networks of neighboring cells (3). Whether this occurs after a myofibril is fully formed, or occurs as new sarcomeres are added to the ends of a developing myofibril has yet to be determined. Additionally, it is uncertain if contraction-driven myofibril development and organization drives AJ – and subsequent desmosome and gap junction – relocalization or if ICD maturation drives myofibril alignment and integration. Regardless of the order, it is clear that contraction, myofibril alignment, and ICD localization are intimately linked to contractile force in pre- and post-natal heart development.

Interestingly, planar cell polarity complex proteins are expressed in cardiomyocytes. Key members of that complex have important roles during embryonic heart development. Disruption of basal markers *Scrib* or *Vangl2* result in disruption of N-cadherin localization and ventricular wall development (163). Downstream planar cell polarity signaling through Rac1, a small GTPase responsible for actin polymerization and

cell migration, is important for heart development (164). Loss of Rac1 in a heart progenitor cell population results in a decreased right ventricle (165). Importantly, ventricular wall development requires apical-basal polarity of rounded cardiomyocytes that are regulated through the receptor CRUMBS and Neuregulin signaling in zebrafish (166, 167). However, there has been little investigation into the reorientation of typical planar cell polarity proteins during ICD rearrangement, or what their roles are – if any – in adult myocardium.

1.3.5 Force, Extracellular Matrix, and Focal Adhesion Crosstalk

Just as it is necessary for individual cells to establish and maintain adhesion, cells must also make stable connections with the surrounding extracellular matrix (ECM). This is accomplished through another complex adhesive structure known as focal adhesions (FAs). FAs are heterodimeric integrin-mediated adhesions that bind specific ECM proteins (168). To date, there are over 150 known associated FA proteins, and these members are spatially separated into different modules within the FA, whose role is a function of location within the three-dimensional structure (168, 169). Although the number of associated FA proteins is extensive, FAs and AJs share very few common proteins. However, a major component of both AJs and FAs, vinculin, plays integral roles at both complexes (as stated above for AJs).

FAs are the direct cellular sensors and translators to changes in ECM stiffness. This is initiated by the transmembrane integrins, where stiff substrates result in increased integrin expression and high-affinity conformational changes in their extracellular domains (170). To counterbalance an increase in ECM stiffness, cells will contract their

actin-myosin cytoskeletons, and this converts the integrin-ECM bond into stable, long-lived states (171, 172). During this process of sensing and responding, increased stiffness will recruit vinculin for force-induced FA stabilization (173, 174). Vinculin is responsible for force-based assembly and disassembly of FAs in epithelial cells (168, 169). As force increases, FAs increase in size and number in fibroblasts and cardiomyocytes (175, 176). Unlike FAs, the effects of ECM stiffness on AJs is poorly understood and not well studied. Two groups measured the output of FA signaling as a function of substrate stiffness and cell-cell adhesion in either epithelial or vascular smooth muscle cells and found that the increased cell-cell adhesions dampened the signaling response from FAs (114, 177). Another study found increased N-cadherin expression as a part of a stiffness-activated FA pathway in MEFs and vascular smooth muscle cells (178); however, neither of these directly translate to cardiomyocytes (discussed below). Lastly, AJs and FAs appear to work together in cell migration: AJs do not impede the speed or force of FA-mediated migration, but AJs provide the directionality in the movement of a multicellular sheet (179).

As stated, vinculin is an integral mechanosensing ligand at FAs and AJs, where it strengthens both adhesions as a response to intracellular or extracellular tension. Recent work in epithelial cells has demonstrated critical phosphorylation sites on vinculin that regulate its localization as a function of tension. At AJs, vinculin is specifically phosphorylated at Y822; this phosphorylation was not detected at vinculin localized to FAs in either quiescent or increased-stiffness states. They determined that force applied to E-cadherin activated Abelson tyrosine kinase to phosphorylate vinculin, and this post-translational modification was required to recruit vinculin to AJs (115). At FAs, Src-mediated phosphorylation of vinculin at Y100 and Y1065 is necessary to mediate FA

stiffness-dependent strengthening (180). However, it is unclear if either of these pathways are present in cardiomyocytes.

The importance of understanding cell-cell, cell-ECM crosstalk is crucial when considering heart function and heart health. While many of these studies have provided great insight into AJ and FA biology, little work has addressed the role of differential vinculin recruitment and how that effects healthy and diseased heart. The stiffness of the ECM in the heart is fine-tuned to match the contractile properties of cardiomyocytes (3, 181, 182). Increased ECM stiffness results in decreased contraction force in cardiomyocytes (182). Importantly, increased ECM stiffness alters force transmission between neighboring cardiomyocytes. On mimics of healthy ECM, cardiomyocytes will transmit force across cells to their neighbors. However, with increased stiffness, there is increased FA size, number, and a reorientation of force vectors into the ECM rather than across the tissue (3). It remains to be investigated if these changes in stiffness result in differential recruitment of vinculin to FAs at the expense of AJs, leaving cell-cell adhesions weakened and vulnerable, incapable of withstanding the amount of force coupled myofibrils create at the ICD.

1.4 Addressing Cardiomyocyte Adhesion

The work undertaken in the course of this study can be seen as a two-pronged approach to address the same problem: how do cardiomyocytes specialize their AJs to manage the increased stress of their natural environment? The first method of approach is a large-scale proximity proteomics screen to identify unique components of the

cardiomyocyte AJ compared to the epithelial AJ and how these differences confer adhesion. The second approach is a dive into the properties of the well-characterized αE-catenin-vinculin interaction and how this interaction holds up in the cardiomyocyte. The specialization of junctions in the heart continues to be the driving question in our lab, with the hopes of providing deep insight into normal and diseased cardiac tissue, and promoting better targeted cellular and molecular approaches to treatment of damaged tissue.

1.5 Proximity Proteomics and Adherens Junction Components

Investigating protein-protein interactions in a native state has been a decades-long challenge. *In vitro* biochemical assays are helpful but may not represent physiological interactions. Co-immunoprecipitation provides *in vivo* interactions, but can only represent strong interactions, where weak, transient interactions are lost in cell lysis and blotting. Additionally, it is becoming increasingly evident that protein-protein interactions are mediated by complexes providing additional limitations to traditional protein-protein interaction techniques. Commonly used methods, such as yeast two-hybrid or crosslinking and pulldowns fail to capture larger complexes or introduce errors of false identification with promiscuous crosslinking. Biochemical approaches and reconstitution assays run into problems with protein solubility and a loss of the native cellular environment. A new methodology of labeling proteins in their native cellular environment has been defining complex interaction networks, including at the adherens junction. Proximity labeling proteomics utilizes a promiscuous biotin ligase fused to a protein of

interest (bait) to label neighboring proteins when a bolus of biotin is added to the system (183–185). Biotinylated proteins can be released from lysed eukaryotic cells and isolated with streptavidin-conjugated beads. Lastly, the biotinylated proteins can be identified by mass spectrometry.

This methodology has been used to identify the adherens junction interactome (adhesome) with E-cadherin as the bait in two different epithelial cells lines (186, 187). Additionally, it has been used to analyze differential ligand recruitment to αE-catenin in a stretch-dependent manner (188). A hand-curated list of the adhesome identified 175 published interacting partners (189). Proximity proteomics techniques have identified 303 and 561 unique proteins in and around E-cadherin in two cell types (186, 187). These studies resulted in 114 common proteins and identified a rich pool of adapter proteins associated with the membrane, actin cytoskeleton, or microtubules (187). This technique exposes new interacting partners and signaling pathways associated with the AJ that have previously remained unknown to the field and opened up new areas of investigation. We chose to use this methodology to determine cell-type specific differences in the AJ adhesome within cultured cardiomyocytes (151).

1.6 αE-catenin Ligands

From the proximity proteomics study, we localized two previously identified αE-catenin ligands at the cardiomyocyte ICD, vinculin and afadin. In fact, both of these ligands were highly ranked in protein abundance, indicating their enrichment at the ICD. Vinculin has been previously studied in the heart, primarily in the context of

myofibrillogenesis and cardiac development. The role of afadin at the ICD is even less understood with minimal research conducted thus far. I chose to characterize the roles of these two established ligands at the cardiomyocyte ICD to provide a deeper understanding of the AJ-actin interfaces and requirements.

1.6.1 Vinculin

Vinculin is an intensely studied protein with functionality at cell-cell and cell-ECM adhesions (**stated 1.3.5**). Vinculin was first identified 40 years ago in chicken and localized strongly with actin stress fibers and cell-ECM adhesions (190). Since then, vinculin has been at the center of studies on migration (191), cell-ECM adhesions (169), cell-cell adhesions (120), signaling (115), and development (192). Structurally, vinculin and αE-catenin share similarities in their domains and overall structures (46, 108). Vinculin contains a head, neck, and tail domain held in an autoinhibited conformation (193). To date, no one ligand has been demonstrated to be sufficient in releasing the autoinhibited state; instead vinculin requires activation from the binding of two or more ligands (173, 194).

As stated, vinculin plays integral roles at focal adhesions and supporting roles at the AJ. However, vinculin also plays integral roles in heart development and cardiac biology. Mice null for vinculin are embryonically lethal, due to a failure in cardiac function and severely reduced cardiomyocyte number (192). A loss of a single allele of vinculin gave rise to disorganized ICDs and a predisposition to cardiomyopathy (195). Tissue-specific loss of vinculin in the heart also demonstrated disrupted ICDs and sudden cardiac death (196). Additionally, vinculin is required for proper myofibrillogenesis; isolated

cardiomyocytes treated with antisense oligodeoxynucleotides had poorly organized myofibrils and undivided Z-disks (197). Human patients carrying a missense mutation in vinculin are more susceptible to hypertrophic cardiomyopathy where patients have increased interstitial fibrosis and a loss of vinculin from the ICD (198). Patient samples taken from dilated cardiomyopathy-induced end-stage heart failure showed a modest increase in vinculin expression and poor localization to the ICD and costameres (199). However, recent work has shown that increased vinculin expression appears to be a byproduct of age. Older monkeys increased expression of vinculin, among other cytoskeletal proteins that are associated with cardiac disease. However, when vinculin is overexpressed at a young age in flies, it results in increased cardiac output and a marked increase in lifespan (200). Vinculin function in the heart is complicated as it localizes to two major structural adhesive elements, yet there is little understanding of how this localization is regulated or balanced in the heart.

1.6.2 Afadin

Afadin is a loosely studied junctional ligand with ties to both the AJ and nectin junctions. It was first identified over twenty years ago in rat brains and found to be localized to cadherin-based cell-cell contacts (201). Since then, it has been found to play a role with various different junctional components and in different tissue types. In neurons, afadin is involved in synaptic junctional formation and assists in forming and remodeling synapses in the hippocampus (202). In development, loss of afadin results in a loss of cellular integrity and polarization in the neuroepithelium (203). Additional studies in epithelial cells demonstrate that afadin is involved in directed cell migration (204),

barrier function in intestinal epithelia (205), and breast cancer cell migration (206). The actual role of afadin in any of these scenarios is multifaceted and complicated. Afadin contains an actin binding domain that binds the side of actin and a PDZ-domain that interacts with nectins. Nectins are transmembrane adhesion molecules that associate with the AJ; afadin binds the intracellular tail of nectins and is thought to stabilize their localization by linking them to the actin cytoskeleton (207). While there are additional signaling events facilitated by afadin (204, 206), its interaction with the AJ is of great interest to us. αE-catenin contains an afadin binding site (47) and afadin was recently demonstrated to be a tension-dependent scaffolding molecule found at epithelial tricellular junctions, localized with AJs (208).

Previous afadin studies have focused on epithelia and neurons, and a loss of afadin is embryonically lethal shortly after the development of the three germ layers (203). However, its initial discovery also marked a robust localization to the ICD in heart sections (201). This observation was not pursued for twenty years. With the increased knowledge of ICD proteins and their role in cardiac disease (7, 55) Zankov, *et al*, investigated the role of afadin at the ICD. They found that afadin exhibits cardio-protective effects against cardiac remodeling due to chronic pressure overload. Hearts null for afadin showed increased fibrosis and apoptosis of cardiomyocytes, and they postulate that afadin, at the ICD, regulates TGF-β signaling (209). This cardiac study indicates that localization of afadin to the milieu found at the ICD could result in functions otherwise unknown for AJ ligands.

2.0 The N-cadherin interactome in primary cardiomyocytes as defined by quantitative proximity proteomics.

This text was published in *Journal of Cell Science.* doi: 10.1242/jcs.221606

2.1 Overview

The junctional complexes that couple cardiomyocytes must transmit the mechanical forces of contraction while maintaining adhesive homeostasis. The adherens junction (AJ) connects the actomyosin networks of neighboring cardiomyocytes and is required for proper heart function. Yet little is known about the molecular composition of the cardiomyocyte AJ or how it is organized to function under mechanical load. Here we define the architecture, dynamics and proteome of the cardiomyocyte AJ. Mouse neonatal cardiomyocytes assemble stable AJs along intercellular contacts with organizational and structural hallmarks similar to mature contacts. We combine quantitative mass spectrometry with proximity labeling to identify the N-cadherin (CDH2) interactome. We define over 350 proteins in this interactome, nearly 200 of which are unique to CDH2 and not part of the E-cadherin (CDH1) interactome. CDH2-specific interactors are comprised primarily of adaptor and adhesion proteins that promote junction specialization. Our

results provide novel insight into the cardiomyocyte AJ and provide a proteomic atlas for defining the molecular complexes that regulate cardiomyocyte intercellular adhesion.

2.2 Introduction

Heart function requires mechanical coupling and chemical communication between cardiomyocytes through a specialized adhesive structure called the intercalated disc (ICD). The ICD is formed from three junctional complexes: adherens junctions (AJs) and desmosomes that physically link opposing cardiomyocytes, and gap junctions that electrically couple cardiomyocytes (7, 8, 210). AJs and desmosomes link the actin and intermediate filament (IF) cytoskeletons, respectively, to the ICD and provide structural integrity and mechanical strength to the cell-cell contact. ICD formation requires multiple adhesion, cytoskeletal and signaling proteins, and mutations in these proteins can cause cardiomyopathies (211). However, the molecular composition of ICD junctional complexes remains poorly defined.

The core of the AJ is the cadherin-catenin complex (15, 212). Classical cadherins are single-pass transmembrane proteins with an extracellular domain that mediates calcium-dependent homotypic interactions. The adhesive properties of classical cadherins are driven by the recruitment of cytosolic catenin proteins to the cadherin tail: p120-catenin (CTNND1) binds to the juxta-membrane domain and β-catenin (CTNNB1) binds to the distal part of the tail. β-Catenin, in turn recruits αE-catenin (CTNNA1) to the cadherin-catenin complex. α-Catenin is an actin-binding protein and the primary link

between the AJ and the actin cytoskeleton (41–44). In mice, loss of AJ proteins in the heart – N-cadherin (CDH2), β-catenin, αE-catenin or αT(Testes)-catenin (CTNNA3) – causes dilated cardiomyopathy (17, 53, 96, 213). Mutations in αT-catenin, an α-catenin homolog expressed predominantly in the heart and testes, and the β-catenin homolog plakoglobin (JUP) have been linked to arrhythmogenic right ventricular cardiomyopathy (57, 214), as have disruptions in β-catenin signaling (215).

The AJ is best understood in the context of epithelia, where it regulates intercellular adhesion, cell motility and polarity (216, 217). The AJ can both sense and respond to mechanical force (50, 218), though the molecular mechanism remains largely undefined. In epithelia, the AJ associates with a panoply of proteins that regulate adhesion, signaling and protein turnover. Recent proteomic studies have begun to define the cadherin interactome and have offered new insight into the molecular complexes that regulate AJ biology in epithelia (186, 187). Yet it is unclear if these complexes are shared between cell types or whether specific proteins are recruited to AJs to meet specific physiological needs. For example, in cardiomyocytes the AJ is thought to anchor myofibrils to the ICD to transmit force between cells. If and how the cardiomyocyte AJ proteome is tuned to meet the mechanical demands of myocyte contraction is not known.

Here we describe efforts to define the molecular complexes associated with N-cadherin at cardiomyocyte cell-cell contacts. We use a combination of light and electron microscopy to reveal that primary neonatal cardiomyocytes assemble junctional complexes along developing intercellular contacts with structural hallmarks reminiscent of the ICD in adult heart tissue. We show that cardiomyocyte AJ proteins are stable with dynamics similar to epithelia. We use proximity proteomics to identify N-cadherin-

associated proteins along cardiomyocyte cell-cell contacts. We define a robust repertoire of interactors, comprised primarily of adaptor and adhesion proteins unique to cardiomyocytes. Our results offer novel insight into the critical adhesion complexes that connect cardiomyocytes and provide a proteomic platform for deciphering how molecular complexes are organized to regulate cardiomyocyte adhesion and cellular organization.

2.3 Results

2.3.1 Organization of primary cardiomyocyte intercellular contacts

Primary cardiomyocytes isolated from rodent neonates retain the ability to establish cell-cell contacts in culture (55, 219). Neonatal cardiomyocytes from mice are also amenable to transient transfection and adenoviral infection (220). To begin to define the junctional complexes at newly formed contacts in neonatal cardiomyocytes, we first examined the recruitment of endogenous CDH2, the core of the AJ. Mouse neonatal cardiomyocytes were isolated from P0-P2 pups and plated on isotropic Collagen I substrates at high density to promote intercellular interactions. After 2-3 days in culture, neonatal cardiomyocytes had established CDH2-positive contacts around much of their perimeter (**Fig. 2-1A, B**). Myofibril formation is evidenced by the periodic, sarcomeric organization of the Z-line marker α-actinin (ACTN2) (**Fig. 2-1C**). Notably, CDH2 localization is not uniform along contacts; instead, it is discontinuous (**Fig. 2-1B**, white arrows) and often concentrated at sites of myofibril coupling between cells (**Fig.2-1B**, inset).

We then examined the localization of other primary components of the ICD junctional complexes: AJ, desmosomes and gap junctions. As expected, the AJ proteins CTNNA1 (**Fig. 2-1D**) and CTNNB1 (**Fig. 2-1E**) showed patterns of localization identical to CDH2. Two desmosome proteins, JUP and plakophilin 2 (PKP2), also showed patterns of localization nearly identical to the AJ (**Fig. 2-1E, G**). JUP can bind directly to classical cadherins (221) and PKP2 can bind to CTNNA3 where it is thought to link the AJ to intermediate filaments at hybrid junctions, where AJ and desmosome proteins are mixed in mammalian hearts (54, 222). The desmosomal cadherin desmoglein 2 (DSG2) also concentrated at cell-cell contacts, but its localization was more restricted than the AJ with some contacts lacking DSG2 (**Fig. 2-1D**, white arrows mark CTNNA1 positive, DSG2 negative contacts). Finally, the gap junction protein Connexin 43 (GJA1) showed a punctate pattern of localization along contacts (**Fig. 2-1F**). Thus, the primary ICD junctional complexes are recruited to neonatal cardiomyocyte cell-cell contacts.

We then sought to define the actin architecture at contacts. We used platinum replica electron microscopy (PREM) to examine actin organization with single filament resolution (223). Cardiomyocytes are enshrouded by a dense cortical cytoskeleton that masks the underlying myofibril network and its association with junctional complexes (**Fig. 2-1H**, junctions highlighted in purple). We then used thin section transmission electron microscopy (TEM) to examine junction architecture. Thin section TEM revealed myofibrils coupled along electron-dense contacts (**Fig. 2-1I, J**; junction highlighted in purple). The contacts are highly convoluted, and many nascent junctions adopt a chevron-like appearance (**Fig. 2-1J**). In addition to adherens junctions, desmosomes and gap junctions are also observed (**Fig. 2-1J**), consistent with the immunostaining. Importantly,

the junctional topology of cultured cardiomyocytes is similar to that observed in adult hearts, where the angled junctions may help to balance shear versus tensile stresses during contraction (224). Taken together, we conclude that neonatal cardiomyocytes build junctional complexes with many of the organizational and structural hallmarks of adult heart tissue.

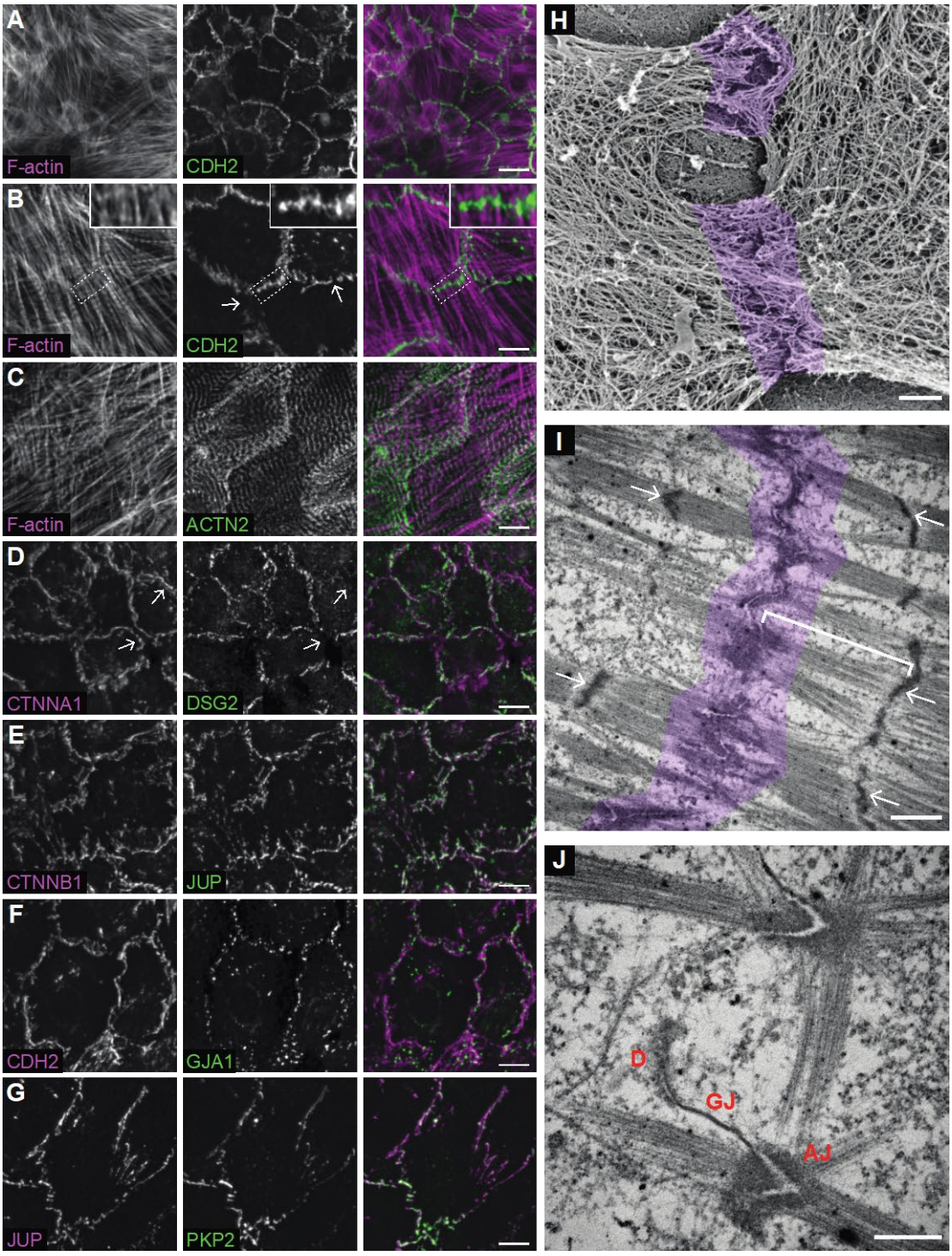

Figure 2-1 Cardiomyocyte cell-cell contact organization and architecture.

A-G. Mouse neonatal cardiomyocytes plated to confluency, fixed 48-72 hrs post-plating and stained for: F-actin and CDH2 (A & B), F-actin and ACTN2 (C), CTNNA1 and DSG2 (D), CTNNB1 and JUP (E), CDH2 and GJA1 (F), and JUP and PKP2 (G). Individual channels and merge shown. All images

are maximum projections of deconvolved Z-stacks. In (B), the white arrows mark gaps in CDH2 staining along contacts and the inset is a magnification of the boxed contact that highlights myofibril integration at contacts. In (D), white arrows mark CTNNA1 positive, DSG2 negative contacts. H. Platinum replica electron microscopy image of two connected cardiomyocytes. Cell-cell contact is highlighted in purple. I-J. Thin section electron microscopy images of cardiomyocyte cell-cell junctions. In (I), the cell-cell contact is highlighted in purple, white arrows point to Z-discs and the white bar defines a membrane-proximal sarcomere. In (J), desmosome (D), gap junction (GJ) and adherens junction (AJ) are labeled. Scale bar is 20 μm in A; 10 μm in B-G; 500 nm in H; 1 μm in I; 500 nm in J.

2.3.2 Adherens junction proteins dynamics

We next examined the dynamics of CDH2 and associated catenin proteins in cardiomyocytes. GFP-tagged CDH2, CTNNB1, JUP, CTNNA1 and CTNNA3 were individually transfected into cardiomyocytes. All fusion constructs localized to cell-cell contacts, as expected (**Fig. 2-2A**). Protein dynamics were measured by fluorescent recovery after photobleaching (FRAP) in dense cells that had been plated for 48-72 hours (**Fig. 2-2A**). Fluorescence recovery over ten minutes was quantified, plotted and fit to double exponential curve (**Fig. 2-2B**). The mobile fractions of junctional CDH2 (34.4%), CTNNB1 (32.3%), JUP (26.5%), CTNNA1 (36.4%) and CTNNA3 (36.1%) were all similar to each other (**Fig. 2-2C**). Notably, these fractions were nearly identical to those observed in epithelial cells (43) indicating that the majority (~2/3) of cadherin/catenin complexes are immobile components of the AJ plaque.

We then assessed the recovery rates of the mobile fractions for both the fast and slow pools (**Fig. 2-2C**). For the cytoplasmic catenins, the fast pool recovery halftimes

(6.6–13.4 sec) could reflect an unbound, cytosolic population of protein near cell contacts. Alternatively, the pool could be caused by photoswitching (225). The fast pool recovery of the transmembrane CDH2 (24.9 sec) likely represents photoswitching because we do not expect diffusion of new CDH2 during this initial time frame. Importantly, the fast pool for all components is relatively small (16–27%) and the slow pool represents the dynamics of the majority of the junction population. Here, the half-times of fluorescence recovery were also similar: CDH2 (315.2 sec), CTNNB1 (255.2 sec), JUP (237.6 sec), CTNNA1 (360.0 sec) and CTNNA3 (221.5 sec). This reflects the tight associations between core components of the cadherin-catenin complex (44) and suggest that the multiprotein complex is exchanged as a unit along contacts. While E-cadherin (CDH1), CTNNB1 and CTNNA1 were found to have similar rates of recovery at epithelial cell-cell contacts, the rates were approximately an order of magnitude faster, in the realm of 26–40 sec (43). It is unclear what underlies this difference, but it could reflect differences in CDH2-mediated *trans* interactions (104, 226) or stronger association with the actin cytoskeleton. Together, our results suggest that cardiomyocytes form stable AJs with properties similar to epithelia.

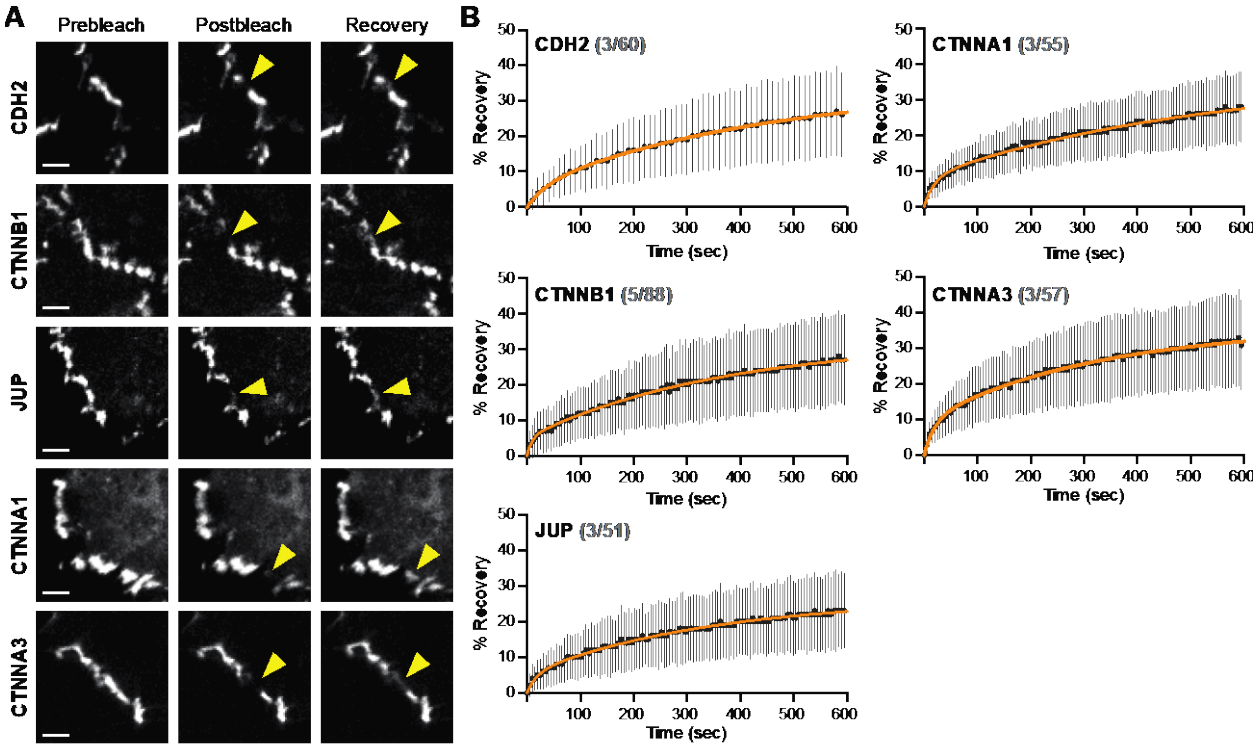

C

	Mobile Fraction (%)	Recovery Halftime (sec)	
		Fast, %Fast	Slow
CDH2	34.4 (32.4–37.9)	24.9 (17.8–33.8), 16%	315.2 (268.3–401.2)
CTNNB1	32.3 (31.3–33.5)	6.6 (4.3–9.5), 16%	255.2 (234.5–281.2)
JUP	26.5 (25.5–27.9)	12.6 (7.9–18.4), 20%	237.6 (209.9–279.8)
CTNNA1	36.4 (34.0–40.3)	13.4 (10.1–17.2), 22%	360.0 (302.7–453.8)
CTNNA3	36.1 (35.1–37.3)	13.4 (10.7–16.4), 27%	221.5 (200.5–249.2)

Figure 2-2 Adherens junction protein dynamics at cardiomyocyte cell-cell contacts.

A. Representative prebleach, postbleach and recovery images from FRAP studies of cells expressing GFP-tagged CDH2, CTNNB1, JUP, CTNNA1 or CTNNA3. Yellow arrows mark the FRAP region along a cell-cell contact. B. Plot of FRAP recovery fraction over time. At each time point, the mean recovery fraction is shown as a black circle and the standard deviation is represented by black lines. The data were fit to a double exponential curve (orange line). The number of experiments and number of FRAP contacts quantified for each protein is shown in grey (# experiments/# FRAP contacts) C. Summary of the mobile fraction (as percentage) and recovery halftimes (fast and slow pools). The percentage of the fast pool also listed. Scale bar is 50 μm in A.

2.3.3 Cdh2-BioID2 biotinylates proteins at cardiomyocyte cell-cell contacts

Given the unique structural and mechanical qualities of cardiomyocyte cell-cell contacts, we next sought to define the molecular complexes along the junctional membrane. We used proximity proteomics to identify proteins near CDH2 by fusing the biotin ligase BioID2 (184) to the C-terminal tail of Cdh2 (**Fig. 2-3A**). This technique has been used with success to define the CDH1 interactome in epithelia (186, 187) and define CTNNA1 force-dependent molecular interactions (188). We cloned the Cdh2-BioID2 fusion into an adenoviral expression system and made Cdh2-BioID2 adenovirus that would allow us to infect primary cardiomyocytes and express low levels of Cdh2-BioID2 for imaging and protein analysis (**Fig. 2-3B**). We were able to reproducibly infect >90% of cardiomyocytes at a low multiplicity of infection (MOI). The Cdh2-BioID2 fusion localized to cell-cell contacts (HA stain, **Fig. 2-3C**), similar to endogenous CDH2 (**Fig. 2-1A, B**). Importantly, when biotin (50 μM) was added to the culture, Cdh2-BioID2 labeled proteins along cell-cell contacts (SA stain in **Fig. 2-3E**; compare to uninfected control in **Fig. 2-3D**). Biotin addition and concomitant labeling did not disrupt cell-cell contacts (**Fig. 2-3E**) and optimal biotinylation was achieved after 24 hours (**Fig. S2-1**). In addition to the prominent junction labeling, a smaller population of biotinylated proteins was observed at Z-discs (**Fig. 2-3F, G**). Finally, we were able to precipitate biotinylated proteins from lysates of infected cells cultured with biotin (**Fig. 2-3H**). Thus, Cdh2-BioID2 localizes to cardiomyocyte cell-cell contacts and labels proximal proteins that can be isolated for proteomic analysis.

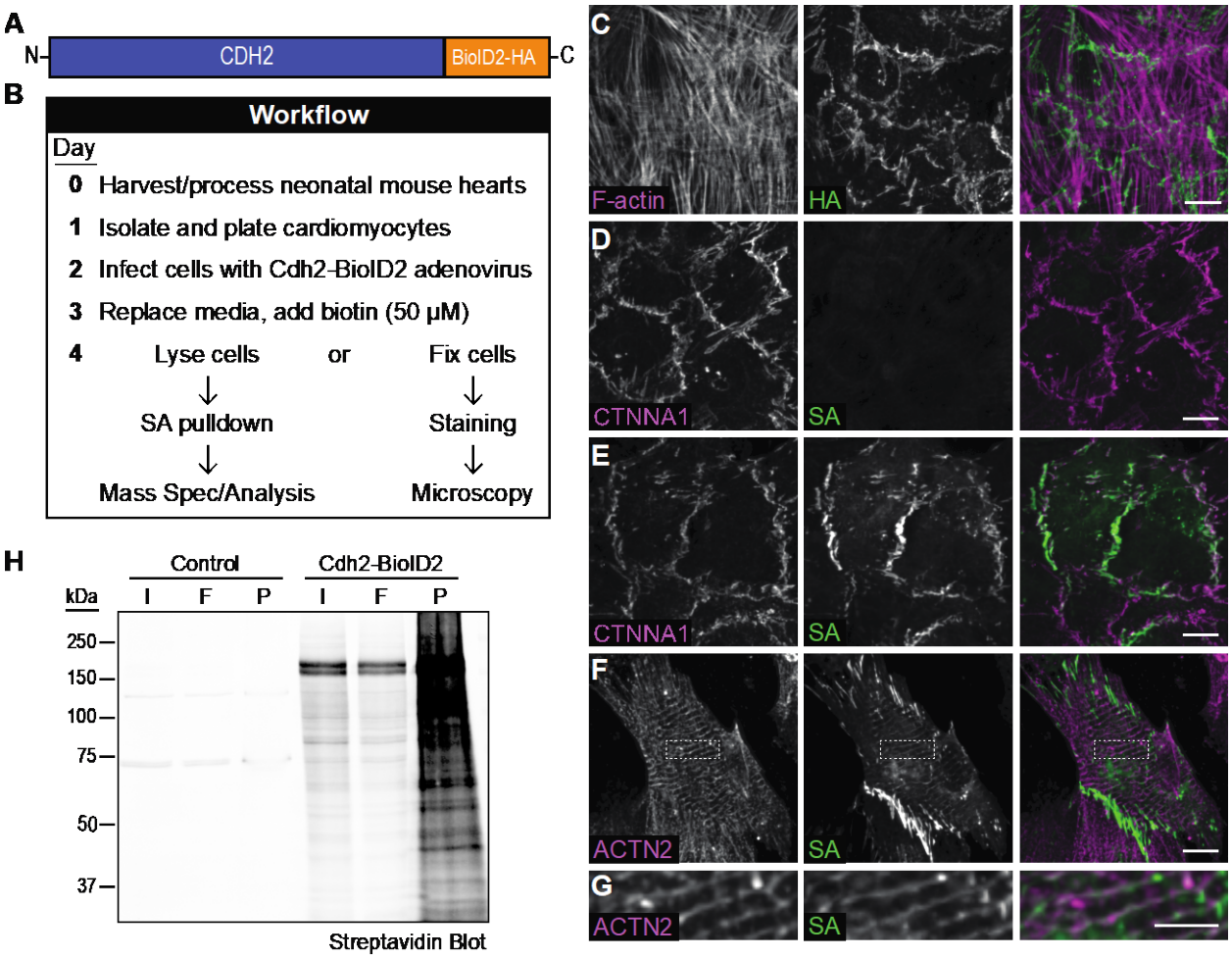

Figure 2-3 CDH2-BioID2 localizes to cell contacts and labels junctional proteins

A. Cartoon schematic of CDH2-BioID2 fusion. B. Experimental workflow for infecting primary cardiomyocytes, labeling with biotin and protein fixation/isolation. All images are maximum projections of deconvolved Z-stacks. C-G. Staining of Cdh2-BioID2 infected cardiomyocytes. C. Cdh2-BioID2 infected cardiomyocytes were stained for F-actin (magenta in merge) and HA (green in merge) to identify the HA-tagged fusion construct. D, E. Uninfected (D) and Cdh2-BioID2 infected (E) cardiomyocytes were stained for CTNNA1 and labeled with a streptavidin (SA) conjugated to CY3 to identify biotinylated proteins. F, G. Cdh2-BioID2 infected cardiomyocytes stained for ACTN2 and biotin (SA). (G) is a high mag image of the boxed region in (F) highlighting biotinylated proteins along Z-lines. H. Streptavidin western blot of pulldowns from control and Cdh2-BioID2 infected

cardiomyocytes. Initial material (I), flow through (F) and precipitated material (P) marked. Scale bar is 10 μm C-F; 5 μm in G.

2.3.4 Quantitative proximity proteomics reveals the cardiomyocyte CHD2 interactome

We used quantitative mass spectrometry (MS) to define the CDH2 interactome. For each replicate, 4 million cells were infected with Cdh2-BioID2 adenovirus, biotin was added to the media and the cells were harvested following the workflow in **Fig. 2-3B**. Uninfected control samples were treated identically to Cdh2-BioID samples (i.e., 50 μM biotin added 48 hrs post-plating and cells harvested 24 hrs after biotin addition). Six Cdh2-BioID2 replicates and six control replicates were collected and analyzed.

MS sample analysis revealed a total of 5117 peptides from 917 proteins (**Fig. 2-4A, B**). The mean coefficient of variance for the Cdh2-BioID2 replicates was ~30% (**Fig. S2-2**). When single unique peptides were excluded, the list was reduced to 4687 peptides from 487 proteins (**Fig. 2-4B**). To define Cdh2-BioiD2 enriched proteins, we established thresholds of fold change ≥ 10 and $p < 0.001$ (**Fig. 2-4A**, dashed grey lines). These thresholds culled the list to a final 365 proteins from 354 genes (**Fig. 2-4B**).

The relative abundance of these 365 proteins is plotted in **Fig. 2-4C** and the 35 most abundant proteins are listed in **Table 2-1**. Among the most abundant proteins were core components of the AJ, including CTNNB1, JUP, CTNND1 and CTNNA1. These same proteins were also abundant in the CDH1 interactome (186, 187). The desmosome components DSG2 and PKP2 were also abundant hits, as were CTNNA3 and the α-

catenin ligands vinculin (VCL) and afadin (AFDN) (47, 227–229). The abundance of desmosomal proteins DSG2 and PKP2 could reflect the proximity of AJs and desmosomes along developing cardiomyocyte junctions and/or the proposed intermingling of junctional components in hybrid junctions (55). The enrichment of VCL and AFDN, two actin-binding proteins that help anchor the AJ to actin (230, 231), likely reflects the importance of these proteins in connecting the AJ to the myofibril network.

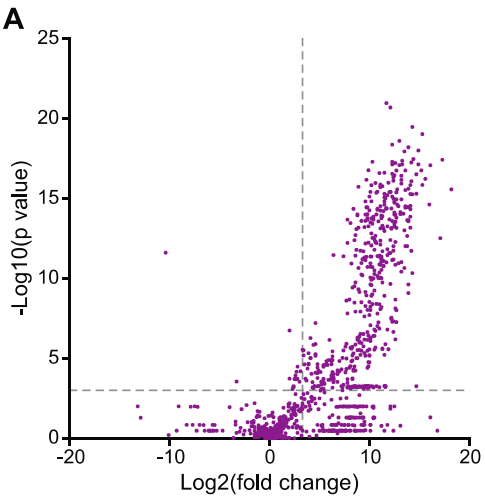

B

Total Identified	
Peptides	5117
Proteins	917
> 1 Unique Peptides	
Peptides	4687
Proteins	487
Cdh2-BioID2 vs. Control p < 0.001 & Fold Change > 10	
Proteins	**365**
Genes	**354**

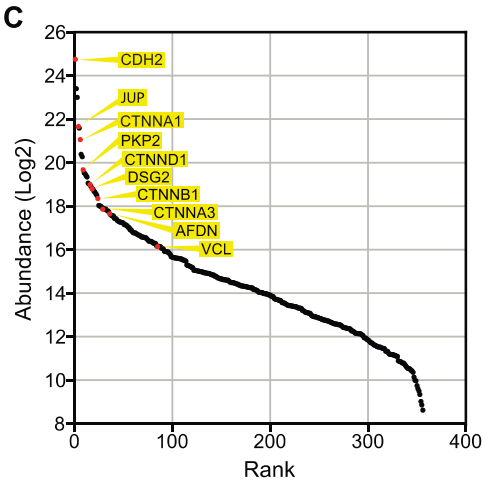

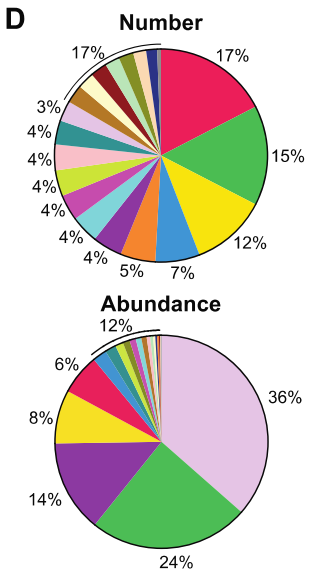

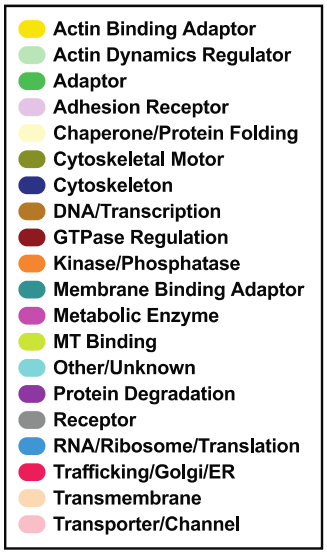

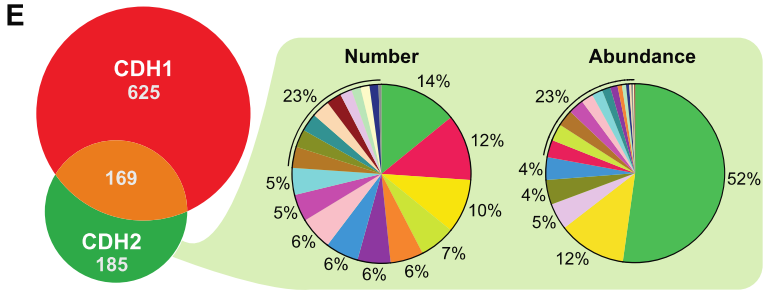

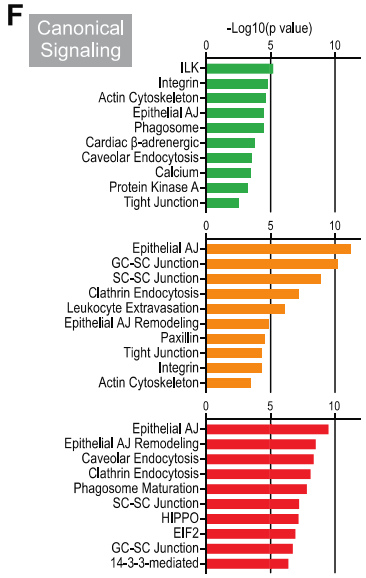

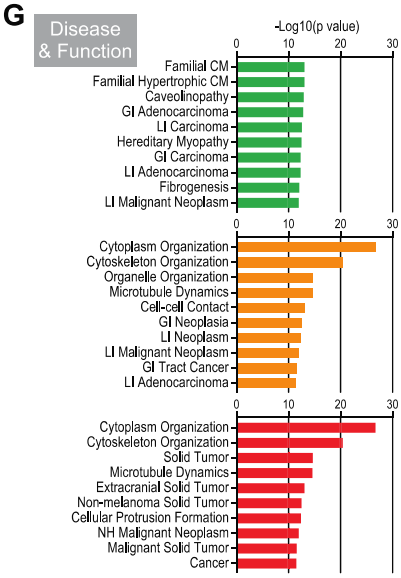

Figure 2-4 Quantitative mass spectrometry identifies CDH2 interactome

A. Plot of p value ($-Log_{10}$) versus fold change (Log_2) of identified proteins. Dashed grey lines mark p = 0.001 (y axis) and fold change = 10 (x axis). B. Summary of identified peptides and proteins. C. Rank plot of abundance (iBAQ mass, Log_2). Proteins of interest are marked as red circles and labeled. D. Protein distribution by assigned category based on number (top pie chart) or abundance (iBAQ) (bottom pie chart). E. Venn diagram of CDH2 interactome in cardiomyocytes (green) versus CDH1 interactome from epithelial cells (red). 169 proteins are shared (orange). Distribution of the CDH2 only pool (minus CDH2, 184 proteins) based on number (left) or abundance (right). F, G. IPA enrichment analysis of CDH2 only (green), CDH2/CDH1 shared (orange) and CDH1 only (red) groups in canonical signaling pathways (F) or disease and function (G). Abbreviations: AJ, Adherens Junction; CM, Cardiomyopathy; GC, Germ Cell; GI, Gastrointestinal; LI, Large Intestine; NH; Nonhematologic; SC, Sertoli Cell.

2.3.5 The cardiomyocyte CDH2 interactome is distinct from epithelial CDH1 interactome

We assigned each of the 354 genes in the Cdh2-BioID2 interactome into one of 20 functional categories according to information from Uniprot, GeneCards and Entrez (**Fig. 2-4D**), similar to (187). By number, the categories with the most hits were Trafficking/Golgi/ER (17%), Adaptor (15%) and Actin Binding Adaptor (12%). However, when considering protein abundance (iBAQ), the top categories were Adhesion Receptor (36%), Adaptor (24%), Protein Degradation (14%) and Actin Binding Adaptor (8%) (**Fig. 2-4D**). Given the substantial, electron-dense structures built along cardiomyocyte AJs (**Fig. 2-1I, J**), the abundance of adaptor proteins and adhesion receptors could function to help couple myofibrils between cardiomyocytes.

Table 2-1 35 most abundant proteins in the CDH2 interactome

Name	Description	Category	p-Value	Fold change	Mass Relative to CDH2
CDH2	Cadherin 2, N-cadherin	Adhesion receptor	4.8E-10	487	1.000
RPS27A	Ribosomal protein S27a	Protein degradation	4.2E-12	168	0.393
SORBS2	Sorbin and SH3 domain containing 2	Adaptor	2.4E-06	2578	0.159
JUP	Junction plakoglobin	Adaptor	7.1E-07	63	0.120
AHNKA	AHNAK nucleoprotein	Adaptor	5.8E-10	1454	0.112
CTNNA1	Catenin alpha-1, αE-catenin	Actin binding adaptor	2.3E-10	4243	0.078
PICALM	Phosphatidylinositol binding clathrin assembly protein	Trafficking/Golgi/ER	6.1E-06	2858	0.048
RTN4	Reticulon-4	Trafficking/Golgi/ER	1.2E-09	1171	0.045
PKP2	Plakophilin 2	Adaptor	3.2E-05	959	0.030
NEBL	Nebulette	Actin binding adaptor	2.7E-06	3905	0.027
XIRP1	Xin actin binding repeat containing 1	Actin binding adaptor	5.9E-05	380	0.026
ITGB5	Integrin subunit beta 5	Adhesion receptor	2.7E-16	295308	0.025
CSRP3	Cysteine and glycine rich protein 3	Actin binding adaptor	3.5E-04	222	0.024
ANXA2	Annexin A2	Membrane binding adaptor	5.5E-06	24	0.019
CTNND1	Catenin delta 1, p120 catenin	Adaptor	6.5E-06	996	0.019
BICD2	BICD cargo adaptor 2	MT binding	4.0E-05	909	0.018
AHNAK2	AHNAK nucleoprotein 2	Adaptor	2.9E-09	1014	0.017
DSG2	Desmoglein 2	Adhesion receptor	2.3E-07	5522	0.016
NACA	Nascent polypeptide-associated complex α subunit	RNA/Ribosome/Translation	1.3E-06	3137	0.016
MYH6	Myosin 6	Cytoskeletal motor	3.2E-06	11	0.015
MAP4	Microtubule associated protein 4	MT binding	6.7E-07	6048	0.015
EEF1A1	Eukaryotic translation elongation factor 1 alpha 1	RNA/Ribosome/Translation	6.4E-08	24	0.014
PLIN4	Perilipin 4	Metabolic Enzyme	1.2E-08	394	0.013
CTNNB1	Catenin beta 1, β-catenin	Adaptor	3.0E-13	136626	0.012
SNAP23	Synaptosome associated protein 23	Trafficking/Golgi/ER	4.0E-07	1336	0.010
CRIP2	Cysteine rich protein 2	DNA/Transcription	5.1E-07	1103	0.009
PALM2	Paralemmin 2	Adaptor	2.9E-06	1414	0.009
SHROOM1	Shroom family member 1	Actin binding adaptor	1.8E-05	1022	0.009
CTNNA3	Catenin alpha 3, αT-catenin	Actin binding adaptor	5.4E-08	6617	0.009
CAVIN1	Caveolae associated protein 1	Trafficking/Golgi/ER	8.3E-07	1093	0.009
LRRC59	Leucine rich repeat containing 59	RNA/Ribosome/Translation	4.6E-06	720	0.009
EFHD2	EF-hand domain family member D2	Adaptor	3.4E-06	868	0.008
FHL1	Four and a half LIM domains 1	Adaptor	1.8E-04	319	0.008
MYL3	Myosin light chain 3	Cytoskeletal motor	4.5E-04	38	0.008
PAKAP	Paralemmin A kinase anchor protein	Adaptor	3.3E-05	354	0.008

CDH2 specific hits are in bold.

We then compared the Cdh2-BioID2 hits with CDH1 interactome from epithelia (186, 187). There are 169 proteins shared between the two interactomes (**Fig. 2-4E**) and

185 proteins unique to CDH2 in cardiomyocytes. The distribution of the CDH2-only hits was similar to the entire population (**Fig. 2-4D**), with adaptor proteins forming the largest class in number and abundance (**Fig. 2-4E**). Actin-binding adaptors, adhesion receptors and cytoskeletal motor proteins were also enriched in the CDH2-only pool (**Fig. 2-4E**). By abundance, adaptor proteins (Adaptor, Actin Binding Adaptor and Membrane Binding Adaptor classes) account for 65% of the CDH2-only pool, highlighting the specialized molecular machinery required for intercellular adhesion in cardiomyocytes.

To gain further insight into the potential similarities and differences between CDH2 and CDH1 interactomes, we performed enrichment analysis using Ingenuity Pathway Analysis (IPA). We examined the CDH2, CDH1 and CDH2/CDH1 protein sets in canonical signaling and disease & function pathways. The CDH1 and CDH2/CDH1 sets were both enriched for AJ, cell-cell and endocytosis signaling (**Fig. 2-4F**). In contrast, the CDH2-specific pool showed less enrichment overall, though the emergence of cardiac β-adrenergic and calcium signaling pathways could reflect how the CDH2 interactome is tuned to cardiac function (**Fig. 2-4F**). The top enriched disease & function pathways for the CDH1 and CDH2/CDH1 protein sets were cellular organization and cancer-related categories (**Fig. 2-4G**). In contrast, the CDH2-specific pool was enriched for a variety of cardiomyopathies (**Fig. 2-4G**). These results suggest that, in cardiomyocytes, CDH2 recruits and organizes unique molecular complexes to regulate cell-cell adhesion and signaling.

2.3.6 Differential gene expression contributes to the specialized adhesion complexes in cardiomyocytes

During development, differential gene expression plays an essential role in establishing cell identity and function. Underlying their specialized role in cardiac contraction, cardiomyocytes express a unique set of genes. To determine if differential gene expression contributes to the CDH2 interactome, we identified cardiomyocyte or heart enriched genes in gene expression profiling data and compared these enriched genes to the CDH2, CDH1 and shared protein sets. We identified 1319 cardiomyocyte-enriched genes (CEGs) from RNA sequencing (RNA-seq) data collected at 11 points during the differentiation of human induced pluripotent stem cells (hiPSCs) to cardiomyocytes (232). CEGs comprised 22% (78/354) of the CDH2 interactome. Comparative analysis revealed that 52 CEGs were unique to CDH2 (**Fig. 2-5A**), representing 28.1% (52/185) of the CDH2 hits (**Fig. 2-5C**). In contrast, the number of CEGs present in the CDH1 or CDH2/CDH1 sets was lower, representing just 4.6% and 15.3%, respectively, of the hits for each class (**Fig. 2-5C**). We also calculated the percentage of CDH2, CDH1 and CDH2/CDH1 CEGS in the total CEG pool (1319 CEGs). Fisher's exact test indicated that CEGs were highly enriched in the CDH2 and CDH2/CDH1 sets, but not the CDH1 set (**Fig. 2-5C**).

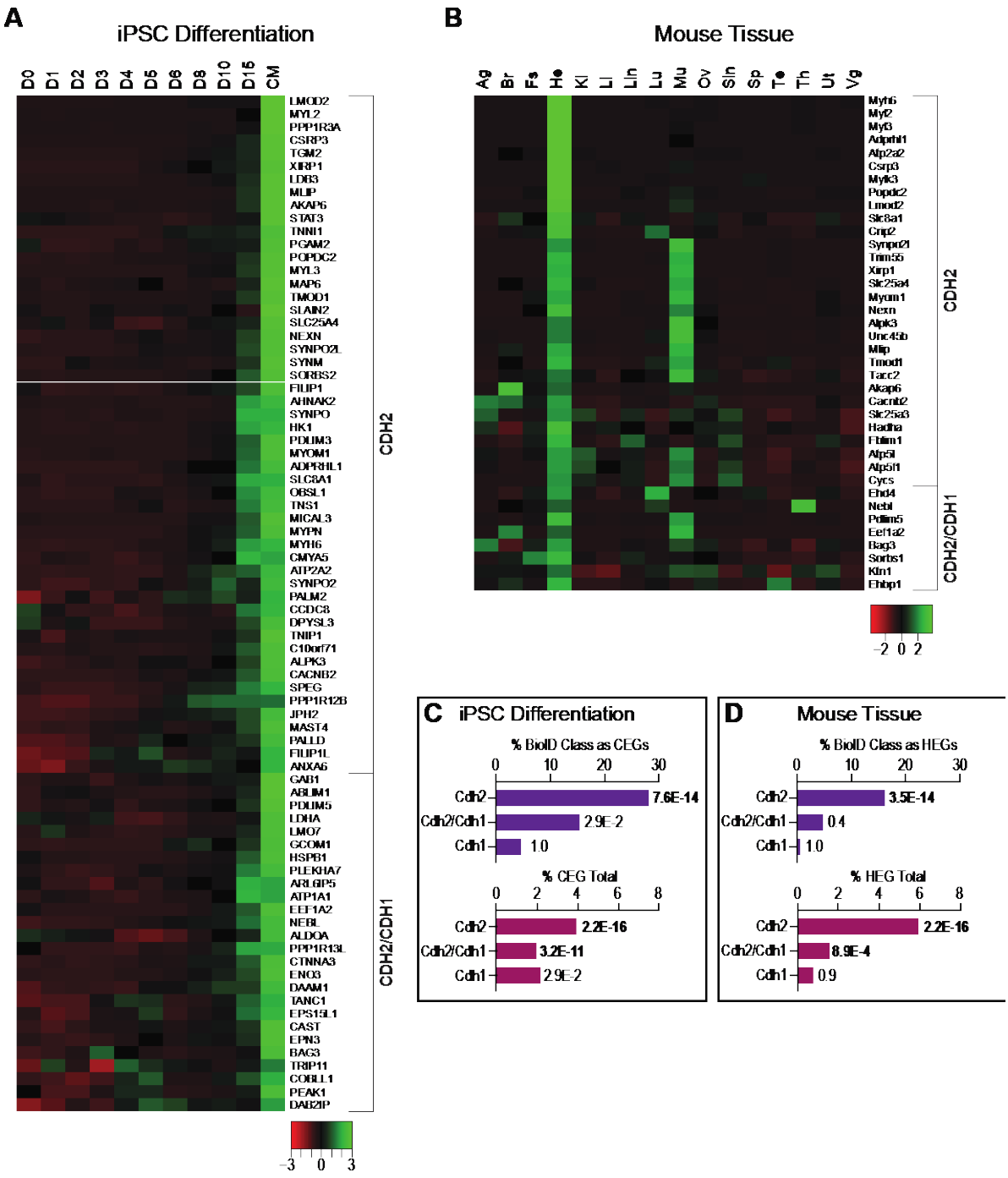

Figure 2-5 Differential gene expression contributes to the cardiomyocyte CDH2 proteome

A. Heat map of CDH2 or CDH2/CDH1 expression profiles during iPSC differentiation into cardiomyocytes (CM), day 0 (D0) to day 15 (D15). B. Heat map of CDH2 or CDH2/CDH1 expression profiles in mouse tissues. Ag (adrenal gland), Br (brain), Fs (fore stomach), He (heart), Ki (kidney), Li

(liver), Lin (large intestine), Lu (lung), Mu (muscle), Ov (ovary), Sin (small intestine), Sp (spleen), Te (testis), Th (thymus), Ut (uterus) and Vg (vesicular gland). C, D. Top, % BioID Class as CEGS/HEGs: percentage of each BioID class as cardiomyocyte enriched genes (CEGs) or heart enriched genes (HEGs). Bottom, % CEG Total: fraction of those BioID CEGs/HEGs in the total CEG/HEG population. P value of Fisher's exact test shown. Significant values are in bold.

We also analyzed tissue-enriched genes from adult mice. Using RNA-seq data from mouse tissues (233), we identified 504 heart-enriched genes (HEGs). HEGs comprised 10.7% (38/354) of CDH2 interactome. Of those, 30 HEGs were present in the CDH2 unique set, representing 16.1% of the CDH2 hits and 6.0% of total HEGs (**Fig. 2-5B, D**). HEGs were highly enriched in the CDH2 and CDH2/CDH1 sets, but not the CDH1 set (**Fig. 2-5D**). Similar results were observed in gene expression data from human tissues (**Fig. S2-3**). Together, these results suggest that cardiomyocyte and heart signature gene expression contribute significantly to the CDH2 interactome. Nonetheless, these enriched genes contribute to approximately 10-20% of the CDH2 interactome. The remaining 80-90% of the CDH2 interactome reflects distinct recruitment and organization at the protein level. Thus, while differential gene expression is a significant contributor to interactome identity, the primary driver of AJ specialization in cardiomyocytes is the recruitment of universal adaptor proteins to build specific, multiplex protein complexes.

2.3.7 CDH2 interactome protein network

To better understand how molecular complexes could be assembled at cardiomyocyte AJs, and how these complexes might differ from epithelia AJs, we

connected and organized the CDH2 interactome (**Fig. 2-6A**). We defined a new interactome group – ICD proteins (curated from the human protein atlas (234)) – and compared it to the CDH2 and CDH1 interactomes. The three-way comparison (**Fig. 2-6B**) defined four groups of proteins: CDH2, CDH2/CDH1, CDH2/ICD and CDH2/CDH1/ICD (**Fig. 2-6A**). All proteins were color-coded to match their assigned group. We then constructed a hierarchical classification with CDH2 at the top (see Methods for details). All protein-protein interactions were based on published, experimental data. The classification produced four tiers of interactors: 11 primary, 62 secondary, 177 tertiary and 48 quaternary (**Fig. 2-6A**). 52 of the Cdh2-BioID hits could not be connected to any other protein in the network. The hierarchal organization reveals that the percentage of Cdh2-BioID unique hits (green) increases from 0 to 70% as the distance from CDH2 increases, whereas the percentage of CDH2/CDH1 (orange) and CDH2/CDH1/ICD (pink) groups decreases from >90% to 25% (**Fig. 2-6C, D**). This suggests that the primary complex (1° and 2° tiers) is largely shared between CDH2 and CDH1, but that specific, specialized interactors are recruited outside (3° and 4° tiers) the primary complex to regulate junction assembly and function in cardiomyocytes. Also noteworthy is the abundance of CDH2 (green) hits versus CDH2/ICD (purple) or CDH2/CDH1/ICD (pink) hits. These green-labeled proteins reflect potentially new, previously unassigned ICD components with potential roles in cadherin and cardiomyocyte adhesion biology.

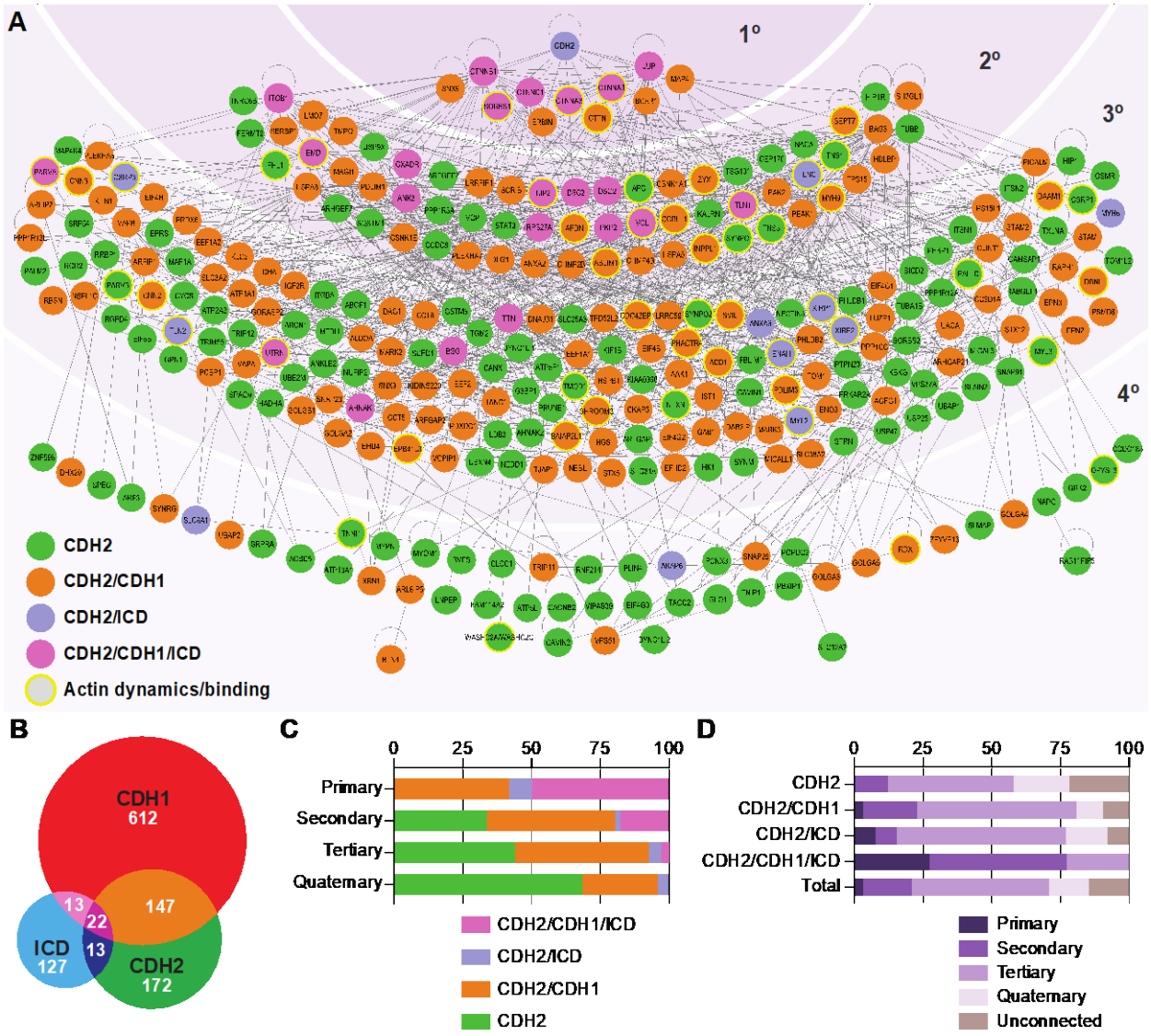

Figure 2-6 Cardiomycoyte CDH2 interactome

A. Interaction network of CDH2 interactome organized into four tiers based using Ingenuity Pathway Analysis. All protein-protein interactions supported by published, experimental data. Hierarchical classification was done manually around CDH2. Primary interactors bind CDH2 directly. Secondary interactors bind primary interactors but not CDH2. Tertiary interactors bind secondary interactors. Quaternary interactors bind tertiary interactors or to outermost tier proteins. Bottom left legend defines group classification. B. Venn diagram between CDH2 interactome, CDH1 interactome and ICD

curated proteins. C. Distribution of groups within each interactome tier. D. Distribution of tier and unconnected proteins within each group and the total collection.

2.3.8 Identified adapter proteins localize to cell-cell contacts

Cardiomyocyte AJs must connect contractile myofibrils, placing unique demands on the proteins that physically connect actin to the cadherin complex. We identified over 100 adaptor proteins in the CDH2 interactome (**Fig 2-4D**, adaptor, actin binding adaptor and membrane binding adaptor) and nearly half of these adaptor proteins bind actin or regulate actin dynamics (**Fig. 2-6A**, actin-associated proteins highlighted with yellow), including the actin-binding proteins VCL and AFDN, both top-ranked hits (**Fig. 2-4C** and Table **2-1**). We examined the localization of 27 adaptor and actin-associated proteins by transiently expressing fluorescently-tagged proteins in cardiomyocytes (**Fig. 2-7**, **Fig. S2-4**). Seventeen of the tested proteins localized to cell-cell contacts (**Fig. 2-7A-F**, **Fig. S2-4A**; summarized in **Fig. 2-7G**). FRMD4A, VCL, AFDN and FBLIM1 localized primarily to cell-cell contacts (**Fig. 2-7A-D**). As expected, VCL also localized to cell-substrate contacts (**Fig. 2-7B**). AFDN and FBLIM were also present at Z-discs (**Fig. 2-7C, D**). Supervillin (SVIL) and Synaptopodin 2 (SYNPO2) localized primarily to Z-discs but were also observed colocalizing with CDH2 at contacts (**Fig. 2-7E, F**; **Fig. S2-4B**). Representative images for showing the localization of PLEKHA6, TJP1 (paralog of TJP2), CTTN, EMD, DAAM1, LDB3, FERMT2, TMOD1, BCAR1, NEXN and FILIP1 are shown in Fig. S4A. DBN1 formed filamentous structures along the actin cytoskeleton with limited localization to cell-cell contacts and LNPK localized to the endoplasmic reticulum (**Fig. S2-4A**). The remaining eight proteins were primarily cytoplasmic or formed aggregates when

overexpressed (**Fig. S2-4A**). These could represent false positives, though three of the hits – PARVA, COBLL1 and TLN1 – have been reported to associate with CDH1 (Guo, 2014). Notably, 9 of the 17 proteins recruited to cell-cell contacts are unique to the CDH2 interactome (**Fig. 2-7H**, highlighted in green) and represent proteins that could promote AJ specialization in cardiomyocytes.

2.3.9 Dynamic shuttling between AJs and Z-discs

The ICD can be thought of as the terminal Z-disc because, for a membrane-tethered myofibril, the ICD functions as the terminal end of the sarcomere (**Fig. 2-1I**). Our localization analysis identified 4 proteins with strong localization to Z-discs and cell-cell contacts: SYNPO2, SVIL, EMD and LDB3 (**Fig. 2-7E, F**; **Fig. S2-4A**). In Cdh2-BioID2 expressing cardiomyocytes, biotinylated proteins were detected at cell-cell contacts as well as at Z-discs (**Fig. 2-1 3G, H**). We questioned if proteins could shuttle between the AJ and Z-discs. We first analyzed the dynamics of GFP-tagged SYNPO2 and SVIL by FRAP (**Fig. 2-7I, J**). Both proteins were dynamic, with large mobile fractions (~75%) and fast recovery halftimes (97 for SYNPO2 and 73 seconds for SVIL). We then tracked the movement of SYNPO2 further using the photoconvertible protein mEos3.2. Photoconverted SYNPO2-mEos3.2 shuttled from Z-discs or cell-cell to distal Z-discs within minutes (**Fig. 2-7K, L**). We speculate that Z-disc proteins are recruited dynamically to the AJ to promote myofibril assembly and integration along cell-cell contacts. Thus, the ICD AJ plays an important role in guiding both cardiomyocyte adhesion and cytoskeleton organization.

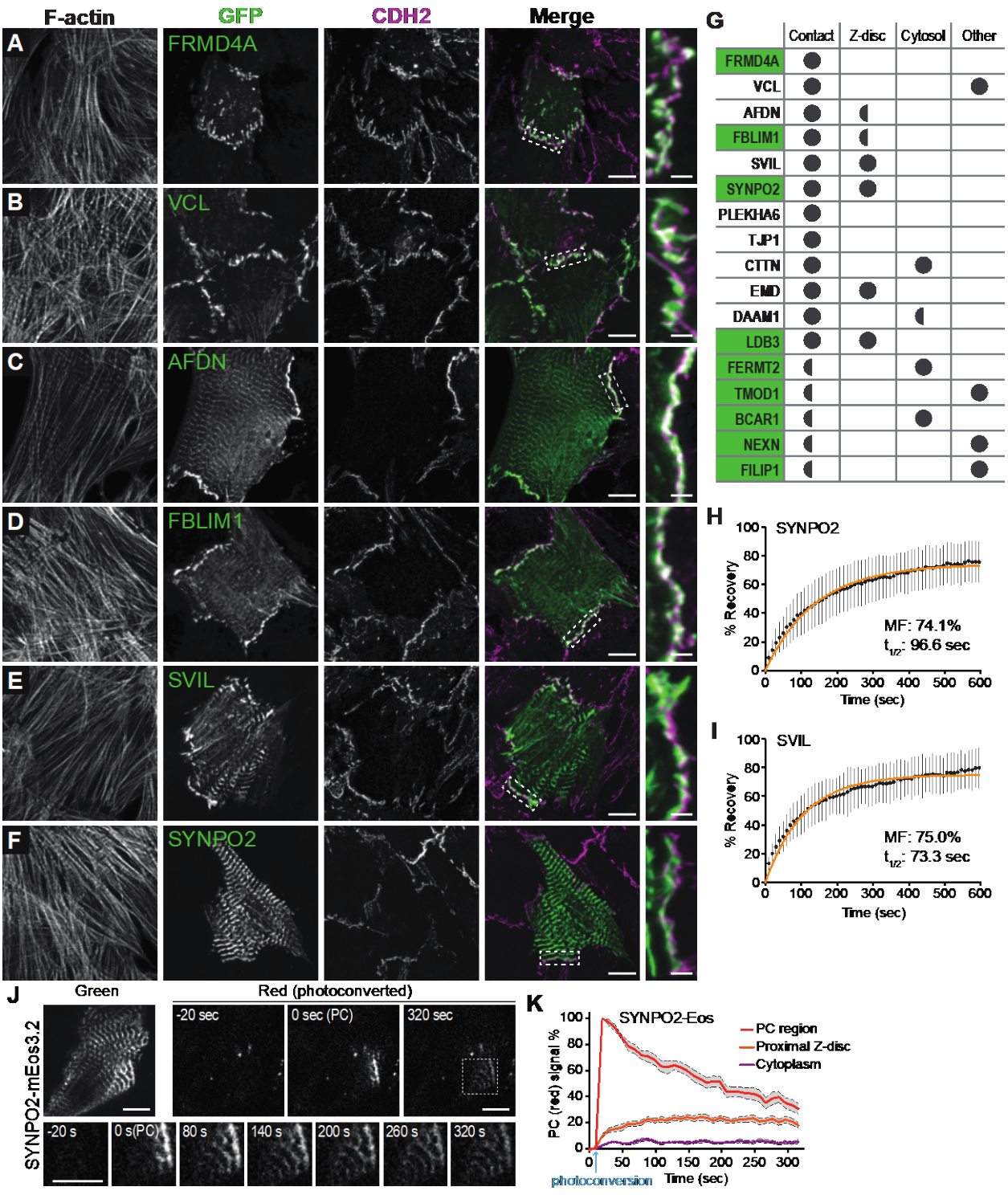
F-actin
GFP
CDH2
Merge
A
FRMD4A
B
VCL
C
AFDN
D
FBLIM1
E
SVIL
F
SYNPO2
G
Contact
Z-disc
Cytosol
Other
FRMD4A
VCL
AFDN
FBLIM1
SVIL
SYNPO2
PLEKHA6
TJP1
CTTN
EMD
DAAM1
LDB3
FERMT2
TMOD1
BCAR1
NEXN
FILIP1
H
SYNPO2
% Recovery
MF: 74.1%
t1/2: 96.6 sec
Time (sec)
I
SVIL
% Recovery
MF: 75.0%
t1/2: 73.3 sec
Time (sec)
J
Green
Red (photoconverted)
SYNPO2-mEos3.2
-20 sec
0 sec (PC)
320 sec
-20 s
0 s(PC)
80 s
140 s
200 s
260 s
320 s
K
SYNPO2-Eos
PC region
Proximal Z-disc
Cytoplasm
PC (red) signal %
photoconversion
Time (sec)

Figure 2-7 CDH2 interactome proteins localize to cell-cell contacts and z-discs

A-F. Cardiomyocytes transfected with GFP-tagged Cdh2-BioID hits. Cells were fixed 24 hours post-transfection and stained for Cdh2 and F-actin. All images are maximum projections of deconvolved Z-stacks. Individual and merged GFP (green) and CDH2 (magenta) channels shown. Far right column is a magnification of boxed contact in Merge image. G. Summary of GFP-Cdh2-BioID interactome localization to cell-cell contacts, Z-discs, cytosol or other. Full circle indicates robust localization; half circle indicates modest localization. Proteins highlighted in green are unique to the CDH2 interactome. Representative images for PLEKHA6, TJP1 (paralog of TJP2), CTTN, EMD, DAAM1, LDB3, FERMT2, TMOD1, BCAR1, NEXN and FILIP1 are shown in Fig S4. H, I. Plot of FRAP recovery fraction over time for SYNPO2 (30 FRAP regions from 2 experiments) and SVIL (18 FRAP regions from 2 experiments) at Z-discs. At each time point, the mean recovery fraction is shown as a black circle and the standard deviation is represented by black lines. The data were fit to a single exponential curve (orange line). Mobile fraction percentage (MF) and recovery halftimes ($t_{1/2}$) listed. SYNPO2 data is from 30 FRAP regions from 2 independent experiments; SVIL data is from 18 FRAP regions from 2 independent experiments. J. Dynamics of photoconverted SYNPO2-mEos3.2 in transfected cardiomyocytes. Green channel shows total SYNPO2-mEos3.2 protein. Red channel shows photoconverted protein before activation (-20 sec (seconds)), immediately after photoconversion (0 sec (PC)) and after 320 sec. Bottom montage shows a magnified view of photoconverted protein (boxed region in top right 320 sec panel) over time. K. Quantification of photoconverted SYNPO2-mEos3.2. Mean percentage of photoconverted protein (red signal) for the photoconverted area (PC region, red line), Z-disc 2-3 microns outside the photoconverted region (Proximal Z-disc, orange line) and cytoplasm 2-3 microns outside the photoconverted region (Cytoplasm, purple line) plotted over time. Dashed lines and grey region around mean define the standard error of the mean. Time of photoconversion marked with a blue arrow. Data is from 12 photoconverted cells from 2 independent experiments. Scale bar is 10 μm in A-F, J.

2.4 Discussion

Our results provide new details into the architecture of the developing ICD and define the proteins that organize the AJ in cardiomyocytes. This work builds off past studies of the cadherin-catenin interactome in epithelia (186–188) to expand the AJ protein atlas to include the cardiomyocyte, a unique contractile system. Our molecular and proteomics data reveal how the cardiomyocyte AJ recruits a unique set of cytoskeletal, scaffold and signaling proteins to build this critical mechanical junction and guide cardiomyocyte organization and adhesion.

2.4.1 Core adhesion complexes are conserved

The cadherin-catenin complex is recruited to developing contacts and, not surprisingly, the catenins (CTNNB1, JUP, CTNND1, CTNNA1, CTNNA3) are among the most robust hits in the CDH2 proteomic screen (**Table 2-1**). FRAP studies revealed that the complex is largely immobile (~1/3 is mobile) and that the entire complex is exchanged along contacts similar to epithelia (43), though the recovery rate is markedly slower (discussed below). These properties are not unexpected given current AJ dogma. Biochemical studies have demonstrated that β-catenin binds with high affinity to αE-catenin and that the β-catenin/αE-catenin complex binds strongly to the cadherin tail to create a stable complex (44). The molecular interactions that underlie the core cadherin-catenin complex are likely conserved between epithelia and cardiomyocytes. Consistent with this, Cdh1 expression can restore intercellular adhesion and myofibril coupling in cultured Cdh2-null cardiomyocytes (14) and ectopic, cardiac-specific expression of Cdh1

in Cdh2-null embryos can rescue early heart development (27). The ability of Cdh1 to rescue basic cadherin functions in Cdh2-deficient cardiomyocytes underscores how the core cadherin-catenin complex, and its basic properties, are conserved between epithelia and cardiomyocytes.

The desmosome components DSG2, JUP and PKP2 were also among the more abundant proteins isolated in the proteomic screen (**Table 2-1**). DSG2 localization was more restricted than the AJ and appeared to be preferentially localized near sites of myofibril integration (**Fig. 2-1D**; Merkel and Kwiatkowski, unpublished observations). DSG2 (and desmosome development) may be favored at more stable or mature AJs, consistent with EM analysis (**Fig. 2-1J**). Interestingly, recent evidence suggests that CDH1 can recruit DSG2 through direct extracellular *cis* interactions to promote desmosome assembly at nascent contacts in epithelial cells (73). A similar interaction between CDH2 and DSG2 could promote desmosome assembly along cardiomyocyte junctions. In contrast to DSG2, JUP and PKP2 showed near identical localization patterns to the AJ (**Fig. 2-1E, G**). JUP can bind directly to classical cadherins (221) and was a robust hit in CDH1 proteomic screens (186, 187). PKP2, an armadillo protein related to CTNND1, is a multifunctional protein that binds desmosomal cadherins, JUP and desmoplakin (DSP) (235). We speculate that both JUP and PKP2 may be recruited to AJs during the initial stages of contact formation to promote desmosome assembly, similar to their proposed role in epithelia (59). Note that PKP2 can also bind directly to CTNNA3 and has been proposed to link the AJ to intermediate filaments at hybrid junctions, where AJ and desmosome proteins are mixed in mammalian hearts (54, 222).

2.4.2 AJ specialization is driven by ancillary adapter proteins

We identified 365 proteins from 354 genes in the CDH2 interactome. Of these, 169 hits were shared with the CDH1 interactome while 185 hits were unique to CDH2. By abundance, 65% of the CDH2 pool was composed of adaptor proteins (**Fig. 2-4E**). Analysis of the protein-protein interactions revealed that shared components occupied the inner tiers of the network whereas CDH2-specific adaptors occupied the outer tiers (**Fig. 2-6A**) The assembled interaction network reflects the hierarchy of protein binding required to form the molecular complexes along cardiomyocyte contacts. Critical to these assemblages are the catenin proteins, CTNND1, CTNNB1, JUP, CTNNA1 and CTNNA3. All catenin proteins are known to bind directly to a number of other proteins. For example, in addition to binding CTNNB1/JUP and actin, CTNNA1/CTNNA3 can interact with VCL, AFDN, PKP2 and ZO1/2 (6). These proteins, in turn, can associate with a wide-range of cytoskeletal and signaling proteins. We speculate that the catenins coordinate the organization of molecular complexes at the cardiomyocyte AJ to regulate adhesion and signaling.

Collectively, the primary function of these adaptor proteins is likely to strengthen the mechanical connection between the AJ and the actin cytoskeleton along the ICD membrane. Myofibrils are coupled to AJs at substantial, electron dense structures (**Fig. 2-1I, J**), consistent with a large assemblage of proteins organizing into an adhesive plaque to anchor the contractile filaments. Likewise, the recovery halftime of the cadherin-catenin complex at cardiomyocyte cell-cell contacts is an order of magnitude slower than at epithelial junctions (**Fig. 2-3C**; (43)), possibly due to stronger connections to the actin

cytoskeleton mediated through actin binding proteins. While adaptor proteins could function to strengthen the physical connection between the cadherin-catenin complex and actin, they might also promote actin and membrane architectures that function to mitigate the forces of contraction. For example, coupling to myofibrils at an angle along the ICD membrane (**Fig. 2-1I, J**) may help AJs withstand mechanical force during contraction. Membrane and actin-associated adaptor proteins could regulate the formation and maintenance of these unique ICD junctional topologies.

Roughly 140 curated ICD proteins were not detected in the CDH2 interactome (**Fig. 2-7B**), including established CDH2-associated proteins like the gap junction protein Connexin 43 (GJA1). While we observed GJA1 along contacts in our cultured cardiomyocytes, the localization was punctate and differed from CDH2. The absence of GJA1 and other curated ICD proteins from our screen could be due to the physical limitations of BioID2-labeling (the range of biotinylation is limited to ~10 nm, (184)), the absence of surface lysines on a target protein for labeling and/or the maturity of the cell-cell contacts in our system. Alternatively, it could reflect the segregation of molecular complexes along these contacts and highlight the specificity of AJ interactions.

Conversely, only 13 of the 185 CDH2-specific hits are curated ICD proteins. The remaining 172 hits have not been associated with the ICD, thus expanding the atlas of proteins associated with cell adhesion in cardiomyocytes. Note, however, that biotin labeling can occur during many stages of a protein life cycle, thus some hits may not be ICD proteins and instead regulate CDH2 trafficking or degradation. In fact, Trafficking/Golgi/ER proteins were a significant fraction (12%, **Fig. 2-4E**) of the CDH2-specific hits. Likewise, some hits could be false positives: of the 27 adaptor and actin-

associated proteins expressed as GFP-tagged fusions in cardiomyocytes, 8 were cytoplasmic or formed aggregates. However, the GFP tag or expression level could have interfered with the localization of many of these proteins, particularly since some (TLN1, PARVA and COBLL1) are shared with the CDH1 interactome and likely represent conserved interactors (187). Also, since proximity labeling occurs in intact, living cells, false interactions that may arise during cell lysis or precipitation are limited (236). Nonetheless, it is essential that any hit be verified by a secondary method (e.g., cell staining or coprecipitation), and we expect that future work will further define and refine the CDH2 interactome.

2.4.3 The AJ and the Z-disc, linked through the myofibril sarcomere

Cardiomyocytes must be coupled to create a functional syncytium and the AJ serves as the mechanical link between myofibrils and the ICD membrane. The contractile unit of the myofibril is the sarcomere whose lateral boundaries are defined by Z-discs where the barbed ends of actin filaments are interdigitated and crosslinked. Z-discs are connected to the lateral membrane (sarcolemma) and the surrounding extracellular matrix by specialized adhesive complexes called costameres. In cardiomyocytes, the AJ functions as the terminal Z-disc for the membrane proximal sarcomere (**Fig. 2-1I**). While cardiomyocyte organization almost certainly requires coordination between the AJ and Z-disc/costamere (224), the molecular details remain largely unexplored and undefined. We identified a number Z-disc proteins in our proteomic screen (**Table S2-1**), including SVIL (237), SYNPO2 (238), EMD (239, 240), BAG3 (241), LDB3 (242), NEBL (243), PDLIM3 & PDLIM5 (244), FHL1 (245), TTN (246) and ZYX (247). We observed that at least 4 –

SVIL, SYNPO2, EMD and LDB3 – localize to both Z-discs and cell-cell contacts (**Fig. 2-7E, F**; **Fig. S2-4A**). We showed that SYNPO2 and SVIL are dynamic proteins and that SYNPO2 can shuttle between junctions and Z-discs. We speculate that the AJ recruits Z-disc proteins to coordinate myofibril assembly and integration at contacts. Additional studies are expected to reveal how such coordination is regulated at the molecular level.

2.4.4 The developing ICD in neonatal cardiomyocytes

We took advantage of the innate ability of primary neonatal cardiomyocytes to reestablish cell-cell contacts *in situ* to express tagged AJ proteins and explore their dynamics and label CDH2-associated proteins. Primary neonatal cardiomyocytes plated on isotropic substrates form cell-cell contacts around their entire perimeter (**Fig. 2-1**), similar to cardiomyocytes in the developing and perinatal heart (157). The stereotypical, elongated cardiomyocyte morphology with aligned myofibrils and ICDs restricted to the bipolar ends develops postnatally (74, 157, 248), though the mechanisms of this polarization remain unclear. Thus, while our proteomic results offer a snapshot of the CDH2 interactome at developing cell-cell contacts rather than at mature ICDs, this transitional stage has *in vivo* relevance and these results provide a significant advance in defining the cadherin interactome in cardiomyocytes. In addition, we were able to generate quantitative MS data from a relatively small sample of cultured primary cardiomyocytes. A similar experimental protocol could be used to examine changes in the CDH2 interactome from mutant cardiomyocytes or from cardiomyocytes cultured under varying conditions (e.g., soft versus stiff substrates). Alternatively, it could be used to define the CDH2 proteome in differentiated iPSCs or modified to express in an AAV

system to examine the CDH2 proteome *in vivo* during heart development or disease. Future work is expected to build on this newly defined AJ network to provide important insight into how the molecular complexes that regulate AJ function change in response to injury or disease.

2.5 Materials and Methods

2.5.1 Plasmids

Murine Cdh2 in pEGFP-N1 (CDH2-EGFP) was a gift from James Nelson. CTNNA3-EGFP was described previously (58). Plasmid pEGFP-C1-rat-l-afadin (AFDN) was gift from Yoshimi Takai (249). Plasmids mEmerald-JUP-N-14 (Addgene 54133), mEmerald-beta-catenin-20 (CTNNB1, Addgene 54017), mEmerald-alpha1-catenin-C-18 (CTNNA1, Addgene 53982), mEmerald-ZO1-C-14 (TJP1, Addgene 54316), mEmerald-Vinculin-23 (VCL, Addgene 54302), mEmerald-Talin-C-18 (TLN1, Addgene 62763), mEmerald-Parvin-N-16 (PARVA, Addgene 54215) and mEmerald-Migfilin-C-14 (FBLIM1, Addgene 54181) were gifts from Michael Davidson. Emerin pEGFP-C1 (EMD, Addgene 61993) was a gift from Eric Schirmer (250). GFP-cortactin (CTNN1, Addgene 26722) was a gift from Anna Huttenlocher (251). EGFP-supervillin (SVIL, Addgene 13040) was gift from Elizabeth Luna (252). Drebin-YFP (DBN1, Addgene 40359) was a gift from Philip Gordon-Weeks (253). pEGFP Kindlin2 (FERMT2, Addgene 105305) was gift from Kenneth Yamada. pHAGE2 Lnp-mCherry (LNPK, Addgene 86687) was a gift from Tom Rapoport (254). HA-p62 (SQSTM1, Addgene 28027) was a gift from Qing Zhong (255).

pDONR223_TRIM55_WT (Addgene 81829) was a gift from Jesse Boehm, William Hahn and David Root (256). MCS-BioID2-HA (Addgene 74224) was a gift from Kyle Roux (184). pAdTrack-CMV (Addgene 16405) was a gift from Bert Vogelstein (257). Sqstm1 and Trim55 were subcloned into pEGFP-N1.

To create the Plekha6, Frmd4a, Daam, Synpo2, Ldb3, Tmod1, Nexn, Filip1, Csrp1, Dpysl3, Cobll1 and Phldb1 constructs, RNA was first isolated and purified from adult mouse heart using an RNeasy Fibrous Tissue Mini kit (Qiagen) and reverse transcribed to create cDNA using Transcriptor High Fidelity cDNA Synthesis Kit (Roche). Gene specific primers were designed against the 5' and 3' ends of each gene to generate full-length clones by PCR. PCR products were cloned directly into pEGFP-N1 (Plekha6, Synpo2, Ldb3, Nexn, Csrp1, Dpysl3, Cobll1 and Phldb1) or pEGFP-C1 (Frmd4a, Daam1, Tmod1 and Filip1) to create EGFP fusions. Synpo2 was also cloned into mEos3.2-N1 (Addgene 54525), a gift from Michael Davidson and Tao Xu (258). Assembled clones were verified by sequencing.

2.5.2 Antibodies

Primary antibodies used for immunostaining were: anti-N-cadherin (1:250, Thermo Fisher Scientific 33-3900), anti-α-Actinin (1:250, Sigma A7811), anti-Desmoglein 2 (1:250, Abcam ab150372), anti-αE-catenin (1:100, Enzo Life Science ALX-804-101-C100), anti-β-Catenin (1:100, BD Transduction Laboratories 610154), anti-γ-Catenin (1:100; Cell Signaling 2309), anti-Connexin-43 (1:100, Proteintech 15386-1-AP), anti-Plakophilin 2 (1:10, Progen 651101) and anti-HA (1:100, Sigma 11867423001).

Streptavidin-Cy3 (1:300, Jackson Immunoresearch 016-160-084) was used to label biotinylated proteins. Secondary antibodies used were goat anti-mouse or anti-rabbit IgG labeled with Alexa Fluor 488, 568 or 647 dyes (1:250, Thermo Fisher Scientific). F-actin was visualized using Alexa Fluor dye conjugated phalloidin (1:100-1:250, Thermo Fisher Scientific).

2.5.3 Cardiomyocyte isolation and culture

All animal work was approved by the University of Pittsburgh Division of Laboratory Animal Resources. Primary cardiomyocytes were isolated from Swiss Webster or Black 6 mouse neonates (P1-P3) as described (58, 220). For protein isolation, Swiss Webster-derived cardiomyocytes were plated onto 35 mm dishes (1 x 10^6 cells/dish) coated with Collagen Type I (Millipore). For immunostaining, cardiomyocytes were plated onto 35 mm MatTek dishes with 10 mm insets coated with Collage Type I. Cardiomyocytes were plated in plating media: 65% high glucose DMEM (Thermo Fisher Scientific), 19% M-199 (Thermo Fisher Scientific), 10% horse serum (Thermo Fisher Scientific), 5% FBS (Atlanta Biologicals) and 1% penicillin-streptomycin (Thermo Fisher Scientific). Media was replaced 16 hours after plating with maintenance media: 78% high glucose DMEM, 17% M-199, 4% horse serum, 1% penicillin-streptomyocin, 1 μM AraC (Sigma) and 1 μM Isoproternol (Sigma). Cells were cultured in maintenance media for 2-4 days until lysis or fixation.

2.5.4 Immunostaining and confocal microscopy

Cells were fixed in 4% EM grade paraformaldehyde in PHEM buffer (60 mM PIPES pH 7.0, 25 mM HEPES pH 7.0, 10 mM EGTA, pH 8.0, 2 mM $MgCl_2$ and 0.12 M Sucrose) or PHM (no EGTA) buffer for 10 minutes, washed twice with PBS and then stored at 4°C until staining. Cells were permeabilized with 0.2% Triton X-100 in PBS for 4 minutes and washed twice with PBS. Cells were then blocked for 1 hour at room temperature in PBS + 10% BSA (Sigma), washed 2X in PBS, incubated with primary antibodies in PBS + 1% BSA for 1 hour at room temperature, washed 2X in PBS, incubated with secondary antibodies in PBS + 1% for 1 hour at room temperature, washed 2X in PBS and then mounted in Prolong Diamond (Thermo Fisher Scientific). All samples were cured at least 24 hours before imaging.

Cells were imaged on a Nikon Eclipse Ti inverted microscope outfitted with a Prairie swept field confocal scanner, Agilent monolithic laser launch and Andor iXon3 camera using NIS-Elements (Nikon) imaging software. Maximum projections of 3-5 μm image stacks were created and deconvolved (3D Deconvolution) in NIS-Elements (Nikon) for presentation.

2.5.5 FRAP experiments

FRAP experiments were conducted on a Nikon swept field confocal microscope (describe above) outfitted with a Tokai Hit cell incubator and Bruker miniscanner. Actively contracting cells were maintained at 37°C in a humidified, 5% CO_2 environment. User-

defined regions along cell-cell contacts (CDH2, CTNNB1, JUP, CTNNA1 and CTNNA3; Fig 2) or Z-discs (SYNPO2 and SVIL; Fig 7) were bleached with a 488 laser and recovery images collected every 5 or 10 seconds for 10 minutes. FRAP data was quantified in ImageJ (NIH) and average recovery plots were measured in Excel (Microsoft). For Fig 2, FRAP recovery plots represent data from >50 contacts from at least three separate transfections of unique cell preps. For Fig 7, FRAP recovery plots represent data from 30 (SYNPO2) or 18 (SVIL) Z-discs from two independent transfections of unique cell preps. Curves were either fit to a double exponential formula (Fig 2) or a single exponential formula (Fig 7), whichever fit the recovery data the best, to determine the mobile fraction and half time of recovery in Prism (Graphpad).

2.5.6 Photoconversion experiments

Transfected cardiomyocytes were cultured and imaged similar to FRAP experiments. User-defined regions at contacts and Z-discs were photoconverted by 300 millisecond exposure to a 405 laser and the dynamics of the photoconverted protein tracked every 10 seconds over 5 minutes. Photoconversion data was quantified in ImageJ (NIH) and changes in signal intensity measured over time in Excel (Microsoft) and plotted in Prism (Graphpad). To establish the photoconverted signal range for each event, the signal intensity of the red photoconverted protein in the region of interest was measured just before and immediately after exposure to the 405 laser. Photoconverted signal was also measured at a Z-disc and similar sized cytoplasmic region 2-3 microns from the photoconverted region over the course of the experiment. Changes in signal intensity of these proximal regions relative to the photoconverted region were plotted over time.

2.5.7 Electron Microscopy

Cardiomyocytes were cultured on collagen-coated MatTek dishes and fixed as described above. After fixation and washing, cells were incubated with 1% OsO4 for one hour. After several PBS washes, dishes were dehydrated through a graded series of 30% to 100% ethanol, and then infiltrated for 1 hour in Polybed 812 epoxy resin (Polysciences). After several changes of 100% resin over 24 hours, cells were embedded in inverted Beem capsules, cured at 37°C overnight and then hardened for 2 days at 65°C. Blocks were removed from the glass dish via a freeze/thaw method by alternating liquid Nitrogen and 100°C water. Ultrathin (60nm) sections were collected on to 200-mesh copper grids, stained with 2% uranyl acetate in 50% methanol for 10 minutes and 1% lead citrate for 7 minutes. Samples were photographed with a JEOL JEM 1400 PLUS transmission electron microscope at 80kV with a Hamamatsu ORCA-HR side mount camera.

For platinum replica electron microscopy (PREM), cardiomyocytes were first washed with PBS and then extracted for 3 minutes in PHEM buffer (without fixative) plus 1% TritonX-100 and 10 μM phalloidin (unlabeled). Following extraction, cells were washed 3x in PHEM buffer (without fixative) plus 5 μM phalloidin and fixed for 20 minutes in PHEM buffer plus 2% glutaraldehyde. Cells were washed and stored in PBS at 4°C until processing. Fixed samples were processed for PREM as described (259). Replicas were imaged in grids on the JEOL JEM 1400 PLUS transmission electron microscope described above.

2.5.8 Adenovirus production

Mouse *Cdh2* ORF was first amplified from CDH2-EGFP by PCR and cloned into MCS-BioID2-HA to fuse BioID2 to the C-terminal tail of N-cadherin. The Cdh2-BioID2 fusion was then subcloned into pAdTrack-CMV plasmid. Recombinant adenovirus was produced by transforming the pAdTrack-CMV-Cdh2-BioID2 plasmid into pAdEasier-1 E.coli cells (a gift from Bert Vogelstein, Addgene 16399) (257). Virus packaging and amplification were performed according to the protocol described by Luo and colleagues (260). Virus particles were purified using Vivapure AdenoPACK 20 Adenovirus (Ad5) purification & concentration kit (Sartorius). Adeno-X qPCR Titration Kit (Clontech) was used to calculate virus titer by quantitative PCR on an Applied Biosystems 7900HT.

2.5.9 Adenovirus infection and biotin labeling

Each experimental replicate included four 35 mm dishes with 1 x 10^6 cells each (4 x 10^6 total). Cardiomyocytes were infected one day after plating with Cdh2-BioID2 adenovirus at an MOI of 2. 24 hours later (48 hours post-plating), the media was replaced with fresh maintenance media plus 50 μM biotin in both Cdh2-BioID2 infected and control uninfected samples. The next day (72 hours post-plating), cells were harvested for protein isolation and mass spec. Cell lysate preparation and affinity purification were performed according to published protocols (184, 185).

2.5.10 Western blotting

Protein samples were separated on an 8% SDS-PAGE gel and transferred onto a PVDF membrane (Bio-Rad). The membrane was blocked in TBST + 5% BSA, washed in TBST, incubated with IRDye 680RD Streptavidin (1:1000, LI-COR) in TBST, washed twice in TBST and washed once in PBS. The membrane was scanned using a LI-COR Odyssey Infrared Imager.

2.5.11 Mass spectrometry and statistical analysis

All protein samples were run on precast Mini-PROTEAN TGX 10% SDS-PAGE gels (Bio-Rad) at 120 volts for 5 min so that the proteins migrated into the gel about 1 cm^2. Gels were stained in Coomassie blue and a single, ~1 cm gel slice was excised for each sample and submitted for processing. Excised bands were digested with trypsin as previously described (261). Briefly, the excised gel bands were destained with 25mM ammonium bicarbonate in 50% acetonitrile (ACN) until no visual stain remained and the gel pieces were dehydrated with 100% ACN. Disulfide bonds were reduced in 10mM dithiothreitol (DTT, Sigma-Aldrich Corporation) at 56°C for 1 hour and alkylated with 55mM iodoacetamide (IAA, Sigma-Aldrich Corporation) for 45 minutes at room temperature in the dark. Excess DTT and IAA were removed by dehydration in 100% ACN before rehydration in 20 ng/µL trypsin (Sequencing Grade Modified, Promega Corporation) in 25 mM ammonium bicarbonate and digested overnight at 37°C. The peptides were extracted from gel pieces in a solution containing 70% ACN/5% formic and desalted with Pierce C18 Spin Columns (Thermo Fisher Scientific) according to

manufacturer's protocol, dried in a vacuum centrifuge and resuspended in 18 µL of 0.1% formic acid. A pooled instrument control (PIC) sample was prepared by combining 4 µL from each of the 12 samples and used to monitor instrument reproducibility.

Tryptic peptides were analyzed by nLC-MS/MS using a nanoACQUITY (Waters Corporation) online coupled with an Orbitrap Velos Pro hybrid ion trap mass spectrometer (Thermo Fisher Scientific). For each nLC-MS/MS analysis, 1 µL of peptides was injected onto a C_{18} column PicoChip 25 cm column packed with Reprosil C18 3 µm 120 Å chromatography with a 75 µm ID and 15 µm tip (New Objective). Peptides were eluted off to the mass spectrometer with a 66 minute linear gradient of 2-35% ACN/0.1% formic acid at a flow rate of 300 nL/min. The full scan MS spectra were collected over mass range m/z 375-1800 in positive ion mode with an FTMS resolution setting of 60,000 at m/z 400 and AGC target 1,000,000 ms. The top 13 most intense ions were sequentially isolated for collision-induced dissociation (CID) tandem mass spectrometry (MS/MS) in the ion trap with ITMS AGC target 5,000 ms. Dynamic exclusion (90s) was enabled to minimize the redundant selection of peptides previously selected for MS/MS fragmentation.

The nLC-MS/MS data were analyzed with MaxQuant software (262, 263), version 1.6.0.1. Briefly, the proteomic features were quantified by high resolution full MS intensities after retention alignment and the corresponding MS/MS spectra were searched with Andromeda search engine against the Uniprot mouse database (release November 2017, 82,555 entries) (264). The mass tolerance was set at 20 ppm for the precursor ions and 0.8 Da for the ITMS fragment ions. Andromeda search included specific trypsin enzyme with maximum two missed cleavages, minimum of seven amino acids in length.

Fixed modification carbamidomethyl (C), and variable modifications of oxidation (M), acetyl (Protein N-term), and deamidation (NQ) were considered. Protein identification threshold was set to 1% false discovery rate (FDR) as described previously (262).

Proteins that exhibit statistically significant abundance between CDH2-BioID2 to control were selected as follows. Proteins with a single peptide identification were excluded from the data analysis and Student's t-test on log2 transformed protein intensity was used for the statistical inference to select CDH2-BioID2 interacting proteins. A protein was considered a significant candidate if the t-test p-value was <0.001 and the fold change >10 when compared to the control.

As a surrogate for protein abundance, MaxQuant iBAQ values were used for label-free absolute quantification of identified proteins (265). The average iBAQ value for each protein was determined from the six replicates in the both CDH2 and control samples. The final iBAQ value was determined by subtracting the control average from the CDH2 average.

2.5.12 Bioinformatics analysis

CDH1 BioID proximity proteomics results were from two previous studies (186, 187). The ICD protein list was from a previous curation (234). Venn diagrams comparing the protein lists were generated using BioVenn (266). Pathway and disease & function enrichment analysis was performed using Ingenuity Pathway Analysis (IPA) tools (Qiagen). Gene expression data for the identification of HEGs (Heart Enriched Genes) or CEGs (Cardiomyocyte Enriched Genes) were from previous studies (232, 233, 267). The

heart or cardiomyocyte enriched genes were identified by the Gene Expression Pattern Analyzer (GEPA) algorithm at the threshold of fold change ≥2 (≥2.5 for cardiovascular differentiation from human embryonic cell data set) (268). Three types of expression patterns were selected: 1) exclusive high expression in cardiomyocytes or heart; 2) multiple high expression tissues/cells including heart/cardiomyocytes in which the sum of fragment per kilobase of exon per million reads (FPKM) was greater than the total sample number and the number of pattern samples was no greater than 4; and 3) “gradient” pattern with the highest expression in heart/cardiomyocytes and fold change of the highest and lowest expression is no less than 4. Fisher’s exact tests for overrepresentation analysis of HEGs or CEGs were performed using R (https://www.r-project.org/).

2.5.13 Protein network analysis

The protein interaction map was generated using Ingenuity Pathway Analysis (IPA, Qiagen). Only protein-protein interactions supported by published, experimental data in the manually curated Ingenuity Knowledge Base were considered to build the network. Hierarchical classification was done by grouping the proteins manually using CDH2 at the core. Proteins that bind CDH2 directly were designated as primary interactors. Proteins that bind to primary interactors but not CDH2 were classified as secondary interactors. Proteins that bind secondary interactors were designated as tertiary interactors. Finally, proteins that bind tertiary interactors or to outermost tier proteins were defined as quaternary interactors. 52 proteins could not be linked to the protein network.

3.0 Vinculin anchors contractile actin to the cardiomyocyte adherens junction

This chapter, at the time of this dissertation submission, is presently undergoing revisions at *Molecular Biology of the Cell*.

3.1 Overview

The adherens junction (AJ) couples the actin cytoskeletons of neighboring cells to allow mechanical integration and tissue organization. The physiological demands of intercellular adhesion require that the AJ be responsive to dynamic changes in force while maintaining mechanical load. These demands are tested in the heart, where cardiomyocyte AJs must withstand repeated cycles of actomyosin-mediated contractile force. Here we show that force-responsive cardiomyocyte AJs recruit actin-binding ligands to selectively couple actin networks and promote contact maturation. We employed a panel of N-cadherin-αE-catenin fusion proteins to rebuild AJs with specific actin linkages in N-cadherin-null cardiomyocytes. In this system, vinculin recruitment was required to rescue myofibril integration and desmosome assembly at nascent contacts. In contrast, loss of vinculin disrupted junction morphology and blocked myofibril integration. Our results identify vinculin as a critical link to contractile actomyosin and offer

insight to how actin integration at the AJ is regulated to provide mechanical stability and cellular organization.

3.2 Introduction

Adherens junctions link the actin cytoskeletons of adjacent cells to provide the foundation for multicellular tissue organization. The dynamic demands of cell-cell adhesion require that the AJ be both responsive and resilient to mechanical force. This is especially true in the heart, where the AJ must transmit the mechanical forces of actomyosin contraction while maintaining adhesive homeostasis. How the AJ balances mechanical integration with contractile force to maintain tissue integrity is not clear.

Cardiomyocytes are linked through a specialized cell-cell contact called the intercalated disc (ICD). The ICD is the site of mechanical and electrical continuity between individual cardiomyocytes that allow the heart to function as a syncytium (7, 8, 210). Three junctional complexes form the ICD: the adherens junction (AJ), desmosome and gap junction. The AJ and desmosome are responsible for mechanical integration by coupling the actin and intermediate filament cytoskeletons, respectively, of neighboring cells. Gap junctions permit electrical continuity through the free flow of ions. Importantly, the ICD AJ is the site of myofibril integration between cardiomyocytes and allows contractile force to be transduced across heart tissue (14).

The core of the AJ is the cadherin-catenin complex (15, 16). N-cadherin, the sole classical cadherin expressed in cardiomyocytes (17), is a single-pass transmembrane

protein with an extracellular domain that mediates homotypic, calcium-dependent interactions (23, 24). The adhesive properties of classical cadherins are driven by the recruitment of cytosolic catenin proteins to the cadherin tail: p120-catenin binds to the juxtamembrane domain and β-catenin binds to the distal part of the tail. β-Catenin, in turn, recruits α-catenin to the cadherin-catenin complex. α-Catenin is an actin-binding protein and the primary link between the AJ and the actin cytoskeleton (21, 41, 42, 45).

AJ binding capabilities are modified by the forces of actomyosin contraction, largely through changes in α-catenin conformation (50, 218). Force induces a conformational change in the central M-domain of αE-catenin to reveal binding sites for ligands, many of which bind F-actin (46, 109, 110, 120, 231, 269). The force required to unfurl αE-catenin (5pN) is well within the range of a myosin motor, demonstrating the physiological relevance for this model of regulation (50, 111). The recruitment of actin-binding proteins in response to force is thought to help anchor actin to the AJ (270).

Cardiomyocytes have at least two distinct actin networks at cell-cell contacts – myofibrils and the cortical cytoskeleton (151) – that must be integrated at AJs. Many actin-binding ligands interact with αE-catenin, including vinculin, afadin, ZO-1 and Eplin (271). In epithelia, vinculin is recruited to αE-catenin in a force-dependent manner and this interaction is thought to be important for reinforcing the αE-catenin:actin interaction (120, 231, 272). Likewise, epithelial afadin can also bind αE-catenin in a force-dependent manner (269), where it functions to strengthen the AJ under tension (208). Both vinculin and afadin localize to the ICD (222, 273) and are recruited to cardiomyocyte AJs (151). Vinculin is required for proper heart development and functions in cardiomyocyte

adhesion and contraction (192, 197). Afadin was recently identified as having a cardioprotective role at the ICD, as mice lacking afadin were shown to be more susceptible to stress-induced injury and myopathy (209). How vinculin and afadin function in mechanical coupling at cardiomyocyte AJs is not well understood.

Here we sought to define the individual functions of αE-catenin, vinculin and afadin in coupling actin to cardiomyocyte AJs. We demonstrate that cultured neonatal cardiomyocytes recruit vinculin and afadin to AJs in a force-dependent manner, similar to epithelia. We show that loss of N-cadherin in cardiomyocytes disrupts cell-cell adhesion and dissolves junctional complexes. These phenotypes defined in our *in situ* loss-of-N-cadherin system are strikingly similar to those shown for *in vivo* models (17). We developed a series of N-cadherin:αE-catenin fusions to test how AJ ligand recruitment and actin-binding influences junctional complex assembly, cell contact architecture and myofibril coupling. We show for the first time that vinculin recruitment to the AJ is necessary to couple myofibrils to the developing cell-cell contacts in cardiomyocytes. Our results offer new insight into actin linkage to the AJ and identify vinculin as the key link between contractile actin networks and the cardiomyocyte AJ.

3.3 Results

3.3.1 Force regulates α-catenin ligand recruitment to cardiomyocyte AJs

Vinculin and afadin are recruited to epithelial AJs in a force-dependent manner (120, 231, 269, 272). Vinculin and afadin localize to the ICD in adult heart and proximity proteomics revealed that both are enriched at the AJ in cultured neonatal cardiomyocytes (151). We sought to determine if vinculin and afadin recruitment to cardiomyocyte AJs is tension-dependent. Cultured cardiomyocytes were treated with 100 μM blebbistatin to suppress myosin activity for up to one hour and stained for vinculin or afadin (**Figure 3-1A-D**). Cardiomyocytes ceased contraction within 30 seconds of blebbistatin addition whereas DMSO did not affect contraction (unpublished observation). In blebbistatin-treated cells, both vinculin and afadin were significantly reduced at cell-cell contacts after one hour, with significant loss of vinculin seen after 30 minutes (**Figure 3-1E and F**). This is consistent with a requirement for tension at the AJ to recruit vinculin or afadin and indicates that nascent cardiomyocyte AJs retain the ability to respond to changes in mechanical force.

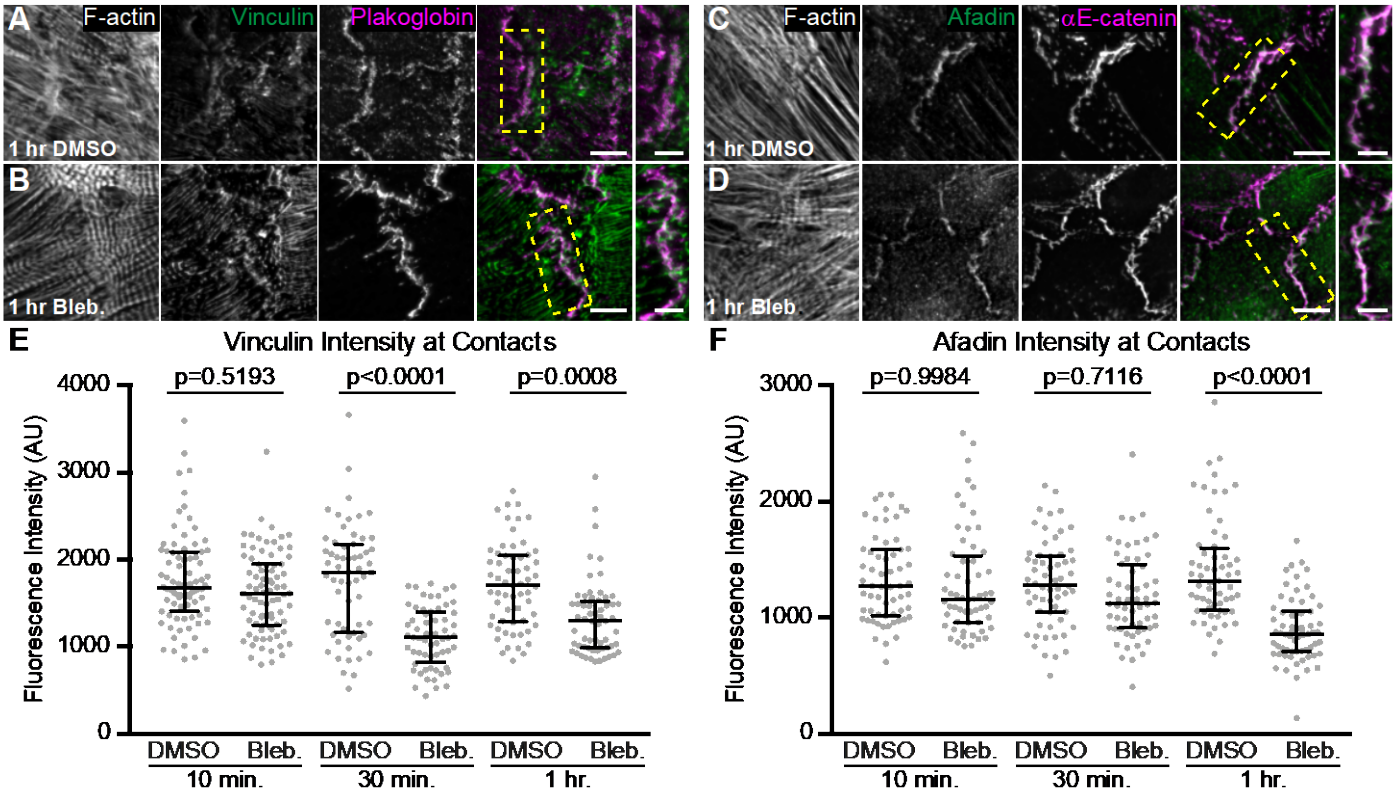

Figure 3-1 Vinculin and afadin recruitment to cardiomyocyte AJs is force dependent

A-D. Mouse neonatal cardiomyocytes were treated for 1 hr with DMSO (A or C) or 100 μM blebbistatin (B and D) before fixation. Cells were stained for F-actin (A-D), vinculin and plakoglobin (A and B), or afadin and αE-catenin (C and D). Images are max projections of 2-3 μm deconvolved stacks. Individual and merged vinculin (green) and plakoglobin (magenta) channels shown in A and B. Individual merged afadin (green) and αE-catenin (magenta) channels shown in C and D. Far right column is a magnification of the boxed contact in merge. E-F. Quantification of vinculin (E) or afadin (F) intensity at cell-cell contacts. Vinculin or afadin signal intensity was measured in cells treated with DMSO or blebbistatin for 10, 30 and 60 minutes before fixation. All data points are plotted. Middle horizontal bar is the median and error bars represent the quartile range. One-way ANOVA, $n \geq 60$ images from at least 3 independent experiments. Scale bar is 10 μm in full images, 5 μm in zoomed images.

3.3.2 Loss of N-cadherin disrupts cardiomyocyte cell-cell contacts

The force-responsive nature of cardiomyocyte AJs led us to question the roles of αE-catenin, vinculin and afadin in linking the AJ to actin. In order to individually test these roles, we developed a system to selectively recruit actin-binding ligands and thus control the actin-binding interfaces at the cardiomyocyte AJ. We first needed to establish a cadherin-null system in which to rebuild AJs. In intact mouse heart tissue, conditional ablation of N-cadherin causes dissolution of all AJ components as well as loss of all desmosomal and gap junction proteins at the ICD (17). We questioned if loss of N-cadherin would disrupt ligand recruitment and junction organization in cultured neonatal cardiomyocytes. Cardiomyocytes from N-cadherin conditional knockout mice ($Ncad^{fx/fx}$; (17)) were isolated and infected with adenovirus expressing Cre-recombinase (hereby referred to as Cre).

In order to determine the time required for N-cadherin depletion post Cre-mediated recombination, we fixed Cre-infected cells at four different time points: 24, 48, 72 and 96 hours post-infection and stained for N-cadherin (**Figure 3-2A-E**). At 24 hours post-infection, N-cadherin levels appeared similar to uninfected cells (**Figure 3-2A and B**). At 48 hours post-infection, N-cadherin levels remained high; however, cell-cell contacts began to appear jagged with N-cadherin clustering along more linear contacts (**Figure 3-2C**). We speculate that declining N-cadherin levels are promoting AJ consolidation and altering junction morphology. Notably, at 72 and 96 hours post-infection, we observed a near complete loss of N-cadherin at cell-cell contacts (**Figure 3-2D and E**; **Supplemental Figure S3-1A and B**).

We next assessed cell contact formation and protein recruitment at 96 hours post Cre infection. In uninfected control cardiomyocytes, AJ markers N-cadherin, β-catenin and αE-catenin were recruited to cell-cell contacts (**Figure 3-2F and G, left column**). Likewise, αE-catenin ligands vinculin and afadin; the gap junction protein connexin 43 (Cx43); and desmosomal markers desmoglein 2 (Dsg2, **Figure 3-2H-K, left column**), plakoglobin, and plakophilin 2 (**Supplemental Figure S3-1C and D, left column**) all localized to cell-cell contacts. In contrast, Cre expression dissolved cell-cell contacts and resulted in a loss of all AJ proteins, αE-catenin ligands, gap junctions and desmosomes (**Figure 3-2H-K**; **Supplemental Figure S3-1C and D, right column**). As expected, N-cadherin is required for cell-cell adhesion in cultured cardiomyocytes and AJ formation is critical for the recruitment and organization of other junctional components.

We sought to determine if cardiomyocyte cell-cell contacts can be restored with exogenous N-cadherin-GFP. Cardiomyocytes were sequentially infected with Cre and then N-cadherin-GFP adenovirus. Expression of N-cadherin-GFP restored cell-cell contacts and the localization of AJ, gap junction and desmosome proteins (**Figure 3-3A-F**; **Supplemental Figure S3-1E and F**). The ability of N-cadherin-GFP to restore cell-cell contacts in an N-cadherin null background demonstrated the dynamic nature of this adhesion system and its tractability for probing cadherin and catenin function further.

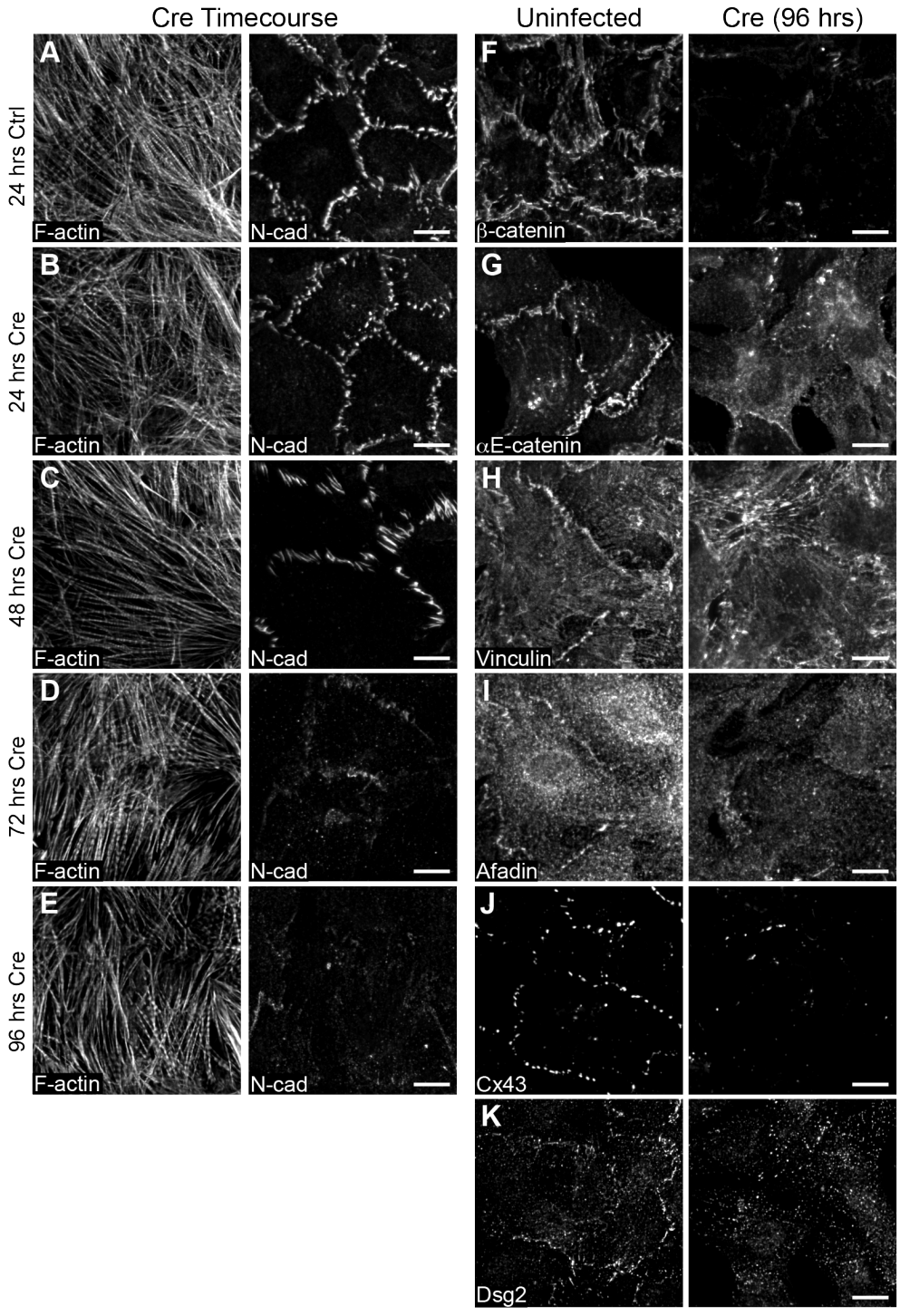
Cre Timecourse
Uninfected
Cre (96 hrs)
24 hrs Ctrl
24 hrs Cre
48 hrs Cre
72 hrs Cre
96 hrs Cre
A
B
C
D
E
F
G
H
I
J
K
F-actin
N-cad
β-catenin
αE-catenin
Vinculin
Afadin
Cx43
Dsg2

Figure 3-2 Loss of N-cadherin disrupts adhesion protein localization

A-E. Neonatal cardiomyocytes from $Ncad^{fx/fx}$ mice were uninfected (A) or infected with adenovirus expressing Cre recombinase (B-E) and fixed over 4 days to assess N-cadherin expression. Cells were stained for F-actin (left panel) and N-cadherin (right panel). F-K. Control and Cre-infected neonatal cardiomyocytes from $Ncad^{fx/fx}$ mice were fixed 96 hours post-infection and stained for AJ components (F, G), AJ adapter proteins (H, I), gap junctions (J), and desmosomes (K). Images are max projections of 2-3 μm deconvolved stacks. Scale bar is 10μm.

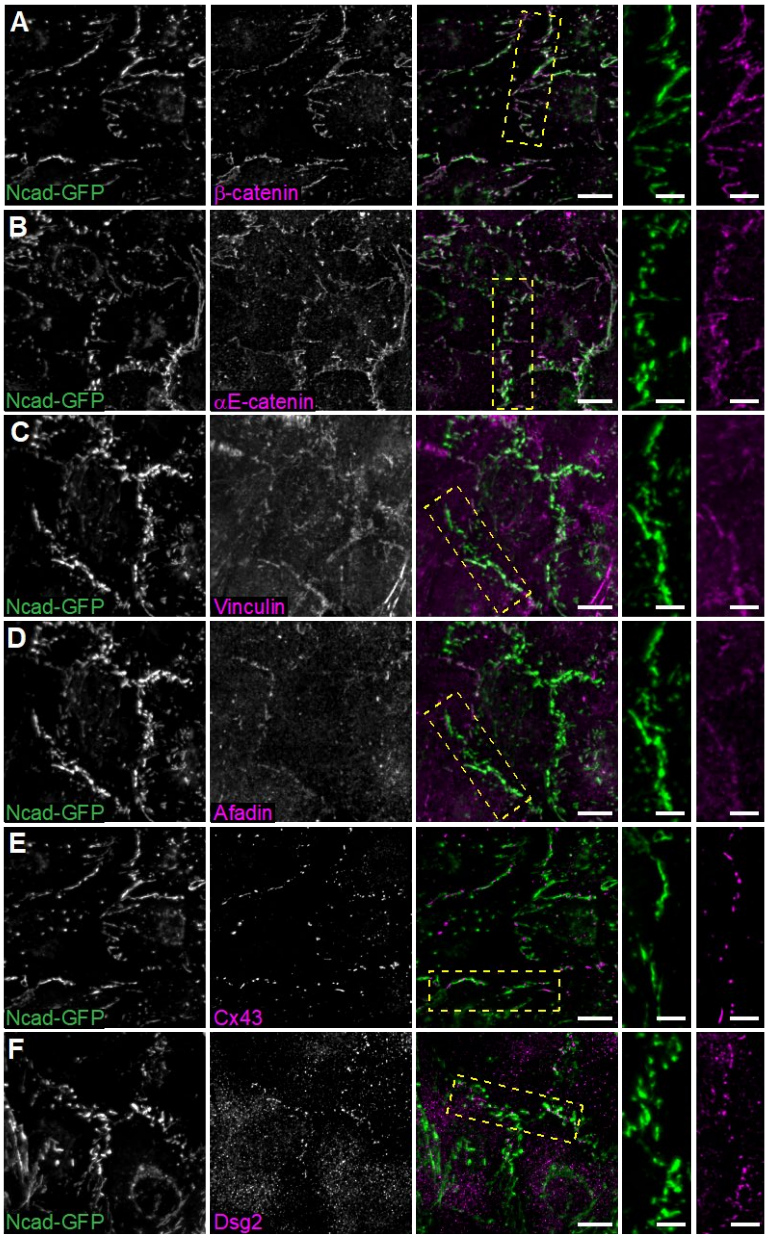

Figure 3-3 N-cadherin-GFP rescues cardiomyocyte junctional complexes

A-F. Neonatal Ncad$^{fx/fx}$ cardiomyocytes infected sequentially with adenoviruses expressing Cre and N-cadherin-GFP, fixed and stained for AJ-associated proteins (A-D), gap junctions (E) and desmosomes (F). Individual and merged N-cadherin-GFP (green) and ICD components (magenta) channels are shown. Far right column is a magnification of the boxed contact in the merge. Images are max projections of 2-3 μm deconvolved stacks. Scale bar is 10μm in full images, 5 μm in zoomed images.

3.3.3 N-cadherin-αE-catenin fusions selectively recruit αE-catenin ligands

We designed a series of N-cadherin-αE-catenin fusion constructs to systematically delineate the individual and combined functions of αE-catenin, vinculin and afadin in AJ-mediated cell-cell adhesion. Fusion constructs were created by taking the extracellular, transmembrane and p-120 binding domains of N-cadherin and fusing them to EGFP followed by the middle (M)-region and actin binding domain (ABD) of αE-catenin (**Figure 3-4A**). The M-region of αE-catenin contains three separate domains: M1, M2 and M3. The vinculin binding site is found in M1 (46) and the afadin binding site spans M2-M3 (47) (**Figure 1-2**). The C-terminal tail of N-cadherin and the N-terminus of αE-catenin were removed to eliminate endogenous β-catenin and αE-catenin recruitment while allowing for proper N-cadherin trafficking (18–20). Within the N-cadherin-GFP-αE-catenin (Ncad-GFP-αEcat) fusion, we introduced various mutations or domain deletions to restrict ligand recruitment and actin-binding interfaces. Ncad-GFP-M1-ABD mimics the core cadherin-catenin complex as it possesses the αE-catenin ABD and contains both vinculin and afadin binding sites. Ncad-GFP-M1-M3 possesses the full M-region of αE-catenin but lacks the ABD and the ability to respond to tension. Ncad-GFP-M1-M2 has an open M-domain that can bind vinculin constitutively but lacks the αE-catenin ABD and afadin binding domain (46). Two constructs were designed to selectively block vinculin recruitment while retaining afadin binding and actin binding through the αE-catenin ABD: Ncad-GFP-M1mutV-ABD, which contains 5 point mutations in M1 that ablate vinculin binding (129), and Ncad-GFP-M2-ABD, which lacks the entire M1 domain. Note that additional ligands may bind αE-catenin M2-M3: we focus on afadin recruitment and use

it as proxy for ligand binding to M2-M3. Lastly, Ncad-GFP-ABD lacks M1-M3, but retains the αE-catenin ABD.

To validate fusion construct localization and ligand recruitment, we first transfected Ncad-GFP-αE-catenin fusion plasmids in to cadherin-deficient epithelial A431D cells (**Supplemental Figure S3-2**). A431D cells do not express classical cadherins but do express other components of the AJ as well as the AJ ligands vinculin and afadin. Thus, we could test the ability of the fusion constructs to restore cell-cell adhesion and selectively recruit ligands. All fusion constructs localized to cell-cell contacts and recruited the predicted ligands (**Supplemental Figure S3-2A-G**).

We then tested the ability of Ncad-GFP-αEcat fusions to restore cell-cell contacts and selectively recruit vinculin or afadin in N-cadherin-null cells. $Ncad^{fx/fx}$ cardiomyocytes were sequentially infected with Cre plus individual adenoviral Ncad-GFP-αEcat fusions. We observed expression and proper localization of the fusion constructs by 24 hours post-infection, which continued through 72 hours post-infection, corresponding with the maximum loss of N-cadherin (**Supplemental Figure S3-1G-M**). All Ncad-GFP-αEcat fusions localized to the membrane and reestablished cell-cell contacts, though the gross morphology of these junctions differed markedly between constructs (**Figure 3-4B-E**). Ncad-GFP-M1-ABD recruited both vinculin and afadin (**Figure 3-4G and K**). This construct also allowed for formation of cell-cell contacts similar to Ncad-GFP (**Figure 3-4B, C, F and G**), indicating that the static Ncad-GFP-αEcat fusion can substitute for the cadherin-catenin-complex. In contrast, Ncad-GFP-M1-M3, which lacked the ABD and the ability to bind actin or respond to tension, failed to recruit vinculin or afadin and formed

poorly organized contacts as expected (**Supplemental Figure S3-2H**). However, the constitutively active Ncad-GFP-M1-M2 enriched vinculin, but not afadin, and restored robust cell-cell contacts (**Figure 3-4H and L**). Ncad-GFP-M1mutV-ABD and Ncad-GFP-M2-ABD both recruited afadin, but not vinculin, and generated long, linear contacts that lacked the jagged contact morphology found in controls (**Figure 3-4E, I and M**; **Supplemental Figure S3-2 I**). Lastly, Ncad-GFP-ABD formed poor contacts that failed to recruit vinculin but did display limited afadin recruitment (**Supplemental Figure S3-2 J**). We speculate that this weak afadin recruitment to cardiomyocyte cell-cell contacts may be mediated by nectins (151, 274). Thus, we were able to specifically recruit αE-catenin ligands to nascent cardiomyocyte contacts and observed morphological changes as a function of the selective association of AJ components. Notably, Ncad-GFP-M1-M2, which only recruits vinculin, formed cell-cell contacts similar to controls whereas Ncad-GFP-M1mutV-ABD and Ncad-GFP-M2-ABD, which do not recruit vinculin, organized linear contacts (**Figure 3-4B and D**; **Supplemental Figure S3-2 I**).

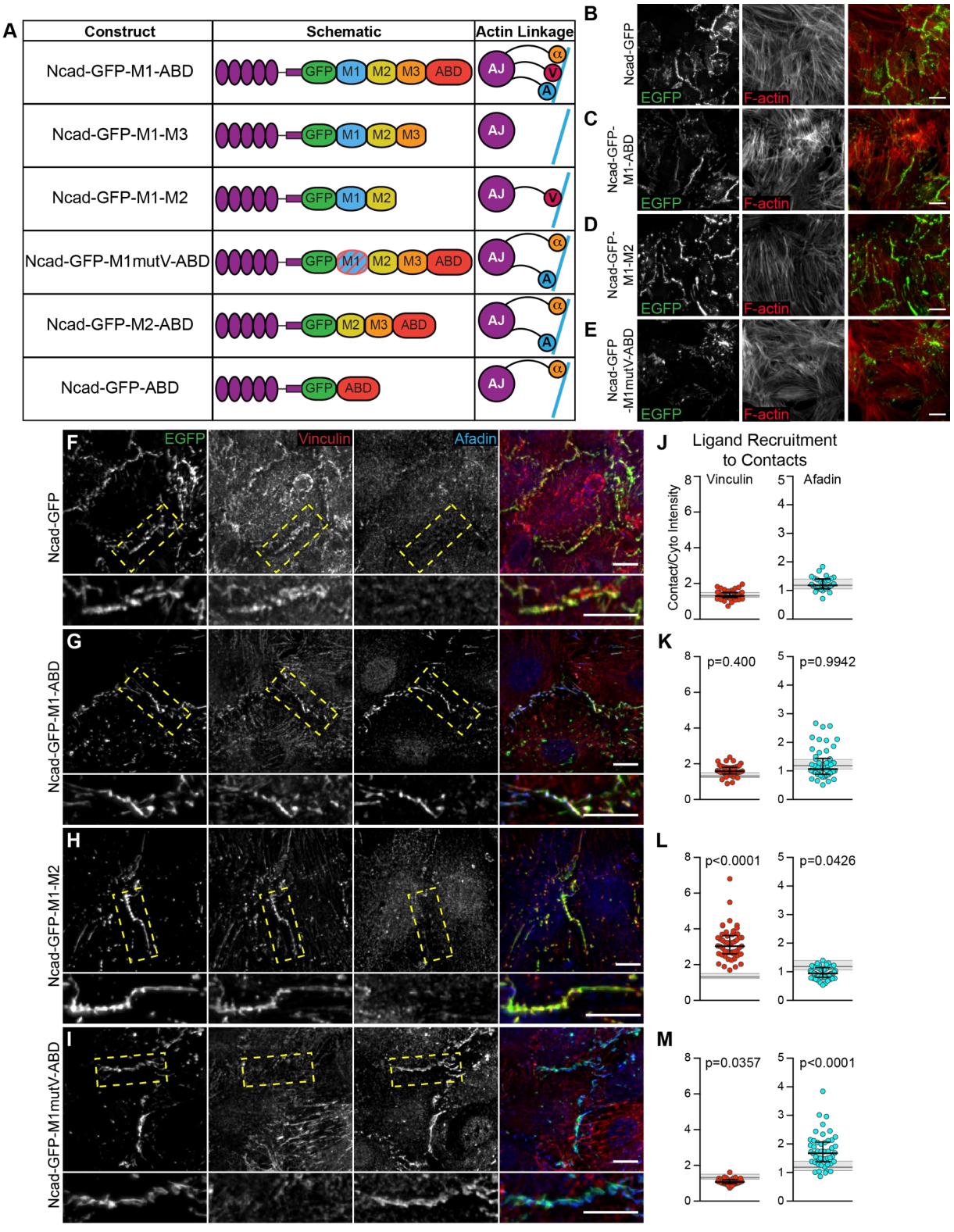
A
Construct
Schematic
Actin Linkage
Ncad-GFP-M1-ABD
Ncad-GFP-M1-M3
Ncad-GFP-M1-M2
Ncad-GFP-M1mutV-ABD
Ncad-GFP-M2-ABD
Ncad-GFP-ABD
GFP
M1
M2
M3
ABD
AJ
α
V
A
B
C
D
E
Ncad-GFP
Ncad-GFP-M1-ABD
Ncad-GFP-M1-M2
Ncad-GFP-M1mutV-ABD
EGFP
F-actin
F
G
H
I
Vinculin
Afadin
J
Ligand Recruitment to Contacts
Contact/Cyto Intensity
K
L
M
p=0.400
p=0.9942
p<0.0001
p=0.0426
p=0.0357
p<0.0001

Figure 3-4 N-cadherin-GFP-αE-catenin fusions selectively recruit ligands to cardiomyocyte cell-cell contacts

A. Table of N-cadherin-GFP-αE-catenin fusion constructs used in this study. Nomenclature, domain schematic, and actin linkage cartoon shown. B-E. Lower magnification images (40X) of $Ncad^{fx/fx}$ cardiomyocytes infected with Cre and N-cadherin-GFP (B) or N-cadherin-GFP-αE-catenin fusion adenoviruses (C-E). Individual and merged EGFP (green) and actin (red) channels are shown. Images max projections of 5 μm stacks. F-I. Cardiomyocytes infected with Cre and N-cadherin-GFP (F) or fusion adenoviruses (G-I), fixed and stained for vinculin and afadin. Individual and merged EGFP (green), vinculin (red) and afadin (blue) channels shown. Images are a max projection of 2-3 μm deconvolved stacks. Bottom image is a magnification of boxed contact. J-M. Quantification of vinculin and afadin intensities at cell-cell contacts. Signal intensity at contacts was divided by the average cytoplasmic intensity and a scatter plot of all data points is shown. The black horizontal line is the median and the error bars define the interquartile range. The shaded gray region in each plot defines the median (thick gray line) and interquartile range (thin gray lines) of vinculin or afadin recruitment observed with full-length N-cadherin-GFP (J) for comparison. One-way ANOVA, significance compared to recruitment with N-cadherin-GFP. $n \geq 50$ images from at least 2 independent experiments. Scale bar is 20 μM in B-E, 10 μm in F-I and 5 μm in zoomed images in F-I.

To assess the effects of ligand recruitment on fusion stability along cell-cell contacts, we performed FRAP (fluorescence recovery after photobleaching) analysis of Ncad-GFP and three key Ncad-GFP-αEcat fusion constructs (**Figure 3-5**). Fluorescence recovery over 15 minutes was quantified, plotted and fit to a double exponential curve. The Ncad-GFP recovery prolife was similar to previously published data from our group (**Figure 3-5A and E**; (151)), consistent with the ability of Ncad-GFP to restore AJs in an N-cadherin-null background. The mobile fraction of Ncad-GFP and all fusion constructs

was ~30%, similar to those observed for AJ components in cardiomyocytes and epithelial cells (**Figure 3-5 I**; (43, 151)). While F-actin binding is critical for AJ formation and extracellular and intracellular cadherin interactions cooperate to regulate AJ assembly (275), our results suggest that AJ plaque (immobile fraction) stability is regulated by cadherin extracellular interactions.

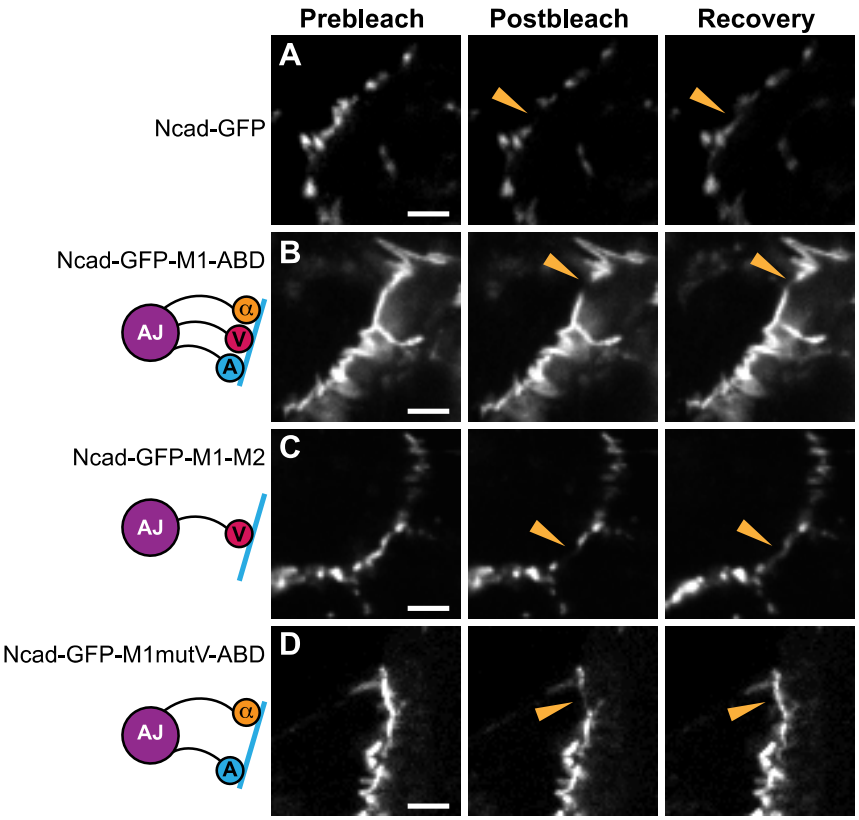

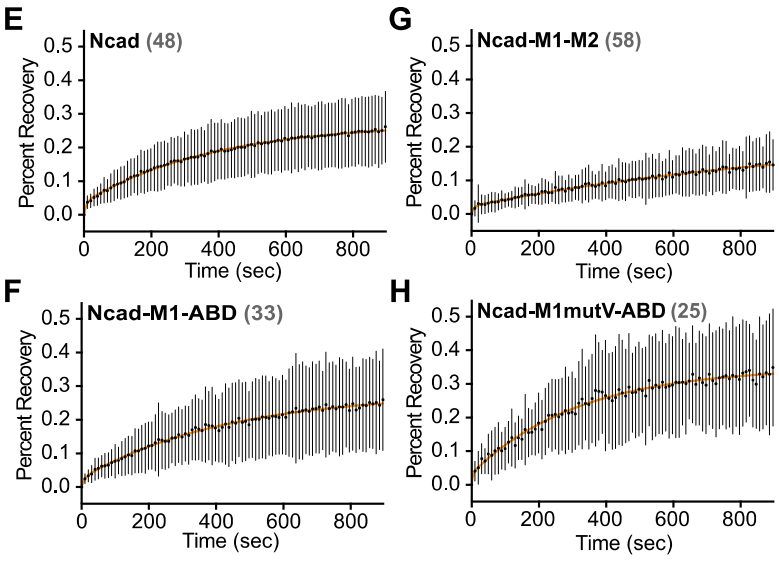

I

Fusion	Mobile Fraction (%)	Recovery Halftime (sec)
Ncad	27.4 (26.0-29.7)	267.3 (254.3-282.5)
Ncad-M1-ABD	28.0 (27.2-29.1)	298.6 (272.8-331.3)
Ncad-M1-M2	24.7 (21.4-30.5)	770.9 (604.8-1073)
Ncad-M1mutV-ABD	34.9 (34.0-36.0)	221.2 (201.0-246.2)

Figure 3-5 N-cadherin-GFP-αE-catenin fusion dynamics at cardiomycoyte cell-cell contacts

A-D. Representative prebleach, postbleach and recovery images from FRAP studies of $Ncad^{fx/fx}$ cardiomyocytes infected with Cre and N-cadherin-GFP or N-cadherin-GFP-αE-catenin fusion adenoviruses. Orange arrowhead marks the FRAP region at a cell-cell contact. E-H. Plot of mean ± s.d. FRAP recovery fraction over 15 minutes. The mean is represented by a black circle and the standard deviation is shown as a black line. The data was fit to a double-exponential curve (orange line). The number of FRAP regions measured for each fusion construct is listed in grey. FRAP data was collected from at least 2 independent infections for each fusion. I. Summary of the mobile fraction (percentage) and recovery halftime (seconds). Scale bar is 5 μm in A-D.

We then analyzed the recovery rates of the mobile fraction slow pools. Ncad-GFP and Ncad-GFP-M1-ABD had similar recovery rates (**Figure 3-5A-B, E-F and I**), consistent with the ability of Ncad-GFP-M1-ABD to reconstitute the AJ. Notably, Ncad-GFP-M1mutV-ABD had a recovery rate faster than Ncad-GFP, suggesting that vinculin regulates the dynamics of the AJ mobile pool (**Figure 3-5D H, and I**)**.** Consistent with this, Ncad-GFP-M1-M2, which binds vinculin constitutively, had a recovery rate that was nearly 3x slower than Ncad-GFP or Ncad-M1-ABD **(Figure 3-5C, G, and I**). We speculate that vinculin anchors the cadherin-catenin complex to actin to limit turnover of the mobile pool without affecting the immobile/mobile pool balance.

3.3.4 Vinculin links the AJ to contractile myofibrils

We then questioned if the differences in cell-cell contact morphology and dynamics observed in cardiomyocytes expressing the Ncad-GFP-αEcat fusions could reflect fundamental changes in actin organization and/or linkage to the AJ. We used thin-section

transmission electron microscopy to assess the ultrastructural organization of the AJ-actin interface. In adult mouse cardiac tissue, the ICD is a contorted, electron-dense structure where myofibrils are coupled between adjacent cells at AJs (151, 224). In wild-type cultured cardiomyocytes, we observed a similar junctional morphology with electron-dense AJs joining myofibrils across cells (**Figure 3-6A and B**, contact highlighted in purple). As expected, loss of N-cadherin dissolved cell junctions and prevented myofibril integration between neighboring cells (**Figure 3-6C and D**). Importantly, AJ structure and myofibril pairing were rescued with N-cad-GFP expression in N-cadherin-null cells (**Figure 3-6E and F**).

Next, we compared the ability of the Ncad-GFP-αE-cat fusions to organize actin along cardiomyocyte cell-cell contacts. Importantly, Ncad-GFP-M1-ABD restored myofibril coupling along thick, electron-dense junctions that were morphologically similar to controls (**Figure 3-6G and H**; compare to **Figure 3-6A and B, E and F**). As expected, lack of actin binding in Ncad-M1-M3 prevented cytoskeletal integration at cell-cell contacts (**Supplemental Figure S3-3A and B**). Strikingly, Ncad-GFP-M1-M2, which connects N-cadherin to actin solely through vinculin, restored myofibril coupling and generated electron-dense junctions morphologically similar to Ncad-GFP-M1-ABD and controls (**Figure 3-6I and J**). In marked contrast, constructs that could bind actin but were incapable of recruiting vinculin failed to restore normal contact morphology or myofibril coupling (**Figure 3-6, K and L**; **Supplemental Figure S3-3, C-F**). Ncad-GFP-M1mutV-ABD and Ncad-GFP-M2-ABD formed thin electron densities along elongated cell-cell contacts, but with little to no myofibril engagement. These results indicate that vinculin recruitment is required to link contractile actin to the cardiomyocyte AJ, as has been

suggested in epithelia (129). Neither the αE-catenin ABD nor afadin recruitment was sufficient to restore myofibril coupling. The increase in electron density along contacts with afadin recruitment suggests it may play a role in actin integration along contacts, but it is not sufficient to couple contractile actin in the absence of vinculin. Together, these results underscore the importance of vinculin in linking the AJ to contractile actin and highlight how αE-catenin coordinates cytoskeletal integration to provide mechanical connections between cells.

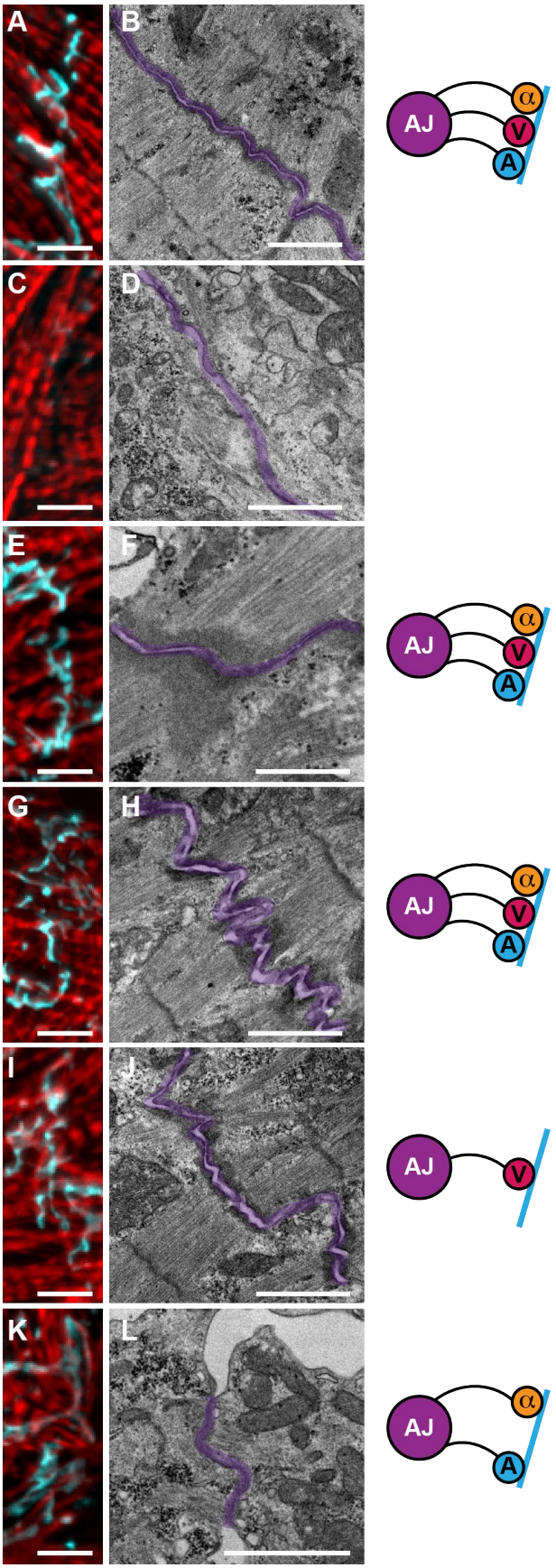
A
B
C
D
E
F
G
H
I
J
K
L
AJ
α
V
A
AJ
α
V
A
AJ
α
V
A
AJ
V
AJ
α
A

Figure 3-6 Vinculin recruitment is required to couple myofibrils to the AJ

$Ncad^{fx/fx}$ cardiomyocytes uninfected (A, B), infected with Cre adenovirus (C, D), or infected with Cre and N-cadherin-GFP-αE-catenin fusion adenoviruses (E-L) were fixed and processed for staining (A, C, E, G, I, K) or thin section TEM (B, D, F, H, J, L). IF images are 2-3 μm deconvolved stacks of N-cadherin staining (A, C) or GFP signal from of N-cadherin-GFP-αE-catenin fusions (E, G, I, K) pseudo-colored blue and stained for F-actin (red). Representative TEM image shown from >60 images from at least three independent experiments. Cell-cell contacts are pseudo-colored purple. Scale bar is 5 μm in A-K; 1 μm in B, D, H, J, L; and 500 nm in F.

3.3.5 Vinculin-binding ligands are not crucial to integration

Myofibrils are a highly specialized, contractile actin network, distinct from actin cables or stress fibers found in epithelial cells. However, the importance of vinculin in linking this unique network to the cardiomyocyte AJ is reminiscent of contractile actin linkages in epithelial cells. Vinculin anchors F-actin to the AJ (120, 231, 272) and can also recruit Ena/VASP proteins to promote actin assembly at junctions under tension (121).To determine if cardiomyocytes use a similar linkage mechanism to epithelial cells, we probed for the Ena/VASP protein Mena (122). Mena is recruited to epithelial contacts under tension (121), is localized to the ICD in heart tissue (276) and was identified in a proximity proteomics screen for N-cadherin-associated protein in cardiomyocytes (151). Immunostaining revealed limited recruitment of Mena to cell-cell contacts in cultured cardiomyocytes (**Supplemental Figure S3-4A**) that was lost after depletion of N-cadherin (**Supplemental Figure S3-4B**). Mena localization was only restored in fusion constructs that recruited vinculin (**Supplemental Figure S3-4D and E vs. S3-4F**). However, we

observed no difference in Mena recruitment between Ncad-M1-M2 and Ncad-M1-ABD despite Ncad-M1-M2 enriching vinculin at cell-cell contacts (**Figure 4-4L**). Thus, while Mena may function in linking contractile F-actin to cardiomyocyte AJs, its recruitment is limited and not correlated with vinculin levels, suggesting a more peripheral role in regulating cardiomyocyte junctional actin.

α-Actinin binds vinculin (277) and αE-catenin (35, 48). α-Actinin crosslinks actin filaments at myofibril Z-discs and is critical for cardiomyocyte organization (247). We did not observe any changes in α-actinin localization with a loss of N-cadherin (**Supplemental Figure S3-5A-B**). However, in Ncad-M1-M2, we observed a modest recruitment of α-actinin to contacts (**Supplemental Figure S3-5D**). We were not able to determine if α-actinin was recruited through vinculin and/or αE-catenin M1-M2. While increased α-actinin recruitment could impact Ncad-M1-M2 dynamics (**Figure 3-5C, F**), enrichment is not required for AJ coupling to F-actin.

3.3.6 Ligand requirements differ for junctional complex assembly

We then wanted to determine if the Ncad-GFP-αEcat fusions could restore the two other major junctional complexes at the ICD: gap junctions and desmosomes. Gap junctions electrically couple cardiomyocytes and their formation is predicated on cadherin localization to cell-cell contacts (11). N-cadherin depletion causes loss of Cx43, the pore-forming protein of gap junctions (**Figure 3-2K**), and Cx43 localization to cell-cell junctions can be restored by expressing Ncad-GFP (**Figure 3-7A**). Importantly, Cx43 contact localization was restored with all Ncad-GFP-αEcat fusions (**Figure 3-7B-D**;

Supplemental Figure S3-6A-C) independent of ligand recruitment or actin engagement. This indicates that N-cadherin delivery to the plasma membrane is sufficient to localize Cx43 to nascent contacts, though gap junction stabilization may require ligand recruitment (195).

Desmosomes also require AJ establishment for assembling along cell-cell contacts (59). Recent works suggests that E-cadherin recruits desmoglein 2 (Dsg2) through direct extracellular *cis* interactions to promote desmosome assembly at nascent contacts in epithelial cells (73). We assessed the ability of the fusion constructs to restore desmosome recruitment after loss of N-cadherin. Interestingly, Dsg2 recruitment was only observed in fusions that could recruit vinculin (**Figure 3-7E-G vs. H**; **Supplemental Figure S3-6D-F**). These data imply that vinculin recruitment could provide a needed mechanical linkage to drive desmosome assembly at nascent cardiomyocyte contacts.

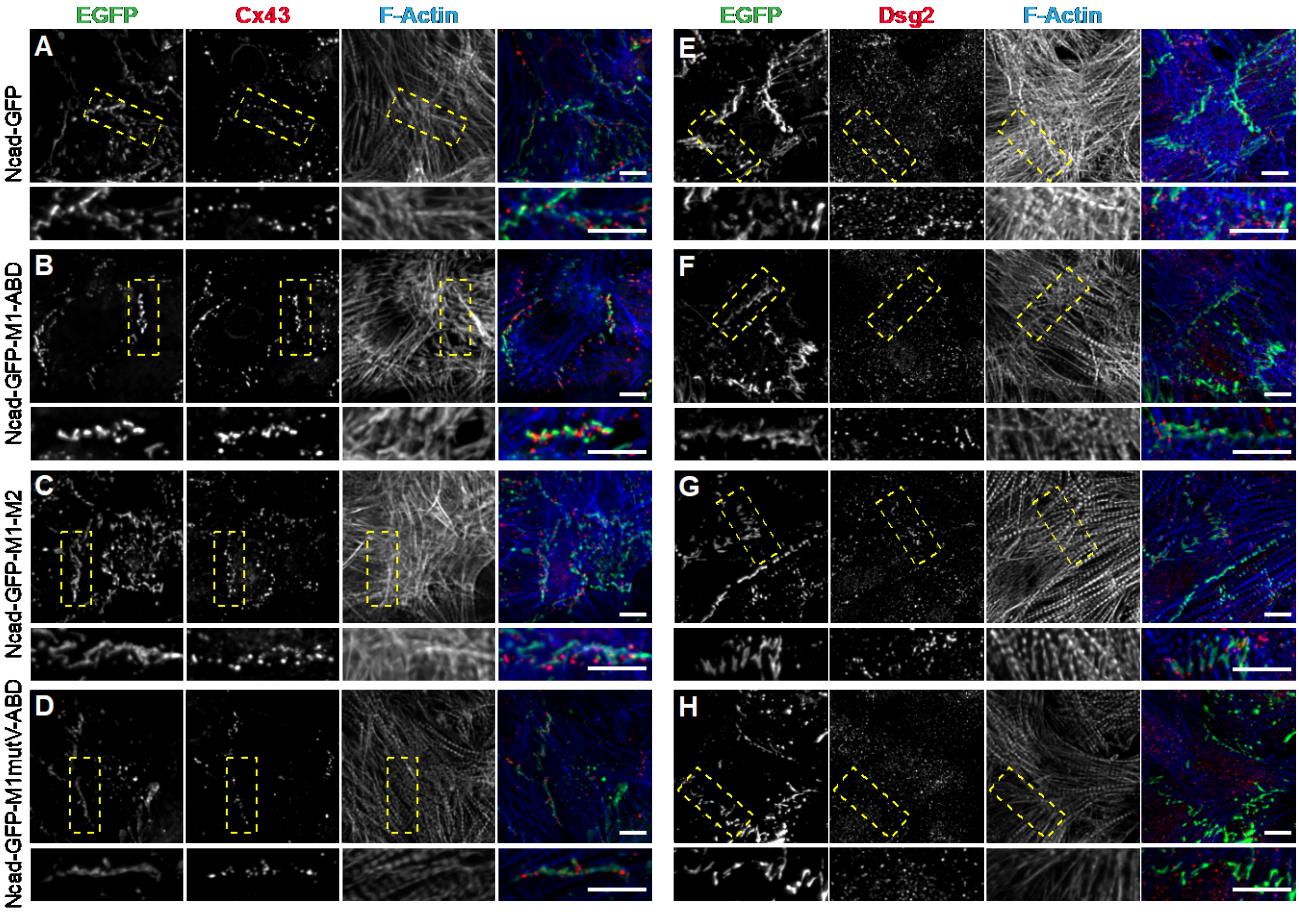
EGFP
Cx43
F-Actin
EGFP
Dsg2
F-Actin
Ncad-GFP
Ncad-GFP-M1-ABD
Ncad-GFP-M1-M2
Ncad-GFP-M1mutV-ABD
A
B
C
D
E
F
G
H

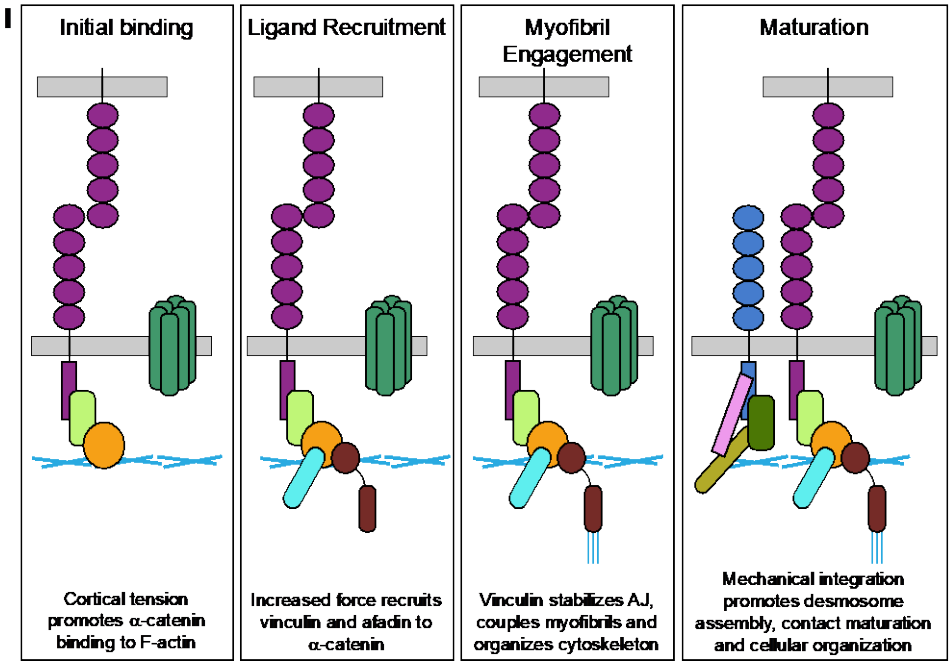
I
Initial binding
Ligand Recruitment
Myofibril Engagement
Maturation
Cortical tension promotes α-catenin binding to F-actin
Increased force recruits vinculin and afadin to α-catenin
Vinculin stabilizes AJ, couples myofibrils and organizes cytoskeleton
Mechanical integration promotes desmosome assembly, contact maturation and cellular organization

Figure 3-7 N-cadherin-GFP-αE-catenin fusions restore junction complexes

N-cadherin-null cardiomyocytes infected with N-cadherin-GFP (A, E) or N-cadherin-GFP-αE-catenin fusion adenoviruses (B-D, F-H). A-D. Cells were fixed and stained for connexin 43 and F-actin. Individual and merged GFP (green), connexin 43 (Cx43, red) and F-actin (blue) channels shown. E-H. Cells were stained for desmoglein 2 and F-actin. Individual and merged GFP (green), desmoglein 2 (Dgs2, red) and F-actin (blue) channels shown. Images are a max projection of 2-3 μm deconvolved stacks. Bottom image is a magnification of boxed contact. Scale bar is 10 μm. I. Schematic of AJ integration with cardiomyocyte actin networks and contact maturation.

3.4 Discussion

Together, our results provide novel insights into the AJ-myofibril linkage in cardiomyocytes. We show that vinculin recruitment through α-catenin is required to couple the cardiomyocyte AJ to contractile actin and promote AJ stability and contact maturation. The mechanical properties of α-catenin thus function to integrate cytoskeletal networks at cardiomyocyte cell-cell contacts to build force-resilient junctions.

Vinculin is recruited to epithelial AJs in a tension-dependent manner where it is thought to help anchor the AJ to actin (120, 231). In addition to creating a new linkage between F-actin and the AJ, vinculin can also recruit ligands such as Mena to promote actin assembly at junctions under tension (121). While Mena localizes to cardiomyocyte cell-cell contacts, we did not observe a concomitant enrichment of Mena with constitutive vinculin recruitment to cardiomyocyte AJs (**Supplemental Figure S3-5**). We did not detect VASP at cardiomyocyte AJs (data not shown). Thus, our results suggest that

vinculin-mediated ligand recruitment may not be the primary driver of increased stability and myofibril integration at the AJ. Instead, the actin binding domain of vinculin may play a critical role in coupling the AJ to contractile actin.

Myofibrils arrange their actin filaments so that the myosin motors exert force as they move toward the barbed end. Recent biophysical data has shown that the vinculin-actin interaction is asymmetrical, where the bond is strengthened when an actin filament is under pointed (-) end-directed load (123). Additional work has demonstrated that differential recruitment of vinculin to sites of high tension in epithelial cells is used to balance tensile and shear forces across cell contacts (272). We propose a model in which tension activates αE-catenin at nascent cardiomyocyte contacts to promote ligand binding (**Figure 3-7I**). Vinculin recruitment, in turn, promotes myofibril binding to strengthen the AJ and orchestrate junctional maturation and mechanical integration. We speculate that vinculin recruitment creates a self-amplifying tension feedback loop to promote junctional planar organization necessary for heart muscle function. Thus, vinculin functions as both a mechanical linchpin and critical organizer of actomyosin and AJ architecture to regulate cardiomyocyte adhesion. We suggest that this is a general mechanism cells use to organize contractile actin networks across various cells types. For example, vinculin is enriched at tricellular junctions in epithelial sheets where contractile actin terminates perpendicularly to AJs (278), similar to cardiomyocytes. Linking to specific actin networks through selective ligand recruitment would allow the AJ to control mechanical load and respond to changes in cellular tension.

Vinculin is a mechano-responsive protein found at both cell-cell and cell-ECM contacts (279). Failing human cardiac tissue shows an increased expression of vinculin

though with a less organized localization pattern (199). Aging non-human primate and mouse models show increased vinculin expression compared to younger animals, with increased localization at both the ICD and cell-ECM adhesions (200). Aging, and ultimately failing, cardiac tissue shows signs of fibrosis resulting in an increased ECM stiffness (280). Increased ECM stiffness has been linked to molecular remodeling of myofibril integration at cell-cell versus cell-ECM adhesions, causing a decrease of force propagation across adhered cardiomyocytes (3). Interestingly, we found that M1-M2 expression caused a loss of vinculin at cell-ECM contacts (data not shown). Consistent with this, vinculin can be selectively enriched at cell-cell contacts or cell-ECM contacts when external tension is applied to either of these areas individually (120, 176). Our results highlight the critical role of vinculin at cardiomyocyte AJs and provide a possible explanation for how changes in ECM stiffness and concomitant cell-ECM adhesion expansion would disrupt the balance of vinculin to impair myofibril integration and decrease cardiac function.

3.5 Materials and Methods

3.5.1 Plasmids

To build the N-cadherin-GFP-αE-catenin fusions, αE-catenin fragments encoding aa273-510, aa273-651, and aa273-906 were cloned into pEGFP-C1 by PCR. Next, Gibson Assembly (NEBuilder HiFi DNA Assembly Kit, New England Biolabs) was used

to clone the N-cadherin fragment aa1-839 into pcDNA3.1 (Thermofisher). Gibson assembly was then used to insert the EGFP-αE-catenin fragments into the pcDNA3.1 N-cadherin aa1-839 backbone, downstream and in-frame with N-cadherin. During construction, a 12 aa glycine and alanine linker was inserted between N-cadherin and αE-catenin to increase flexibility.

The point mutations R329A, R330A, L347A, L348A and Y351A were introduced by site directed mutagenesis (Agilent) in the αE-catenin M-region to inhibit vinculin binding (129).

3.5.2 Cardiomyocyte isolation and culture

All animal work was approved by the University of Pittsburgh Division of Laboratory Animal Resources. Outbred Swiss Webster mice were used to generate wild-type cardiomyocytes for blebbistatin experiments. N-cad$^{fx'fx}$ conditional knockout mice (Jackson Labs, stock #007611, (17)) were used to generate N-cadherin null cardiomyocytes.

Tissue culture dishes or MatTek dishes (35 mm dish with 10 mm microwell) were coated with rat tail Type I collagen (Millipore) diluted to 0.5 μg/μl in PBS for 30 minutes at room temperature. Dishes were dried and treated with UV radiation for 1 hour, after which they were washed with PBS, dried and stored at room temperature in the dark.

Neonatal mouse cardiomyocytes were isolated as described (220). Briefly, mouse pups were sacrificed at P1-P3, the hearts were removed, cleaned, minced, and digested

overnight at 4°C in 20 mM BDM (2,3-Butanedione monoxime) and 0.0125% trypsin in HBSS. The following day, heart tissue was digested further in15 mg/mL Collagenase/Dispase (Roche) in Leibovitz media with 20 mM BDM to create a single cell suspension. Cells were pre-plated for 1.5-2 hours in plating media (65% high glucose DMEM, 19% M-199, 10% horse serum, 5% FBS and 1% penicillin-streptomycin) to remove fibroblasts and endothelial cells Cardiomyocytes were plated on MatTek dishes ($1.5x10^5$) or 12-well dishes ($4.5x10^5$) in plating media. 16 hours post-plating, the plating media was exchanged for maintenance media (78% high glucose DMEM, 17% M-199, 4% horse serum, 1% penicillin-streptomyocin, 1 μM AraC, and 1 μM Isoproternol).

3.5.3 Adenovirus production and infection

N-cadherin-GFP-αE-catenin fusions were expressed as adenoviruses using the AdEasy System as described (151, 260). Briefly, N-cadherin-EGFP-αE-catenin fusions were moved in to pShuttle-CMV using NEBBuilder HiFi DNA Assembly Master Mix (New England Biolabs). Positive clones were transformed into AdEasier *E. coli* cells to generate recombinant adenovirus DNA. Adenoviral plasmids were then transfected into HEK293 cells for virus production. Virus was amplified and purified using AdenoPACK 20 Adenovirus (Ad5) purification & concentration kit (Sartorius). Virus titer was determined by quantitative Polymerase Chain Reaction (qPCR) using Adeno-X qPCR Titration Kit (Clontech) on an Applied Biosystems 7900HT.

Adenovirus expressing Cre (Ad(RGD)-CMV-iCre) was purchased from Vector Biolabs.

$Cdh2^{fx/fx}$ cardiomyocytes were infected with adenovirus Cre at MOI (multiplicity of infection) 75 on the day of plating to achieve 100% infection. 16 hours after virus addition, the media was replaced with maintenance media. 6-8 hours later (22-24 hours after Cre infection) cardiomyocytes were infected with the N-cadherin-GFP-αE-catenin fusion adenovirus at MOI 10-15 to achieve >50% infection rate. Cardiomyocytes were fixed 96 hours after Cre infection for analysis.

3.5.4 Immunofluorescence

Cells were processed for immunofluorescence as follows: cells were fixed in warmed (37°C) 4% EM grade paraformaldehyde in PHM buffer (60 mM PIPES pH 7.0, 25 mM HEPES pH 7.0, 2 mM $MgCl_2$ and 0.12 M Sucrose) for 10 minutes and washed twice with PBS. Cells were permeabilized with 0.2% Triton X-100 in PBS for 4 minutes and washed twice with PBS. Cells were blocked in 10% BSA (Sigma) in PBS for 1 hour at room temperature. Samples were incubated with primary antibodies in PBS + 1% BSA for 1 hour at room temperature, washed 2X in PBS, incubated with secondary antibodies in PBS + 1% for 1 hour at room temperature, washed 2X in PBS and then mounted in Prolong Diamond (Thermo Fisher Scientific). All samples were cured at least 24 hours before imaging.

For blebbistatin experiments, cardiomyocytes (96 hours post-plating) were treated with 100 μM blebbistatin in DMSO or DMSO control or 10 minutes to 1 hour. Cells were incubated at 37°C during treatment. After incubation, cells were first pre-permeabilized in 0.2% Triton X-100 in PBS for 2 minutes, then fixed and labeled as described.

3.5.5 Antibodies

Primary antibodies used for immunostaining were: anti-αE-catenin (1:100; Enzo Life Sciences ALX-804-101-C100), anti-β-Catenin (1:250; BD Transduction Laboratories 610154), anti-Plakoglobin (1:100; Cell Signaling 2309), anti-Vinculin (1:800; Sigma Aldrich V9131), anti-N-cadherin (1:250; Invitrogen 99-3900), anti-l-Afadin (1:500; Sigma Aldrich A0349), anti-Connexin-43 (1:100; ProteinTech 15386-1-AP), anti-Plakophilin 2 (1:10; Progen 651101), anti-Desmoglein 2 (1:250, Abcam EPR6768), anti-α-Actinin (1:250, Sigma A7811), anti-Mena (1:300, mouse monoclonal, a kind gift from Frank Gertler) and anti-Cre Recombinase (1:300, Cell Signaling 12830). Secondary antibodies used were goat anti-mouse or anti-rabbit IgG conjugated to Alexa Fluor-488, 568, or 647 (1:250; Invitrogen). F-actin was visualized using an Alexa Fluor dye conjugated to phalloidin (1:100, ThermoFisher Scientific).

3.5.6 Whole cell lysis and immunoblotting

Cardiomyocytes were cultured on collagen-coated 12-well dishes (see above). 96 hours after plating, cardiomyocytes were lysed with RIPA buffer supplemented with 1X protease inhibitors (Millipore). Lysate protein concentration was determined by BCA Assay (BioRad). 15 μg of lysate was loaded per well and resolved on a 10% SDS PAGE and then transferred to a PVDF membrane. The membrane was blocked in 5% BSA in 1X TBST with 0.02% NaN_3 for 1 hour at room temperature. Primary antibodies (N-cadherin 1:2500, GAPDH 1:750 (Abcam ab9485)) were diluted in 5% BSA in 1X TBST with 0.02% NaN_3 overnight at 4°C, followed by three 15 minute TBST washes. LI-COR

secondary antibodies (Goat anti-mouse 680; goat anti-rabbit 800, 1:15,000) were diluted in 1X TBST with 0.02% NaN_3 and incubated for 1 hour at room temperature. The membrane was washed three times in 1X TBST and once in PBS. The membrane was imaged on a LI-COR Odyssey imaging system. Band intensities were quantified in ImageJ and plotted in Prism (GraphPad).

3.5.7 Confocal microscopy

Cells were imaged with a 100X 1.49 NA objective or a 40X 1.30 objective on a Nikon Eclipse Ti inverted microscope outfitted with a Prairie swept field confocal system, Agilent monolithic laser launch and Andor iXon3 camera using NIS-Elements (Nikon) imaging software. Maximum projections of 2-3 um image stacks were created and deconvolved (3D Deconvolution) in NIS-Elements (Nikon) for presentation. Expression and staining levels were adjusted for presentation purposes in Photoshop (Adobe). All levels were corrected the same across each figure except Figure 6 where the phalloidin labeling of F-actin was modified individually to account for differences in staining and in Figure 5 to account for changes in focal plane/expression for live cell imaging. Note that Ncad-GFP-ABD levels were adjusted individually in Supplemental Figures S2, S3, and S6 as this construct localized to cell-cell contacts less efficiently than the other fusions.

3.5.8 FRAP experiments

FRAP experiments were conducted on a Nikon swept field confocal microscope (describe above) outfitted with a Tokai Hit cell incubator and Bruker miniscanner. Actively

contracting cells were maintained at 37°C in a humidified, 5% CO_2 environment. User-defined regions along cell-cell contacts were bleached with a 488 laser and recovery images collected every 10 seconds for 15 minutes. FRAP data was quantified in ImageJ (NIH) and average recovery plots were measured in Excel (Microsoft). All recovery plots represent data from two independent transfections of unique cell preps. The data were fit to a double-exponential curve to determine the mobile fraction and half time of recovery in Prism (Graphpad). Only recovery rates of the slow pool are reported as this was the dominant mobile pool (87-91%) for all constructs.

3.5.9 Electron Microscopy

Cardiomyocytes were grown on collagen-coated MatTek dishes and fixed as described above. After fixation and washing, cells were incubated with 1% OsO4 for one hour. After several PBS washes, dishes were dehydrated through a graded series of 30% to 100% ethanol, and then infiltrated for 1 hour in Polybed 812 epoxy resin (Polysciences, Warrington, PA). After several changes of 100% resin over 24 hours, cells were embedded in inverted Beem capsules, cured at 37°C overnight and then hardened for 2 days at 65°C. Blocks were removed from the glass dish via freeze/thaw method by alternating liquid Nitrogen and 100°C water. Ultrathin (60nm) sections were collected on to 200-mesh copper grids, stained with 2% uranyl acetate in 50% methanol for 10 minutes and 1% lead citrate for 7 minutes. Samples were photographed with a JEOL JEM 1400 PLUS transmission electron microscope (Peabody, MA) at 80kV with a Hamamatsu ORCA-HR bottom mount camera.

3.5.10 Image analysis

Vinculin and afadin recruitment to the N-cadherin-EGFP-αE-catenin fusion constructs was analyzed in ImageJ. A single plane was selected from the z-stack where the contact was most in focus and IsoJ Dark thresholding was used to create a mask of the EGFP channel to define the region of analysis (cell-cell contacts). The vinculin or afadin signal intensity was then measured within the masked region. Next, three random intensity measurements of vinculin or afadin were taken in the cell cytoplasm and these values were averaged. Finally, the ratio of vinculin or afadin intensity within the mask was divided by the cytoplasmic signal to calculate the contact/cytoplasmic ratio. Colocalization data were plotted with Prism software (GraphPad). A One-way ANOVA with multiple comparisons was performed; $p<0.05$.

Blebbistatin experiments were analyzed in a similar method. A single plane was selected from the z-stack where the contact was most in focus. IsoJ Dark thresholding was used to create a mask of the tension-insensitive marker, and this mask was applied to either the vinculin or afadin channels to determine their intensity at the contact. Intensity values of treated (blebbistatin) and control (DMSO) samples were plotted in Prism software (GraphPad).

4.0 Discussion and Perspectives

4.1 Study Synopses

Proximity proteomics studies have identified and validated previously unknown components of E-cadherin based epithelial AJs (186, 187). We sought to understand both the similarities and differences between E-cadherin based epithelial AJs and N-cadherin based cardiomyocyte AJs. In brief, we found that the core cadherin-catenin complex is conserved between the two proteomics data sets. However, identified proteins located in the tertiary and quaternary interactor field are more unique between the two data sets (**Figure 2-6**). Our results indicate that AJs in different tissue types, or centered around different classical cadherins, will show differential adapter proteins which will specialize signaling and adhesion based on the needs of the tissue. Therefore, if this study was repeated with N-cadherin in neurons, we would expect to identify unique tertiary and quaternary interactors compared to both E-cadherin and the N-cadherin cardiomyocyte data sets.

Our proximity data set also revealed several αE-catenin ligands, including ZO-1, vinculin, and afadin, enriched at the ICD (**Figure 2-4**). Briefly, ZO-1 is a key component of tight junctions and a known interactor with Cx43 involved in its trafficking (93, 281). However, there are no tight junctions in cardiomyocytes and our data set did not identify Cx43. The function of the αE-catenin:ZO-1 interaction has not been explored, but our data suggests that ZO-1 is in close proximity to the AJ where its function is not understood. The function of vinculin and afadin was of greater interest to us as there is

more literature describing their roles in AJ biology, but little understanding of its role at the ICD (109, 112, 208, 269). In our investigations, we demonstrated that vinculin plays a critical role in coupling the myofibril network between neighboring cells. Vinculin itself was able to maintain mechanical continuity between cells, independent of the αE-catenin-actin linkage (**Figure 3-6**).

Largely, our work can be viewed as combining holistic and nuanced approaches to defining mechanisms of cardiomyocyte adhesion. Our work identified 172 proteins that previously had no known localization to the ICD, leaving a vast area of research open to investigators and their favorite protein of interest. From here, we honed in on two αE-catenin ligands to define molecular mechanisms of force-required adhesion. Future work in our lab will be to expand our holistic approach to the desmosome interactome with goals to further define the *area composita* and desmosome-specific signaling pathways. Additionally, we will take the nuanced approach to understand the consequences of differential vinculin recruitment between AJs and FAs in an ECM stiffness-dependent manner. This work will better characterize the molecular outcomes of cardiac remodeling post-myocardial infarction and inform the observation of decreased cardiac output and cellular exhaustion.

4.2 Perspectives

4.2.1 Junctional Crosstalk

Our proximity proteomics studies revealed a close spatial relationship between AJs and desmosomes (**Figure 2-4**). This was unique when compared to the E-cadherin interactome which did not include desmosomal proteins in their top 35 hits (**Table 2-1**) (187). This further solidifies the observation that junctional complexes are highly intermingled in cardiomyocytes (11). Additionally, recent biophysical work showed a physical interaction between E-cadherin and Desmoglein 2 in nascent contact formation in epithelial cells (73). Given the temporal frame for our BioID studies, it could be that N-cadherin and Desmoglein 2 interact to initiate desmosome formation. Biophysical and biochemical data investigating this interaction should be pursued to determine the role of other classical cadherins in their ability to promote desmosome formation.

Our data also showed a close interaction between AJ and Z-disc proteins (**Figure 2-7**). Previous work demonstrated a “transitional zone” adjacent to the ICD where the last Z-disc would be found. This zone contained several Z-disc associated proteins which were thought to provide an anchoring point for titin before handing off the myofibril to the AJ (224). In our work, we demonstrated that traditional Z-disc proteins are highly dynamic and can be seen moving – shuttling – between Z-discs and between the ICD and Z-discs. While we have furthered the understanding of the crosstalk between AJs and Z-discs, the consequences of this shuttling are vastly unknown. It would be of great interest to investigate the localization of these various shuttling proteins during cardiac development and disease. Importantly, there is no evidence detailing the consequences of blocking

protein shuttling or localization imbalances. As cardiomyocytes, and myofibrils in particular, undergo substantial remodeling after a myocardial infarction, or in the progression of cardiomyopathies, it would be of interest to understand and investigate the roles these shuttling proteins have in altering the structure of myofibrils (3, 175).

Developmental studies have shown that the ICD is the result of junctional coalescing over a long period of time, where AJs are first concentrated at myofibril ends, followed quickly by desmosomes, and lastly by GJs, which take the longest to properly localize (12, 156). However, the data does not address how much of this coalescing is due to lateral movement of junctions versus insertion of new junctions at the proper location. It is likely that it is a combinatorial effect, where increased polarity of myofibrils, interacting with AJs, will first drive bipolar morphology. It is unknown if desmosomes or GJs can relocalize without the AJ. Loss of the AJ results in a loss of all other junctions, therefore this question is difficult to assess (17). However, it does appear desmosomes are more dispensable than AJs given that patients can live with desmosomal defects but cannot survive development with core AJ protein defects. It is not known how desmosomal ARVC defects play a role in the *area composita* and whether they create an overall weakness in the myocardium. ARVC patients do not show AJ defects but do show GJ localization defects (11). How the AJ and desmosome cooperate to promote GJ stability and localization is unknown and it would be of interest if ARVC mutations in GJ localization can be overridden through changes in AJ expression or stabilizing the portion of the desmosome that is able to assemble.

4.2.2 Vinculin Functions Under Stress

Several crucial pieces of information are missing from the cardiomyocyte and AJ literature: the number of cadherin molecules expressed in cardiomyocytes, the number of formed AJs, and the number of myofibril bound AJs. Various studies in epithelia have attempted to determine a range of forces that an AJ can handle, and all of those fall short of what an ICD is predicted to experience – even though those values are also rough estimates (3, 50). While cardiomyocytes generate more force on average than epithelial cells, it is not known if individual cadherin-catenin complexes experience more force in a cardiomyocyte compared to an epithelial cell. Cardiomyocytes could handle this problem in one of two ways: increase the number of AJs per actin filament so that force is dispersed across more molecules or specialize the AJ so that it can handle more load. The heart's inherent mechanism of handling this problem would also be seen during cardiac remodeling post-infarction.

Our data demonstrate that vinculin plays a critical role in linking the myofibril network to the cardiomyocyte ICD. This supports the long line of investigation into the role of vinculin in the heart (192, 195, 196, 200). Yet, what makes vinculin so special among actin-binding proteins remains to be understood. We were not able to determine what, if any, additional ligands vinculin localization promoted to the ICD to account for myofibril integration or the longevity of the contacts. Future work should investigate the biochemical and thermodynamic differences in the actin binding domain of various actin binding proteins to elucidate kinetic differences in their bond strength and biophysical differences in their load capacity.

Past work has suggested that vinculin localization and over expression (in flies) is cardioprotective, resulting in better cardiac performance for a longer period of time. Both an increase in expression and enrichment of vinculin to costameres and the ICD was seen (200). However, in tissue samples from failing patients, an increase in expression and localization of vinculin was also noted (199). Therefore, is an increase in vinculin truly cardioprotective, or is it a result of increased load and an indicator for poor performance? Also, there is little speculation for the role of increased vinculin; the presumption is that increased vinculin results in increased linkage at the ICD and better mechanical integration. This hypothesis could tie in to the understanding of how the heart manages force across the AJ. Many unknowns about abnormal, aged, or diseased cardiomyocyte form and function exist, with little understanding on the potential outcome for mechanical integration. However, continued investigation in this area would result in therapeutic implications for investigators and patients.

4.2.3 The Future of Heart Failure Treatment

Cardiovascular disease is the leading cause of death in the United States, and ischemic heart disease is the leading cause of death worldwide (79, 282). The population of the United States is projected to shift where the over 65 demographic contains more individuals than children under the age of 18 (U.S. Census Bureau). As cardiovascular disease is primarily an age-dependent phenomenon, the number of events and hospitalizations is expected to increase (79). In this time frame of an increased aged population, the American Heart Association estimates that nearly half (45.1%) of the US population will have a form of cardiovascular disease, resulting in a cost burden of $1.1

trillion by 2035 (79). Treatments post-MI revolve around management and never succeed in restoring heart function to its previous level. There has been plenty of work in preventative care to promote heart health and hopefully, avoid a cardiac event. However, there has been little advancement in post-cardiac event care and treatment.

Because cardiomyocytes are post-mitotic, they have minimal regenerative capabilities. There has been years' worth of research investigating the possibility of cardiac regeneration or promoting cardiomyocytes to divide (283). A second avenue of research has been differentiating and engrafting pluripotent stem cells (iPSCs), embryonic stem cells (ESC), or allogenic iPSCs into the scarred, infarcted area in large and small mammals (284–286). There are several mechanisms by which these cells can be differentiated into cardiomyocytes, but the ultimate end goal is a multicellular tissue both mechanically and electrically coupled with developed myofibrils (287). The tissue is then grafted into the infarcted area and hearts are monitored for improved cardiac function and decreased scar size. The advancement in this area has been substantial, but is still far from the clinic (282). While the graft can adhere to the neighboring cells, the demonstration of mechanical continuity between host and graft remains poor. Unsurprisingly, the level of GJs is low between the two tissues and the test animals frequently experience arrhythmias that have evaded treatment (285, 286, 288).

A driving area of research should be to investigate methods to promote adhesion between derived cells in the graft as well as increase adhesion among host and graft tissue. Recent data demonstrated an increase in N-cadherin localization between host and graft tissue at the border, but minimal N-cadherin expression between cardiomyocytes in the graft (285). Adult mouse myocardium does not form nascent

contacts in cell culture, and graft studies have not followed animals for the long term to analyze full integration of the graft or full maturation of the grafted tissue (151). The molecular, chemical, and physical cues that drive the initiation of cardiomyocyte adhesion are poorly understood, and this is exemplified in the attempt to treat infarcts with iPCS/ESCs. Future work will focus on promoting intercellular adhesion within the graft as well as encouraging nascent adhesions between host and graft tissue.

Appendix A Supplemental Material for Chapter 2

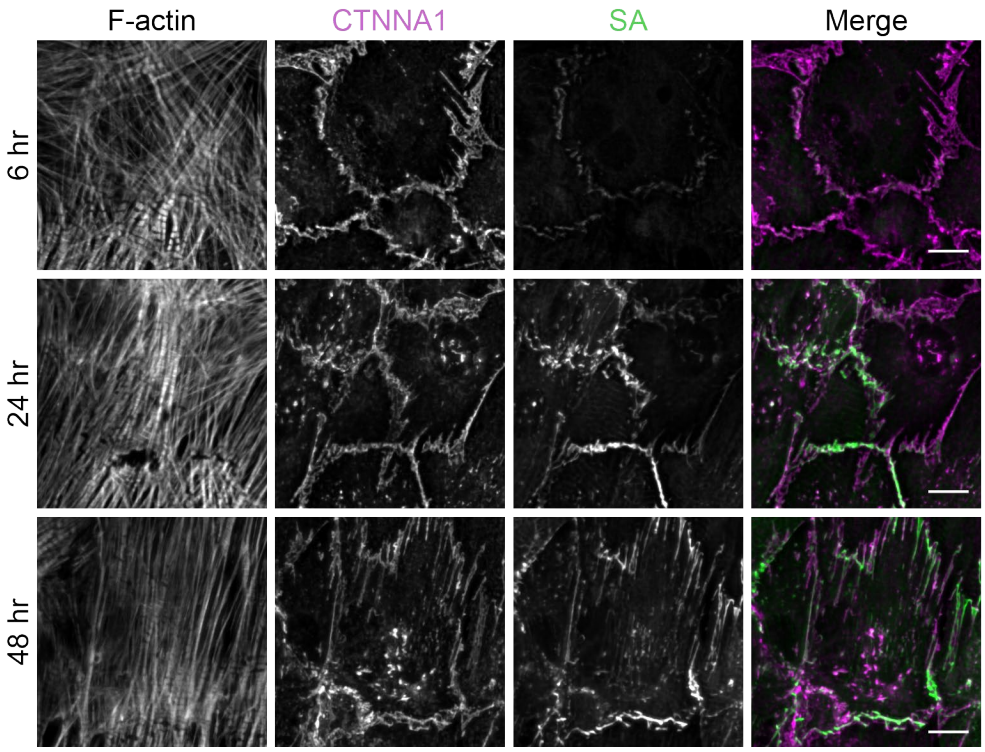

Figure S2-1 (accompanies Figure 3)

Time course of biotin labeling. Cardiomyocytes infected with Cdh2-BioID2 adenovirus were fixed 6, 24 and 48 hours after biotin addition. Cells were stained for F-actin, CTNNA1 and biotin (streptavidin, SA). CTNNA1 (magenta) and SA (green) channels are shown in merge. Scale bar is 10 μm.

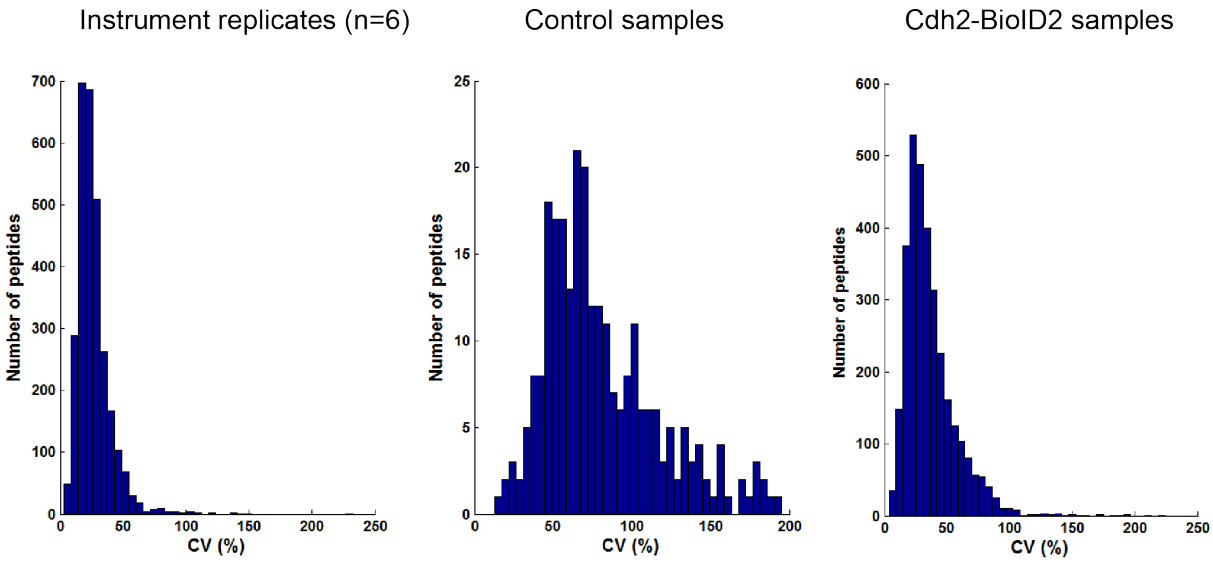

Figure S2- 2 (accompanies Figure 4)

Coefficient of variance (CV) for mass spec analysis of instrument replicates, control samples and experimental (Cdh2-BioID2) samples.

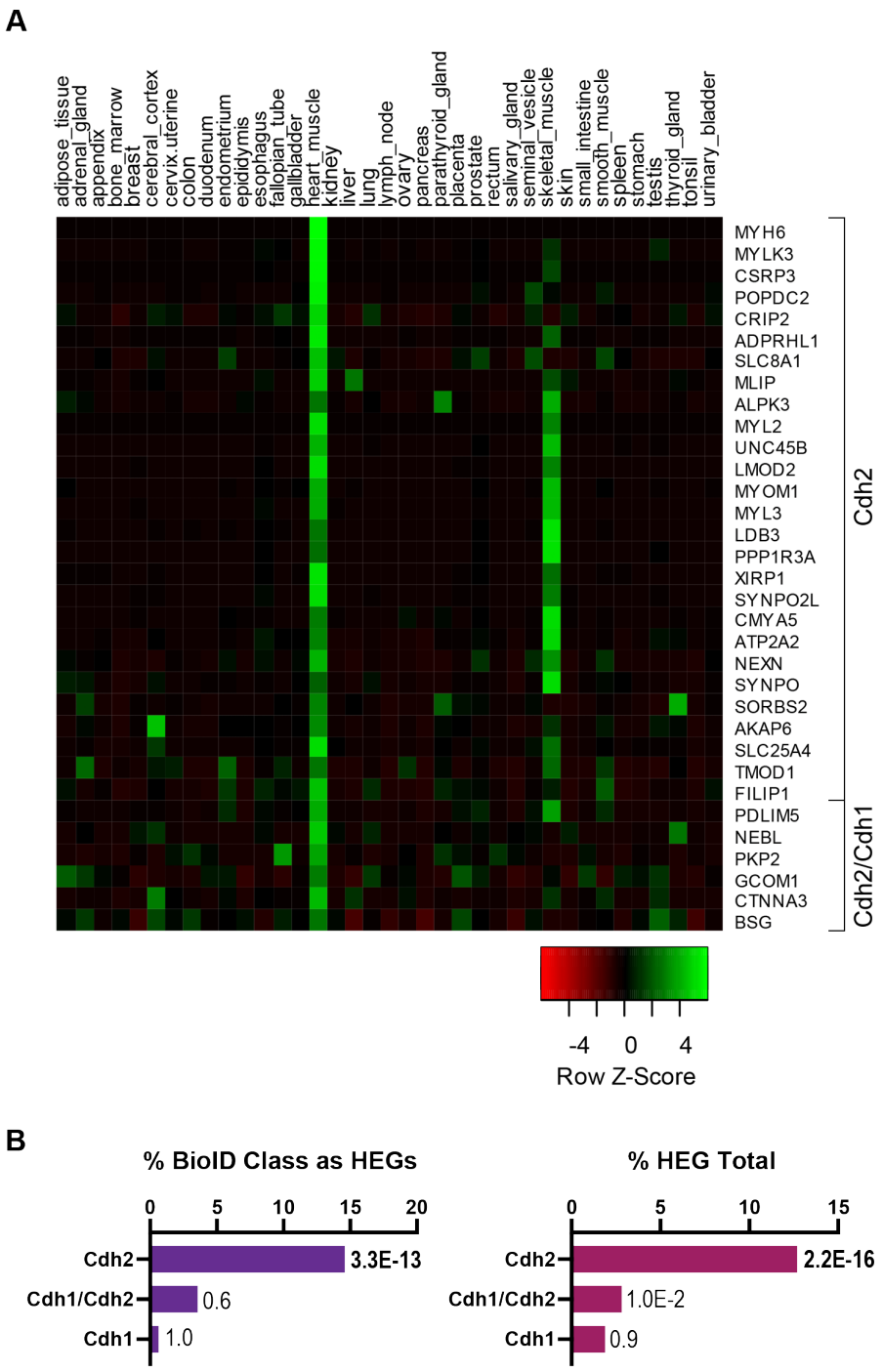

Figure S2- 3 (accompanies Figure 5)

A. Heat map of CDH2 or CDH2/CDH1 expression profiles in human tissues. B. Left, percentage of each BioID class as HEGs. Right, fraction of those BioID HEGs in the total HEG population. P value of Fisher's exact test shown.

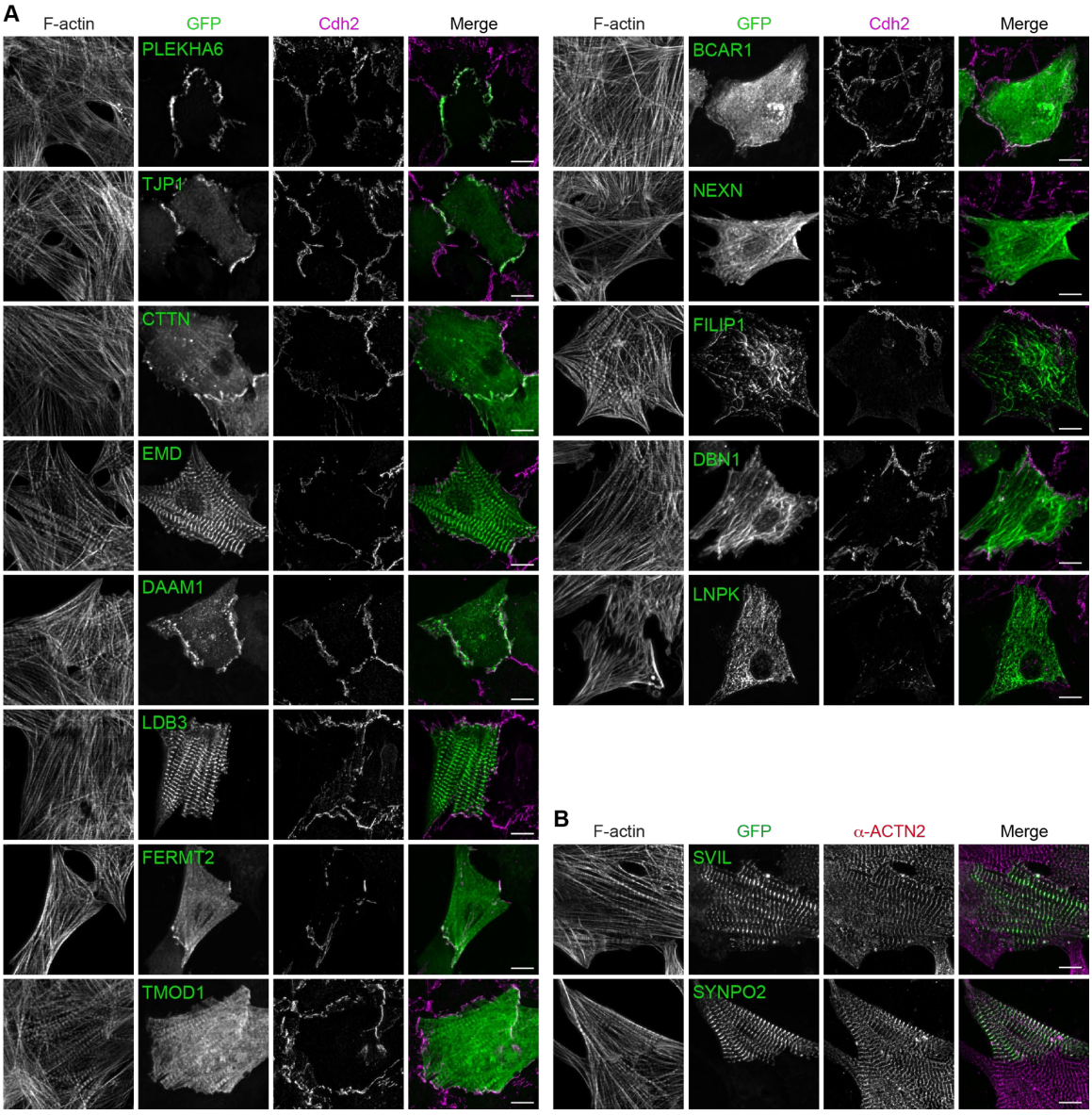

Figure S2- 4 (accompanies Figure 7)

A. CDH2 interactome protein localization. Cardiomyocytes transfected with GFP-tagged Cdh2-BioID hits and stained for Cdh2 and F-actin. Individual and merged GFP (green) and CDH2 (magenta) channels shown. Note that LNPK was tagged with mCherry and DBN1 (paralog of DBNL) was tagged with YFP. Both fusion protein channels were pseudo-colored green for consistent comparison. Tested but not shown are PHLDB1, SQSTM1, TLN1, PARVA, TRIM55, CSRP1, DPYSL3 and COBLL1. All formed aggregates or were cytoplasmic when expressed in cardiomyocytes. B. SVIL and SYNPO2 localize to Z-discs. Cardiomyocytes transfected with EGFP-

tagged SVIL and SYNPO2. Cells were fixed 24 hours post-transfection and stained for ACTN2 and F-actin. Scale bar is 10 μm for A and B.

Appendix B Supplemental Material for Chapter 3

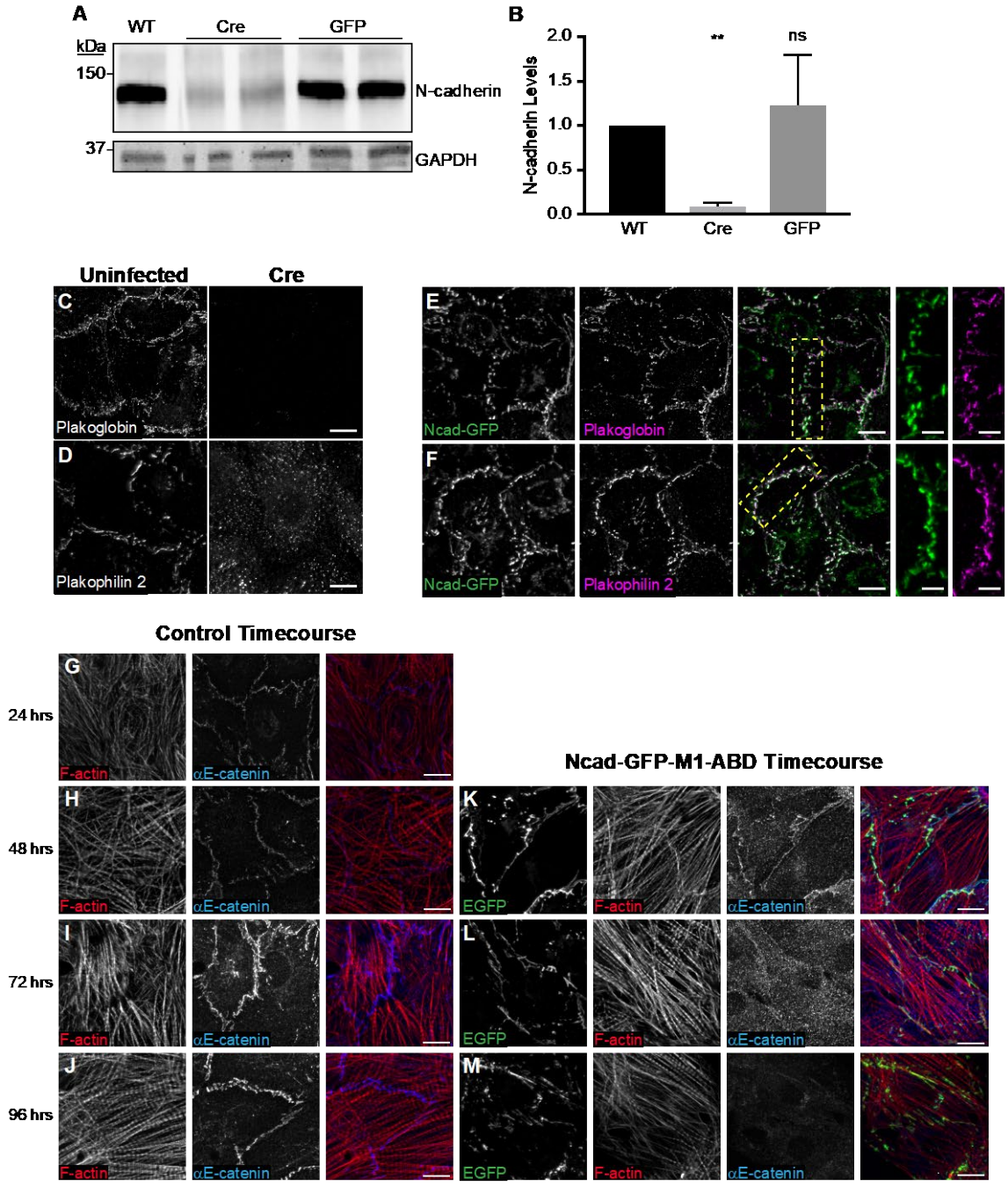

Figure S3-1 Cre-mediated loss of N-cadherin in Ncad$^{fx/fx}$ cardiomyocytes (accompanies Figure 2-2)

A. Representative western blot of cell lysates from $Ncad^{fx/fx}$ cardiomyocytes that were uninfected (WT), infected with Cre recombinase-expressing adenovirus (Cre) or GFP-expressing adenovirus (GFP). Lysates were separated by SDS-PAGE and blotted for N-cadherin (top) and GAPDH (bottom). B. N-cadherin band intensities in A were measured, normalized to WT and plotted. Error bars represent standard deviation from at least three independent experiments. One-way ANOVA, $p<0.01$. C-D. Neonatal cardiomyocytes from $Ncad^{fx/fx}$ mice were either uninfected (left panel) or infected with adenovirus expressing Cre recombinase, fixed and stained for desmosome components plakoglobin (C) and plakophilin (D). E-F. Expression of N-cadherin-GFP in N-cadherin-null cardiomyocytes restored plakoglobin (E) and plakophilin (F) recruitment. Individual N-cadherin-GFP (green) and desmosome components (magenta) channels are shown along with the merge. Far right column is a magnification of boxed contact in the merge. G-M. αE-catenin expression in control (G-J) and Cre/Ncad-GFP-M1-ABD infected $Cdh2^{fx/fx}$ (K-M) cardiomyocytes. G-J. $Cdh2^{fx/fx}$ cardiomyocytes were fixed at four different time points and stained for αE-catenin and F-actin. K-M. $Cdh2^{fx/fx}$ cardiomyocytes were infected with Cre recombinase and Ncad-GFP-M1-ABD adenoviruses, fixed at three separate time points and stained for αE-catenin and F-actin. αE-catenin expression was lost over 96 hours as Ncad-GFP-M1-ABD expression increased. Images are max projections of 2-3 μm deconvolved stacks. Scale bar is 10 μm.

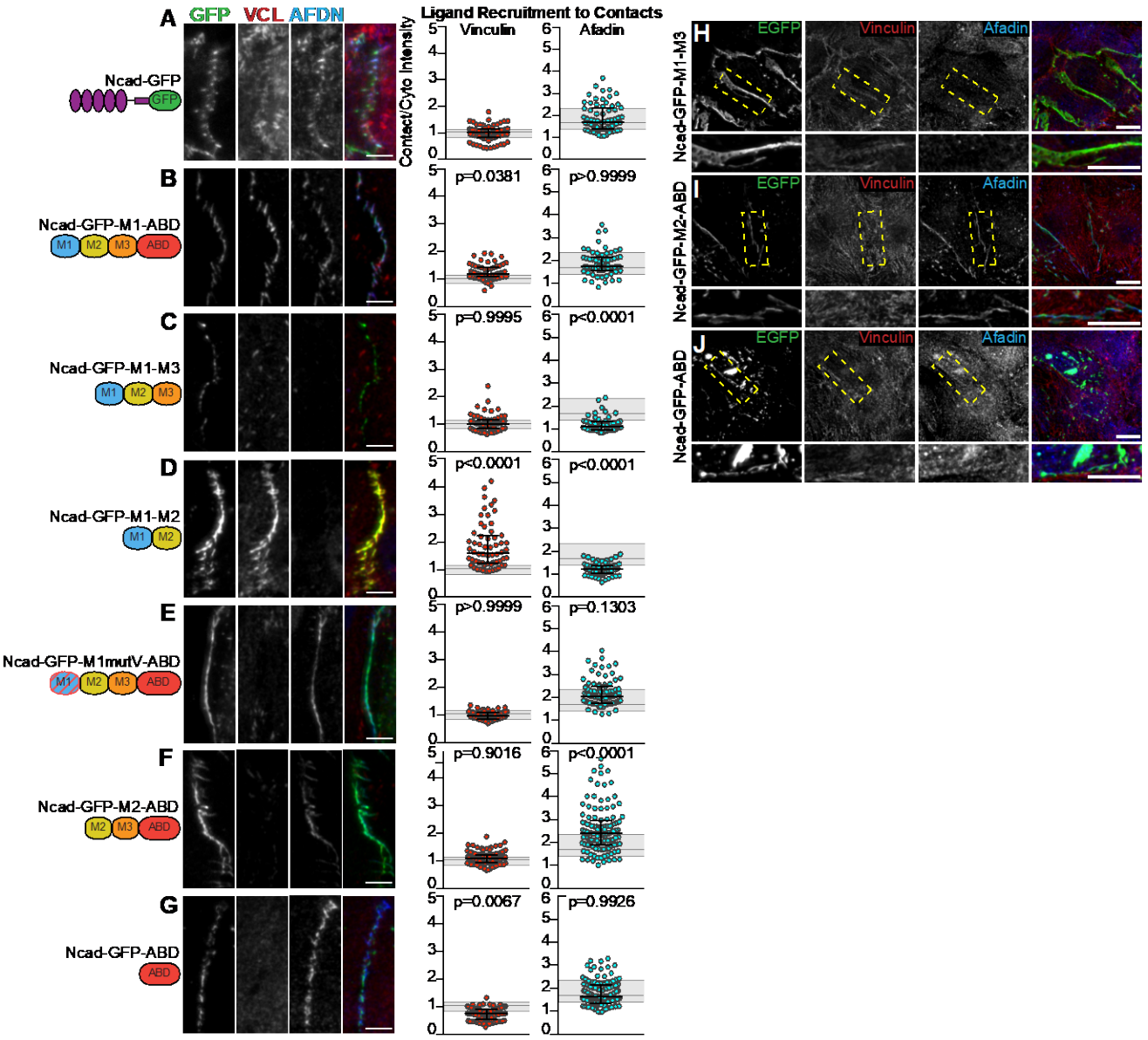

Figure S3- 2 N-cadherin-GFP-αE-catenin fusion ligand recruitment in cadherin-null cells (accompanies Figure 2-4)

Cadherin-null A431D epithelial cells were transfected with N-cadherin-GFP-αE-catenin fusion constructs to test vinculin and afadin recruitment (A-G). Cells were fixed 48 hours post-transfection and stained for vinculin and afadin. Individual fusion constructs (green), vinculin (red), afadin (blue) and merged channels are shown. Images are max projections of 3 μm stacks. Scale bars are 10 μm. Quantification of vinculin and afadin intensities at cell-cell contacts is shown on the right. Signal intensity at contacts was divided by the average cytoplasmic intensity and a scatter plot of all data

points is shown. The black horizontal line is the median and the error bars define the interquartile range. The shaded gray region in each plot defines the median (thick gray line) and interquartile range (thin gray lines) of vinculin or afadin recruitment observed with full-length N-cadherin-GFP (A) for comparison. One-way ANOVA, significance compared to recruitment with N-cadherin-GFP. $n \geq 60$ images from at least 3 independent experiments. H-J. Neonatal cardiomyocytes isolated from $Ncad^{fx/fx}$ mice were infected with Cre and N-cadherin-GFP-αE-catenin fusion adenoviruses. Cells were fixed and stained for vinculin and afadin. Individual and merged GFP (green), vinculin (red) and afadin (blue) channels shown. Images are max projections of 2-3 μm deconvolved stacks. Scale bar is 10 μm.

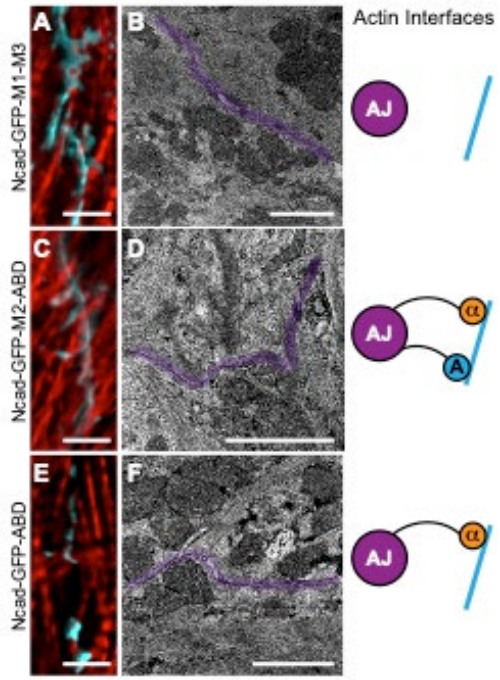

Figure S3- 3 . Immunostaining and TEM of N-cadherin-GFP-αE-catenin fusion constructs (accompanies Figure 2-4)

Ncad$^{fx/fx}$ cardiomyocytes infected with Cre and N-cadherin-GFP-αE-catenin fusion adenoviruses (A-F) were fixed and processed for staining (A, C, E) or thin section EM (B, D, F). IF images are 2-3 μm deconvolved stacks showing GFP signal from of N-cadherin-GFP-αE-catenin fusions pseudo-colored blue and stained for F-actin (red). Scale bar is 5 μm for IF images. Thin section TEM images are representative of >60 images from at least three independent experiments. Cell-cell contacts are pseudo-colored purple. Scale bar is 1 μm for TEM images.

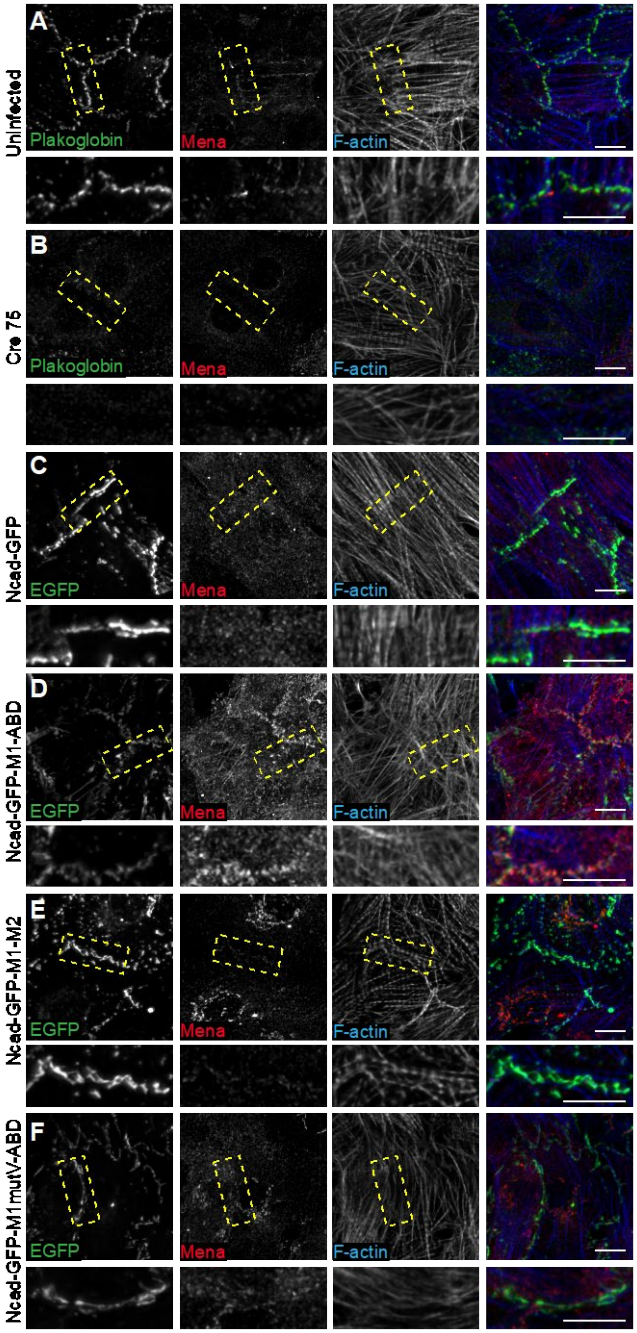

Figure S3- 4 Mena localization with N-cadherin fusion constructs

$Ncad^{fx/fx}$ cardiomyocytes were either uninfected (A), infected with Cre recombinase (B), or infected with both Cre and N-cadherin fusion constructs (C-F). Cells were fixed and stained for Mena and F-actin. Individual and merged GFP (green), Mena (red) and F- actin (blue) channels are shown.

Images are a max projection of 2-3 μm deconvolved stacks. Bottom row in each panel set is a magnification of boxed contact. Scale bar is 10 μm.

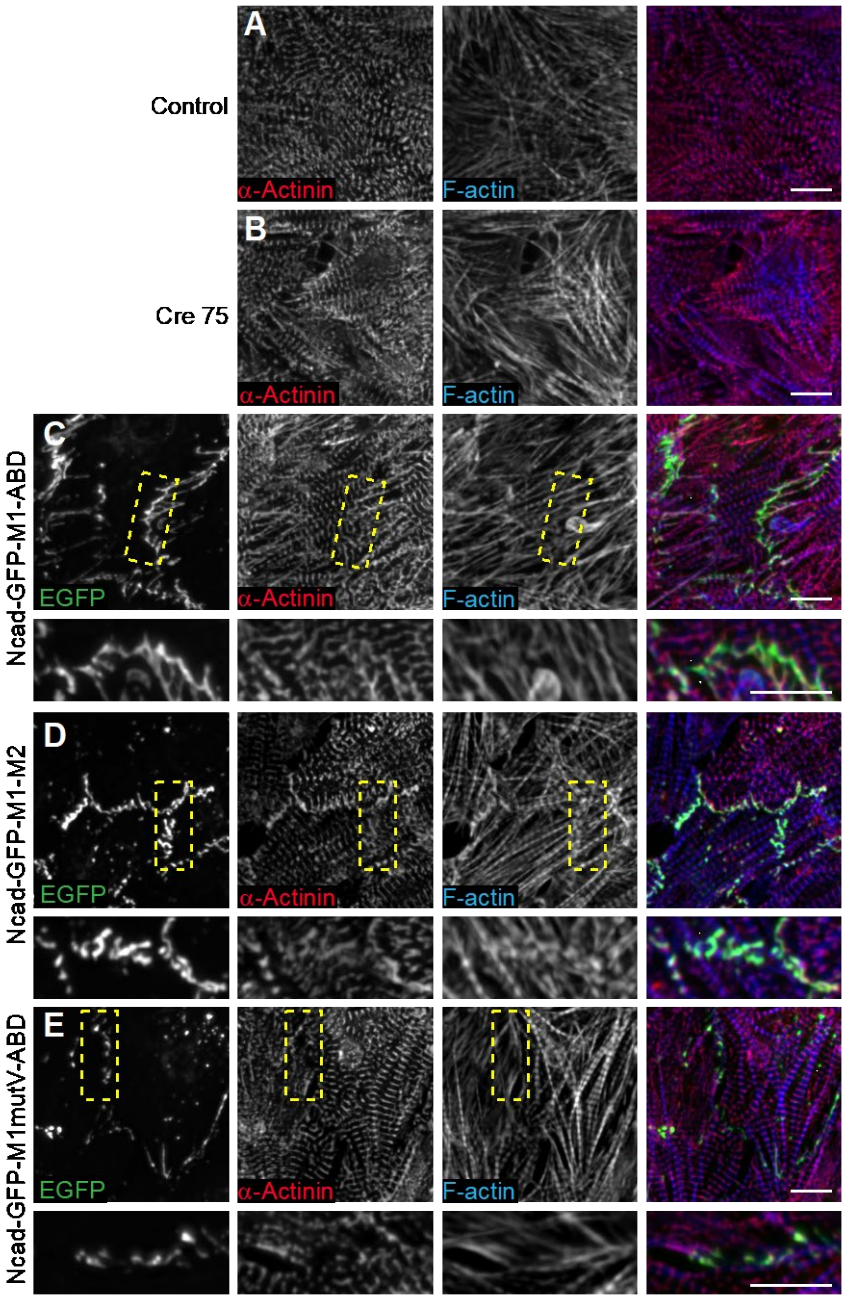

Figure S3- 5 α-Actinin localization with N-cadherin fusion constructs

Ncad$^{fx/fx}$ cardiomyocytes were uninfected (A), infected with Cre recombinase alone (B), or infected with Cre and fusion constructs (C-E). Cells were fixed and stained for α-actinin and F-actin. Individual and merged N-cadherin fusion (green), α-actinin (red) and F-actin (blue) channels are shown. Images

are a maximum projection of 2-3 μm deconvolved stacks. Bottom row in each panel set is a magnification of boxed contact. Scale bar is 10 μm.

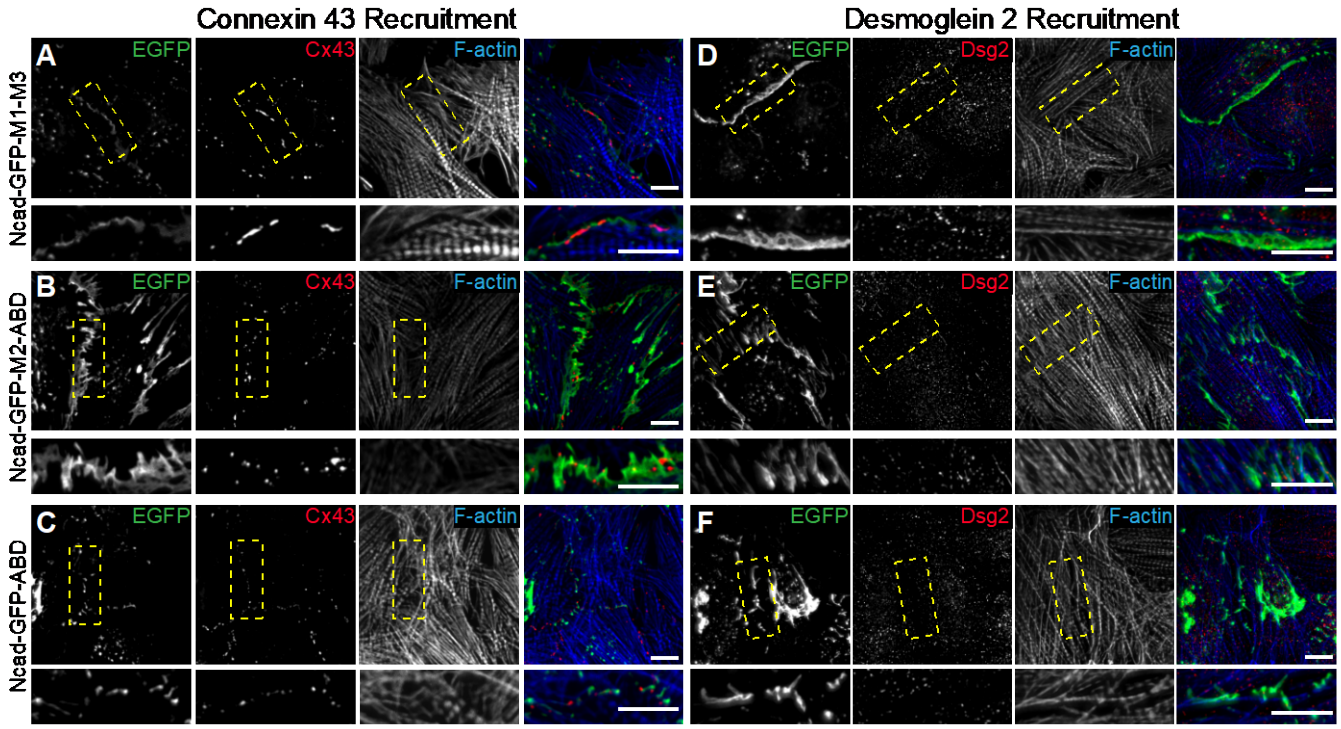

Figure S3- 6 Connexin 43 and Desmoglein 2 localization (accompanies Figure 7)

Neonatal cardiomyocytes isolated from Ncad$^{fx/fx}$ mice were infected with Cre and N-cadherin-GFP-αE-catenin fusion adenoviruses. A-C. Cells were fixed and stained for connexin 43 and F-actin. Individual and merged GFP (green, connexin 43 (Cx43, red) and F-actin (blue) channels shown. Cx43 localization occurs independent of actin binding or ligand recruitment to the fusion constructs. D-F. Cells were fixed and stained for Dsg2 and F-actin. Individual and merged GFP (green), desmoglein 2 (Dsg2, red) and F-actin (blue) channels shown. Dsg2 localization is not seen with rescue of Ncad-M1-M3 (D), Ncad-M2-ABD (E), or Ncad-ABD (F) as none of these constructs can successfully recruit vinculin. Images are a maximum projection of 2-3 μm deconvolved stacks. Bottom images are a magnification of boxed contacts. Scale bar is 10 μm.

Bibliography

1. Liu Z, et al. (2010) Mechanical tugging force regulates the size of cell-cell junctions. *Proc Natl Acad Sci* 107(22):9944–9949.

2. Maruthamuthu V, Sabass B, Schwarz US, Gardel ML (2011) Cell-ECM traction force modulates endogenous tension at cell-cell contacts. *Proc Natl Acad Sci* 108(12):4708–4713.

3. McCain ML, Lee H, Aratyn-Schaus Y, Kleber AG, Parker KK (2012) Cooperative coupling of cell-matrix and cell-cell adhesions in cardiac muscle. *Proc Natl Acad Sci* 109(25):9881–9886.

4. Jacot JG, Martin JC, Hunt DL (2011) Mechanobiology of CM Dev. 43(1):1–13.

5. Sheikh F, Ross RS, Chen J (2013) Cell-Cell Connection to Cardiac Disease Intercalated Disks: Structure and Components. 19(6):182–190.

6. Vite A, Li J, Radice GL (2015) New functions for alpha-catenins in health and disease: from cancer to heart regeneration. *Cell Tissue Res*. doi:10.1007/s00441-015-2123-x.

7. Ehler E (2016) Cardiac cytoarchitecture - why the “hardware” is important for heart function! *Biochim Biophys Acta - Mol Cell Res* 1863(7):1857–1863.

8. Vermij SH, Abriel H, van Veen TAB (2017) Refining the molecular organization of the cardiac intercalated disc. *Cardiovasc Res* 113(3):259–275.

9. Horsley V, Pavlath GK (2004) Forming a Multinucleated Cell: Molecules That Regulate Myoblast Fusion. *Cells Tissues Organs* 176(1–3):67–78.

10. Oren-Suissa M, Podbilewicz B (2007) Cell fusion during development. *Trends Cell Biol* 17(11):537–546.

11. Noorman M, et al. (2009) Cardiac cell-cell junctions in health and disease: Electrical versus mechanical coupling. *J Mol Cell Cardiol* 47(1):23–31.

12. Geisler SB, et al. (2010) Ordered Assembly of the Adhesive and Electrochemical Connections within Newly Formed Intercalated Disks in Primary Cultures of Adult Rat Cardiomyocytes. *J Biomed Biotechnol* 2010(Dcm):1–14.

13. Fenix A, Neininger A, Taneja N, ELife KH-, 2018 U (2018) Muscle-specific stress fibers give rise to sarcomeres in cardiomyocytes. *Elife*:1–33.

14. Luo Y, Radice GL (2003) Cadherin-mediated adhesion is essential for myofibril continuity across the plasma membrane but not for assembly of the contractile apparatus. *J Cell Sci* 116:1471–1479.

15. Ratheesh A, Yap AS (2012) A bigger picture: Classical cadherins and the dynamic actin cytoskeleton. *Nat Rev Mol Cell Biol*. doi:10.1038/nrm3431.

16. Mege R-M, Ishiyama N (2017) Integration of Cadherin Adhesion and Cytoskeleton at Adherens Junctions. *Cold Spring Harb Perspect Biol* 9.

17. Kostetskii I, et al. (2005) Induced deletion of the N-cadherin gene in the heart leads to dissolution of the intercalated disc structure. *Circ Res* 96:346–354.

18. Davis MA, Ireton RC, Reynolds AB (2003) A core function for p120-catenin in cadherin turnover. *J Cell Biol* 163(3):525–34.

19. Wahl JK, Kim YJ, Cullen JM, Johnson KR, Wheelock MJ (2003) N-cadherin-Catenin Complexes Form Prior to Cleavage of the Proregion and Transport to the Plasma Membrane. *J Biol Chem* 278(19):17269–17276.

20. Bianchini JM, et al. (2015) Reevaluating E-catenin monomer and homodimer functions by characterizing E-cadherin/ E-catenin chimeras. *J Cell Biol* 210(7):1065–1074.

21. Buckley CD, et al. (2014) Cell adhesion. The minimal cadherin-catenin complex binds to actin filaments under force. *Science* 346(6209):1254211.

22. Janssens B, et al. (2001) alphaT-catenin: a novel tissue-specific beta-catenin-binding protein mediating strong cell-cell adhesion. *J Cell Sci* 114(Pt 17):3177–88.

23. Shapiro L, Weis WI (2009) Structure and biochemistry of cadherins and catenins. *Cold Spring Harb Perspect Biol* 1(3):a003053.

24. Harrison OJ, et al. (2011) The extracellular architecture of adherens junctions revealed by crystal structures of type i cadherins. *Structure* 19(2):244–256.

25. Liang, Xuan; Gomez, Guillermo; Yap A (2015) Current perspectives on cadherin-cytoskeleton interactions and dynamics. 11–24.

26. Radice GL, et al. (1997) Developmental defects in mouse embryos lacking N-cadherin. *Dev Biol*. doi:10.1006/dbio.1996.8443.

27. Luo Y, et al. (2001) Rescuing the N-cadherin knockout by cardiac-specific expression of N- or E-cadherin. *Development*. doi:10.1016/S1353-2561(98)00008-5.

28. Ferreira-Cornwell MC, et al. (2002) Remodeling the intercalated disc leads to cardiomyopathy in mice misexpressing cadherins in the heart. *J Cell Sci* 115:1623–1634.

29. Bienz M (2005) β-catenin: A pivot between cell adhesion and Wnt signalling. *Curr Biol*. doi:10.1016/j.cub.2004.12.058.

30. Haegel H, et al. (1995) Lack of β-catenin affects mouse development at gastrulation. *Development*.

31. Chen CP, Posy S, Ben-Shaul A, Shapiro L, Honig BH (2005) Specificity of cell-cell adhesion by classical cadherins: Critical role for low-affinity dimerization through beta-strand swapping. *Proc Natl Acad Sci U S A* 102:8531–8536.

32. Gul IS, Hulpiau P, Saeys Y, van Roy F (2017) Evolution and diversity of cadherins and catenins. *Exp Cell Res* 358(1):3–9.

33. Zhou J, et al. (2006) Upregulation of γ-catenin compensates for the loss of β-catenin in adult cardiomyocytes. *Am J Physiol Circ Physiol* 292(1):H270–H276.

34. Bierkamp C, Schwarz H, Huber O, Kemler R (1999) Desmosomal localization of beta-catenin in the skin of plakoglobin null-mutant mice. *Development*.

35. Nieset JE, et al. (1997) Characterization of the interactions of α -catenin with α -actinin and β-catenin/plakoglobin. *J Cell Sci* 110:1013–1022.

36. Peiters T, van Roy F, van Hengel J (2012) Functions of p120ctn isoforms in cell-cell adhesion and intracellular signaling. *Front Biosci* 11(1):1669–1694.

37. Wehrendt DP, et al. (2016) P120-catenin regulates early trafficking stages of the n-cadherin precursor complex. *PLoS One*. doi:10.1371/journal.pone.0156758.

38. Chen X, Kojima SI, Borisy GG, Green KJ (2003) p120 catenin associates with kinesin and facilitates the transport of cadherin-catenin complexes to intercellular junctions. *J Cell Biol*. doi:10.1083/jcb.200305137.

39. Peifer M, Yap AS (2003) Traffic control: p120-catenin acts as a gatekeeper to control the fate of classical cadherins in mammalian cells. *J Cell Biol*. doi:10.1083/jcb.200310090.

40. Nanes BA, et al. (2012) p120-catenin binding masks an endocytic signal conserved in classical cadherins. *J Cell Biol*. doi:10.1083/jcb.201205029.

41. Rimm DL, Koslov ER, Kebriaei P, Cianci CD, Morrow JS (1995) Alpha 1(E)-catenin is an actin-binding and -bundling protein mediating the attachment of F-actin to the membrane adhesion complex. *Proc Natl Acad Sci* 92(19):8813–8817.

42. Drees F, Pokutta S, Yamada S, Nelson WJ, Weis WI (2005) Alpha-catenin is a molecular switch that binds E-cadherin-beta-catenin and regulates actin-filament assembly. *Cell* 123:903–915.

43. Yamada S, Pokutta S, Drees F, Weis WI, Nelson WJ (2005) Deconstructing the cadherin-catenin-actin complex. *Cell* 123(5):889–901.

44. Pokutta S, Choi HJ, Ahlsen G, Hansen SD, Weis WI (2014) Structural and thermodynamic characterization of cadherin· β-catenin·α-catenin complex formation. *J Biol Chem*. doi:10.1074/jbc.M114.554709.

45. Ishiyama N, et al. (2013) An autoinhibited structure of α-catenin and its implications for vinculin recruitment to adherens junctions. *J Biol Chem* 288(22):15913–15925.

46. Choi H-J, et al. (2012) E-catenin is an autoinhibited molecule that coactivates vinculin. *Proc Natl Acad Sci* 109(22):8576–8581.

47. Pokutta S, Drees F, Takai Y, Nelson WJ, Weis WI (2002) Biochemical and structural definition of the l-afadin- and actin-binding sites of alpha-catenin. *J Biol Chem* 277(21):18868–74.

48. Knudsen Ka, Soler Ap, Johnson Kr, Wheelock Mj (1995) Interaction of alpha-actinin with the cadherin/catenin cell-cell adhesion complex via alpha-catenin. *J Cell Biol* 130(1):67–77.

49. Itoh M, Nagafuchi A, Moroi S, Tsukita S (1997) Involvement of ZO-1 in cadherin-based cell adhesion through its direct binding to α catenin and actin filaments. *J Cell Biol*. doi:10.1083/jcb.138.1.181.

50. Charras G, Yap AS (2018) Tensile Forces and Mechanotransduction at Cell–Cell Junctions. *Curr Biol* 28(8):R445–R457.

51. Benjamin JM, et al. (2010) αE-catenin regulates actin dynamics independently of cadherin-mediated cell-cell adhesion. *J Cell Biol* 189(2):339–352.

52. Hansen SD, et al. (2013) E-catenin actin-binding domain alters actin filament conformation and regulates binding of nucleation and disassembly factors. *Mol Biol Cell* 24(23):3710–3720.

53. Sheikh F, et al. (2006) ??-E-catenin inactivation disrupts the cardiomyocyte adherens junction, resulting in cardiomyopathy and susceptibility to wall rupture. *Circulation* 114(10):1046–1055.

54. Goossens S, et al. (2007) A unique and specific interaction between alphaT-catenin and plakophilin-2 in the area composita, the mixed-type junctional structure of cardiac intercalated discs. *J Cell Sci* 120(Pt 12):2126–2136.

55. Franke WW, et al. (2007) The area composita of adhering junctions connecting heart muscle cells of vertebrates - III: Assembly and disintegration of intercalated disks in rat cardiomyocytes growing in culture. *Eur J Cell Biol* 86(3):127–142.

56. Swope D, Cheng L, Li J, Radice G (2011) β- and γ-catenin cooperate to maintain mechanoelectrical coupling in the heart. *Circ Res*.

57. Van Hengel J, et al. (2013) Mutations in the area composita protein at-catenin are associated with arrhythmogenic right ventricular cardiomyopathy. *Eur Heart J* 34(3):201–210.

58. Wickline ED, et al. (2016) Alpha-T-Catenin Is a Constitutive Actin-Binding α-Catenin That Directly Couples the Cadherin-Catenin Complex to Actin Filaments. *J Biol Chem* 291(30):15687–15699.

59. Nekrasova O, Green KJ (2013) Desmosome assembly and dynamics. *Trends Cell Biol* 23(11):537–546.

60. Brasch J, Harrison OJ, Honig B, Shapiro L (2012) Thinking outside the cell: How cadherins drive adhesion. *Trends Cell Biol*. doi:10.1016/j.tcb.2012.03.004.

61. Marcozzi C, Burdett ID, Buxton RS, Magee AI (1998) Coexpression of both types of desmosomal cadherin and plakoglobin confers strong intercellular adhesion. *J Cell Sci*.

62. Chitaev N a, Troyanovsky SM (1997) Direct Ca 2+-dependent Heterophilic Interaction between Desmosomal Cadherins, Desmoglein and Desmocollin, Contributes to Cell-Cell Adhesion. *Cell* 138(1):193–201.

63. Kimura TE, Merritt AJ, Garrod DR (2007) Calcium-independent desmosomes of keratinocytes are hyper-adhesive. *J Invest Dermatol*. doi:10.1038/sj.jid.5700643.

64. Witcher LL, et al. (1996) Desmosomal cadherin binding domains of plakoglobin. *J Biol Chem*. doi:10.1074/jbc.271.18.10904.

65. Hatzfeld M (2007) Plakophilins: Multifunctional proteins or just regulators of desmosomal adhesion? *Biochim Biophys Acta - Mol Cell Res* 1773(1):69–77.

66. Kowalczyk AP, et al. (1997) The amino-terminal domain of desmoplakin binds to plakoglobin and clusters desmosomal cadherin-plakoglobin complexes. *J Cell Biol*. doi:10.1083/jcb.139.3.773.

67. Acehan D, et al. (2008) Plakoglobin is required for effective intermediate filament anchorage to desmosomes. *J Invest Dermatol*. doi:10.1038/jid.2008.141.

68. Nekrasova OE, et al. (2011) Desmosomal cadherins utilize distinct kinesins for assembly into desmosomes. *J Cell Biol* 195(7):1185–1203.

69. Michels C, Buchta T, Bloch W, Krieg T, Niessen CM (2009) Classical Cadherins Regulate Desmosome Formation. *J Invest Dermatol*. doi:10.1038/jid.2009.17.

70. Tinkle CL, Pasolli HA, Stokes N, Fuchs E (2008) New insights into cadherin function in epidermal sheet formation and maintenance of tissue integrity. *Proc Natl Acad Sci*. doi:10.1073/pnas.0807374105.

71. Troyanovsky RB, Klingelhofer J, Troyanovsky S (1999) Removal of calcium ions triggers a novel type of intercadherin interaction. *J Cell Sci*.

72. Tsang SM, et al. (2010) Desmoglein 3, via an interaction with E-cadherin, is associated with activation of Src. *PLoS One*. doi:10.1371/journal.pone.0014211.

73. Shafraz O, et al. (2018) E-cadherin binds to desmoglein to facilitate desmosome assembly. *Elife* 7:1–18.

74. Pieperhoff S, Franke WW (2007) The area composita of adhering junctions connecting heart muscle cells of vertebrates - IV: Coalescence and amalgamation of desmosomal and adhaerens junction components - Late processes in mammalian heart development. *Eur J Cell Biol* 86:377–391.

75. Cowin P, Kapprell HP, Franke WW, Tamkun J, Hynes RO (1986) Plakoglobin: A protein common to different kinds of intercellular adhering junctions. *Cell* 46(7):1063–1073.

76. Li J, Radice GL (2010) A new perspective on intercalated disc organization: Implications for heart disease. *Dermatol Res Pract* 2010(1). doi:10.1155/2010/207835.

77. Awad MM, et al. (2006) DSG2 Mutations Contribute to Arrhythmogenic Right Ventricular Dysplasia/Cardiomyopathy. *Am J Hum Genet* 79(1):136–142.

78. Delmar M, McKenna WJ (2010) The cardiac desmosome and arrhythmogenic cardiomyopathies: From gene to disease. *Circ Res* 107(6):700–714.

79. Benjamin EJ, et al. (2018) *Heart disease and stroke statistics - 2018 update: A report from the American Heart Association* doi:10.1161/CIR.0000000000000558.

80. Rampazzo A, et al. (2002) Mutation in Human Desmoplakin Domain Binding to Plakoglobin Causes a Dominant Form of Arrhythmogenic Right Ventricular Cardiomyopathy. *Am J Hum Genet*. doi:10.1086/344208.

81. Bauce B, et al. (2005) Clinical profile of four families with arrhythmogenic right ventricular cardiomyopathy caused by dominant desmoplakin mutations. *Eur Heart J*. doi:10.1093/eurheartj/ehi341.

82. van Tintelen JP, Entius MM, Bhuiyan ZA, Jongbloed R, Wiesfeld AC, Wilde AA, van der SJ, Boven LG, Mannens MM, van Langen IM, Hofstra RM, Otterspoor LC, Doevendans PA, Rodriguez LM, van Gelder IC, Hauer R (2006) Plakophilin-2 mutations are the major determinant of familial arrhythmogenic right ventricular dysplasia/cardiomyopathy. *Circulation* 113:1650–1658.

83. Syrris P, et al. (2006) Arrhythmogenic Right Ventricular Dysplasia/Cardiomyopathy Associated with Mutations in the Desmosomal Gene Desmocollin-2. *Am J Hum Genet* 79(5):978–984.

84. McKoy G, et al. (2000) Identification of a deletion in plakoglobin in arrhythmogenic right ventricular cardiomyopathy with palmoplantar keratoderma and woolly hair (Naxos disease). *Lancet*. doi:10.1016/S0140-6736(00)02379-5.

85. Kumar NM, Gilula NB (1996) The gap junction communication channel. *Cell*. doi:10.1016/S0092-8674(00)81282-9.

86. Goodenough DA (2002) Connexins, Connexons, and Intercellular Communication. *Annu Rev Biochem*. doi:10.1146/annurev.biochem.65.1.475.

87. Solan JL, Lampe PD (2009) Connexin43 phosphorylation: structural changes and biological effects. *Biochem J*. doi:10.1042/BJ20082319.

88. Severs NJ, Bruce AF, Dupont E, Rothery S (2008) Remodelling of gap junctions and connexin expression in diseased myocardium. *Cardiovasc Res*. doi:10.1093/cvr/cvn133.

89. Unwin PNT, Ennis PD (1984) Two configurations of a channel-forming membrane protein. *Nature*. doi:10.1038/307609a0.

90. Makowski L, Caspar DLD, Phillips WC, Goodenough DA (1977) Gap junction structures. II. Analysis of the X-ray diffraction data. *J Cell Biol*. doi:10.1083/jcb.74.2.629.

91. Elfgang C, et al. (1995) Specific permeability and selective formation of gap junction channels in connexin-transfected HeLa cells. *J Cell Biol*. doi:10.1083/jcb.129.3.805.

92. Bernstein SA, Morley GE (2006) Gap junctions and propagation of the cardiac action potential. *Adv Cardiol*. doi:10.1159/000092563.

93. Toyofuku T, et al. (1998) Direct association of the gap junction protein connexin-43 with ZO-1 in cardiac myocytes. *J Biol Chem* 273(21):12725–12731.

94. Rhett JM, Jourdan J, Gourdie RG (2011) Connexin 43 connexon to gap junction transition is regulated by zonula occludens-1. *Mol Biol Cell* 22(9):1516–1528.

95. Shaw RM, et al. (2007) Microtubule Plus-End-Tracking Proteins Target Gap Junctions Directly from the Cell Interior to Adherens Junctions. *Cell* 128(3):547–560.

96. Li J, et al. (2005) Cardiac-specific loss of N-cadherin leads to alteration in connexins with conduction slowing and arrhythmogenesis. *Circ Res* 97(5):474–81.

97. Kaplan SR, et al. (2004) Remodeling of myocyte gap junctions in arrhythmogenic right ventricular cardiomyopathy due to a deletion in plakoglobin (Naxos disease). *Hear Rhythm*. doi:10.1016/j.hrthm.2004.01.001.

98. Yang Z, et al. (2006) Desmosomal dysfunction due to mutations in desmoplakin causes arrhythmogenic right ventricular dysplasia/cardiomyopathy. *Circ Res* 99(6):646–655.

99. Manias JL, et al. (2008) Fate of connexin43 in cardiac tissue harbouring a disease-linked connexin43 mutant. *Cardiovasc Res*. doi:10.1093/cvr/cvn203.

100. Kaprielian RR, et al. (1998) Downregulation of immunodetectable connexin43 and decreased gap junction size in the pathogenesis of chronic hibernation in the human left ventricle. *Circulation*. doi:10.1161/01.CIR.97.7.651.

101. Sepp R, Severs NJ, Gourdie RG (1996) Altered patterns of cardiac intercellular junction distribution in hypertrophic cardiomyopathy. *Heart*. doi:10.1136/hrt.76.5.412.

102. Rakshit S, Zhang Y, Manibog K, Shafraz O, Sivasankar S (2012) Ideal, catch, and slip bonds in cadherin adhesion. *Proc Natl Acad Sci* 109(46):18815–18820.

103. Harrison OJ, et al. (2010) Two-step adhesive binding by classical cadherins. *Nat Struct Mol Biol* 17(3):348–357.

104. Vendome J, et al. (2014) Structural and energetic determinants of adhesive binding specificity in type I cadherins. *Proc Natl Acad Sci* 111(9):E4175–E4184.

105. Borghi N, et al. (2012) E-cadherin is under constitutive actomyosin-generated tension that is increased at cell-cell contacts upon externally applied stretch. *Proc Natl Acad Sci U S A* 109(31):12568–73.

106. Pokutta S, Drees F, Yamada S, Nelson WJ, Weis WI (2008) Biochemical and structural analysis of alpha-catenin in cell-cell contacts. *Biochem Soc Trans* 36:141–147.

107. Li J, et al. (2015) Structural Determinants of the Mechanical Stability of Alpha Catenin. *J Biol Chem*:1–36.

108. Rangarajan ES, Izard T (2012) The cytoskeletal protein ??-catenin unfurls upon binding to vinculin. *J Biol Chem* 287(22):18492–18499.

109. Yao M, et al. (2014) Force-dependent conformational switch of α -catenin controls vinculin binding. *Nat Commun* 5. doi:10.1038/ncomms5525.

110. Kim T, et al. (2015) Dynamic Visualization of a -Catenin Reveals Rapid , Reversible Conformation Switching between Tension States. *Curr Biol*:1–7.

111. Finer JT, Simmons RM, Spudich JA (1994) Single myosin molecule mechanics: piconewton forces and nonmetre steps. *Nature* 368:561–563.

112. Maki K, et al. (2016) Mechano-adaptive sensory mechanism of α-catenin under tension. *Sci Rep* 6(April):24878.

113. Salbreux G, Charras G, Paluch E (2012) Actin cortex mechanics and cellular morphogenesis. *Trends Cell Biol*. doi:10.1016/j.tcb.2012.07.001.

114. Chu YS, et al. (2004) Force measurements in E-cadherin-mediated cell doublets reveal rapid adhesion strengthened by actin cytoskeleton remodeling through Rac and Cdc42. *J Cell Biol*. doi:10.1083/jcb.200403043.

115. Bays JL, et al. (2014) Vinculin phosphorylation differentially regulates mechanotransduction at cell-cell and cell-matrix adhesions. *J Cell Biol* 205(2):251–263.

116. Kovacs EM, Goodwin M, Ali RG, Paterson AD, Yap AS (2002) Cadherin-directed actin assembly: E-cadherin physically associates with the Arp2/3 complex to direct actin assembly in nascent adhesive contacts. *Curr Biol* 12(5):379–382.

117. Carramusa L, Ballestrem C, Zilberman Y, Bershadsky AD (2007) Mammalian diaphanous-related formin Dia1 controls the organization of E-cadherin-mediated cell-cell junctions. *J Cell Sci*. doi:10.1242/jcs.014365.

118. Cai L, Makhov AM, Schafer DA, Bear JE (2008) Coronin 1B antagonizes cortactin and remodels Arp2/3-containing actin branches in lamellipodia. *Cell* 134(5):828–842.

119. Shewan AM (2005) Myosin 2 Is a Key Rho Kinase Target Necessary for the Local Concentration of E-Cadherin at Cell-Cell Contacts. *Mol Biol Cell*. doi:10.1091/mbc.e05-04-0330.

120. le Duc Q, et al. (2010) Vinculin potentiates E-cadherin mechanosensing and is recruited to actin-anchored sites within adherens junctions in a myosin II-dependent manner. *J Cell Biol* 189(7):1107–1115.

121. Leerberg JM, et al. (2014) Tension-sensitive actin assembly supports contractility at the epithelial zonula adherens. *Curr Biol* 24(15):1689–1699.

122. Krause M, Dent EW, Bear JE, Loureiro JJ, Gertler FB (2003) Ena/VASP Proteins: Regulators of the Actin Cytoskeleton and Cell Migration. *Annu Rev Cell Dev Biol* 19(1):541–564.

123. Huang D, Bax N, Buckley C, Weis W, Dunn A (2017) Vinculin forms a Catch Bond with F-Actin that Depends on Actin Filament Orientation. *Biophys J* 112(3):268a.

124. Nagafuchi A, Ishihara S, Tsukita S (1994) The roles of catenins in the cadherin-mediated cell adhesion: Functional analysis of E-cadherin-α catenin fusion molecules. *J Cell Biol* 127(1):235–245.

125. Imamura Y, Itoh M, Maeno Y, Tsukita S, Nagafuchi A (1999) Functional domains of α-catenin required for the strong state of cadherin-based cell adhesion. *J Cell Biol*. doi:10.1083/jcb.144.6.1311.

126. Pacquelet A, Rørth P (2005) Regulatory mechanisms required for DE-cadherin function in cell migration and other types of adhesion. *J Cell Biol*. doi:10.1083/jcb.200506131.

127. Desai R, et al. (2013) Monomeric α-catenin links cadherin to the actin cytoskeleton. *Nat Cell Biol* 15(3):261–273.

128. Dartsch N, Schulte D, Hägerling R, Kiefer F, Vestweber D (2014) Fusing VE-cadherin to α-catenin impairs fetal liver hematopoiesis and lymph but not blood vessel formation. *Mol Cell Biol* 34(9):1634–48.

129. Chen C-S, et al. (2015) alpha-Catenin-mediated cadherin clustering couples cadherin and actin dynamics. *J Cell Biol* 210(4):647–661.

130. Misra JR, Irvine KD (2018) The Hippo Signaling Network and Its Biological Functions. *Annu Rev Genet* 52(1):65–87.

131. von Gise A, et al. (2012) YAP1, the nuclear target of Hippo signaling, stimulates heart growth through cardiomyocyte proliferation but not hypertrophy. *Proc Natl Acad Sci* 109(7):2394–2399.

132. Xin M, et al. (2012) Regulation of IGF signalling by YAP Governs Cardiomyocyte proliferation and Embryonic Heart Size. 4(196):1–15.

133. Karaman R, Halder G (2018) Cell junctions in Hippo signaling. *Cold Spring Harb Perspect Biol* 10(5). doi:10.1101/cshperspect.a028753.

134. Zhao B, et al. (2007) Inactivation of YAP oncoprotein by the Hippo pathway is involved in cell contact inhibition and tissue growth control. *Genes Dev* 21:2747–2761.

135. Kim N-G, Koh E, Chen X, Gumbiner BM (2011) E-cadherin mediates contact inhibition of proliferation through Hippo signaling-pathway components. *Proc Natl Acad Sci* 108(29):11930–11935.

136. Schlegelmilch K, et al. (2011) Yap1 acts downstream of α-catenin to control epidermal proliferation. *Cell* 144(5):782–795.

137. Silvis MR, et al. (2011) α-Catenin Is a Tumor Suppressor That Controls Cell Accumulation by Regulating the Localization and Activity of the Transcriptional. *Sci Signal* 4(174):1–10.

138. Das Thakur M, et al. (2010) Ajuba LIM Proteins Are Negative Regulators of the Hippo Signaling Pathway. *Curr Biol* 20(7):657–662.

139. Ibar C, et al. (2018) Tension-dependent regulation of mammalian Hippo signaling through LIMD1. *J Cell Sci* 131(5):jcs214700.

140. Rauskolb C, Sun S, Sun G, Pan Y, Irvine KD (2014) Cytoskeletal tension inhibits Hippo signaling through an Ajuba-Warts complex. *Cell* 158(1):143–156.

141. Alégot H, et al. (2019) Recruitment of Jub by α-catenin promotes Yki activity and Drosophila wing growth . *J Cell Sci* 132(5):jcs222018.

142. Xu J, et al. (2018) Yorkie Functions at the Cell Cortex to Promote Myosin Activation in a Non-transcriptional Manner. *Dev Cell* 46(3):271-284.e5.

143. Aragona M, et al. (2013) A mechanical checkpoint controls multicellular growth through YAP/TAZ regulation by actin-processing factors. *Cell* 154(5):1047–1059.

144. Zhou DW, Lee TT, Weng S, Fu J, García AJ (2017) Effects of substrate stiffness and actomyosin contractility on coupling between force transmission and vinculin–paxillin recruitment at single focal adhesions. *Mol Biol Cell* 28(14):1901–1911.

145. Shiba Y, et al. (2012) Human ES-cell-derived cardiomyocytes electrically couple and suppress arrhythmias in injured hearts. *Nature* 489(7415):322–325.

146. Xin M, et al. (2013) Hippo pathway effector Yap promotes cardiac regeneration. *Proc Natl Acad Sci* 110(34):13839–13844.

147. Lin Z, et al. (2014) Cardiac-specific YAP activation improves cardiac function and survival in an experimental murine MI model. *Circ Res* 115(3):354–363.

148. Li J, et al. (2015) Alpha-Catenins Control Cardiomyocyte Proliferation by Regulating Yap Activity. doi:10.1161/CIRCRESAHA.116.304472.

149. Vite A, Zhang C, Yi R, Emms S, Radice GL (2018) Alpha-catenin-dependent cytoskeletal tension controls Yap activity in the heart. *Development*:dev.149823.

150. Witzel HR, et al. (2012) The LIM Protein Ajuba Restricts the Second Heart Field Progenitor Pool by Regulating Isl1 Activity. *Dev Cell* 23(1):58–70.

151. Li Y, et al. (2019) The N-cadherin interactome in primary cardiomyocytes as defined using quantitative proximity proteomics. *J Cell Sci* 132(3):jcs221606.

152. Lindsey ML, Mann DL, Entman ML, Spinale FG (2003) Extracellular matrix remodeling following myocardial injury. *Ann Med* 35:316–326.

153. van den Borne SWM, et al. (2010) Myocardial remodeling after infarction: the role of myofibroblasts. *Nat Rev Cardiol* 7(1):30–37.

154. Jacot JG, McCulloch AD, Omens JH (2008) Substrate stiffness affects the functional maturation of neonatal rat ventricular myocytes. *Biophys J* 95(October):3479–3487.

155. Samarel AM (2005) Costameres, focal adhesions, and cardiomyocyte mechanotransduction. *Am J Physiol Heart Circ Physiol* 289(6):H2291-301.

156. Vreeker A, et al. (2014) Assembly of the cardiac intercalated disk during preand postnatal development of the human heart. *PLoS One* 9(4). doi:10.1371/journal.pone.0094722.

157. Hirschy A, Schatzmann F, Ehler E, Perriard JC (2006) Establishment of cardiac cytoarchitecture in the developing mouse heart. *Dev Biol* 289(2):430–441.

158. Ono S (2010) Dynamic regulation of sarcomeric actin filaments in striated muscle. *Cytoskeleton* 67(11):677–692.

159. Ishiwata T, Nakazawa M, Pu WT, Tevosian SG, Izumo S (2003) Developmental Changes in Ventricular Diastolic Function Correlate With Changes in Ventricular Myoarchitecture in Normal Mouse Embryos. *Circ Res* 93(9):857–865.

160. De Deyne PG (2017) Formation of sarcomeres in developing myotubes: role of mechanical stretch and contractile activation. *Am J Physiol Physiol* 279(6):C1801–C1811.

161. Chan YC, et al. (2013) Electrical stimulation promotes maturation of cardiomyocytes derived from human embryonic stem cells. *J Cardiovasc Transl Res*. doi:10.1007/s12265-013-9510-z.

162. Ribeiro MC, et al. (2015) Functional maturation of human pluripotent stem cell derived cardiomyocytes invitro - Correlation between contraction force andelectrophysiology. *Biomaterials* 51:138–150.

163. Phillips HM, et al. (2007) Disruption of planar cell polarity signaling results in congenital heart defects and cardiomyopathy attributable to early cardiomyocyte disorganization. *Circ Res* 101(2):137–145.

164. Henderson DJ, Chaudhry B (2011) Getting to the heart of planar cell polarity signaling. *Birth Defects Res Part A - Clin Mol Teratol*. doi:10.1002/bdra.20792.

165. Leung C, Lu X, Liu M, Feng Q (2014) Rac1 signaling is critical to cardiomyocyte polarity and embryonic heart development. *J Am Heart Assoc* 3(5):1–14.

166. Jiménez-Amilburu V, et al. (2016) In Vivo Visualization of Cardiomyocyte Apicobasal Polarity Reveals Epithelial to Mesenchymal-like Transition during Cardiac Trabeculation. *Cell Rep* 17(10):2687–2699.

167. Jiménez-Amilburu V, Stainier DYR (2019) The transmembrane protein Crb2a regulates cardiomyocyte apicobasal polarity and adhesion in zebrafish. *Development* 49(April):dev.171207.

168. Kanchanawong P, et al. (2010) Nanoscale architecture of integrin-based cell adhesions. *Nature* 468(7323):580–584.

169. Case LB, et al. (2015) Molecular mechanism of vinculin activation and nanoscale spatial organization in focal adhesions. *Nat Cell Biol* 17(7). doi:10.1038/ncb3180.

170. Larsen M, Artym V V., Green JA, Yamada KM (2006) The matrix reorganized: extracellular matrix remodeling and integrin signaling. *Curr Opin Cell Biol* 18(Figure 1):463–471.

171. Humphrey JD, Dufresne ER, Schwartz M a (2014) Mechanotransduction and extracellular matrix homeostasis I E r. *Nat Publ Gr* 15(12):802–812.

172. Peyton SR, Ghajar CM, Khatiwala CB, Putnam AJ (2007) The emergence of ECM mechanics and cytoskeletal tension as important regulators of cell function. *Cell Biochem Biophys* 47(2):300–320.

173. Carisey A, et al. (2013) Vinculin regulates the recruitment and release of core focal adhesion proteins in a force-dependent manner. *Curr Biol* 23(4):271–281.

174. Grashoff C, et al. (2010) Measuring mechanical tension across vinculin reveals regulation of focal adhesion dynamics. *Nature* 466(7303):263–6.

175. Bajaj P, Tang X, Saif T a., Bashir R (2010) Stiffness of the substrate influences the phenotype of embryonic chicken cardiac myocytes. *J Biomed Mater Res - Part A* 95:1261–1269.

176. Plotnikov S V., Pasapera AM, Sabass B, Waterman CM (2012) Force fluctuations within focal adhesions mediate ECM-rigidity sensing to guide directed cell migration. *Cell* 151(7):1513–1527.

177. Sazonova O V., et al. (2011) Cell-cell interactions mediate the response of vascular smooth muscle cells to substrate stiffness. *Biophys J* 101(3):622–630.

178. Mui KL, et al. (2015) N-cadherin induction by ECM stiffness and FAK overrides the spreading requirement for proliferation of vascular smooth muscle cells. *Cell Rep* 10(9):1477–1486.

179. Dunn AR, et al. (2012) E-cadherin is under constitutive actomyosin-generated tension that is increased at cell-cell contacts upon externally applied stretch. *Proc Natl Acad Sci* 109(31):12568–12573.

180. Auernheimer V, et al. (2015) Vinculin phosphorylation at residues Y100 and Y1065 is required for cellular force transmission. *J Cell Sci* 128(18):3435–3443.

181. McCain ML, Parker KK (2011) Mechanotransduction: The role of mechanical stress, myocyte shape, and cytoskeletal architecture on cardiac function. *Pflugers Arch Eur J Physiol* 462:89–104.

182. Engler AJ, et al. (2008) Embryonic cardiomyocytes beat best on a matrix with heart-like elasticity: scar-like rigidity inhibits beating. *J Cell Sci* 121(Pt 22):3794–3802.

183. Roux KJ, Kim DI, Raida M, Burke B (2012) A promiscuous biotin ligase fusion protein identifies proximal and interacting proteins in mammalian cells. *J Cell Biol* 196(6):801–810.

184. Kim DI, et al. (2016) An improved smaller biotin ligase for BioID proximity labeling. *Mol Biol Cell* 27(8):1188–1196.

185. Le Sage V, Cinti A, Mouland AJ (2016) Proximity-dependent biotinylation for identification of interacting proteins. *Curr Protoc Cell Biol* 2016:17.19.1-17.19.12.

186. Van Itallie CM, et al. (2013) Biotin ligase tagging identifies proteins proximal to E-cadherin, including lipoma preferred partner, a regulator of epithelial cell–cell and cell–substrate adhesion. *J Cell Sci* 127(4):885–895.

187. Guo Z, et al. (2014) E-cadherin interactome complexity and robustness resolved by quantitative proteomics. *Sci Signal* 7(354). doi:10.1126/scisignal.2005473.

188. Ueda S, Blee AM, Macway KG, Renner DJ, Yamada S (2015) Force dependent biotinylation of myosin IIA by α-catenin tagged with a promiscuous biotin ligase. *PLoS One* 10(3):1–15.

189. Zaidel-Bar R (2013) Cadherin adhesome at a glance. *J Cell Sci* 126(2):373–378.

190. Geiger B (1979) A 130K protein from chicken gizzard: Its localization at the termini of microfilament bundles in cultured chicken cells. *Cell*. doi:10.1016/0092-8674(79)90368-4.

191. Seddiki R, et al. (2017) Force-dependent binding of vinculin to α-catenin regulates cell–cell contact stability and collective cell behavior. *Mol Biol Cell* 29(4):380–388.

192. Xu W, et al. (1998) Vinculin knockout results in heart and brain defects during embryonic development. *Development* 125(2):327–37.

193. Borgon RA, Vonrhein C, Bricogne G, Bois PRJ, Izard T (2004) Crystal structure of human vinculin. *Structure*. doi:10.1016/j.str.2004.05.009.

194. Bakolitsa C, et al. (2004) Structural basis for vinculin activation at sites of cell adhesion. *Nature*. doi:10.1038/nature02610.

195. Zemljic-Harpf AE, et al. (2004) Heterozygous inactivation of the vinculin gene predisposes to stress-induced cardiomyopathy. *Am J Pathol* 165(3):1033–1044.

196. Zemljic-Harpf AE, et al. (2007) Cardiac-myocyte-specific excision of the vinculin gene disrupts cellular junctions, causing sudden death or dilated cardiomyopathy. *Mol Cell Biol* 27(21):7522–7537.

197. Shiraishi I, et al. (1997) Vinculin is an essential component for normal myofibrillar arrangement in fetal mouse cardiac myocytes. *J Mol Cell Cardiol* 29:2041–2052.

198. Vasile VC, Ommen SR, Edwards WD, Ackerman MJ (2006) A missense mutation in a ubiquitously expressed protein, vinculin, confers susceptibility to hypertrophic cardiomyopathy. *Biochem Biophys Res Commun* 345(3):998–1003.

199. Heling A, et al. (2000) Increased expression of cytoskeletal, linkage, and extracellular proteins in failing human myocardium. *Circ Res*. doi:10.1161/01.RES.86.8.846.

200. Kaushik G, et al. (2015) Vinculin network-mediated cytoskeletal remodeling regulates contractile function in the aging heart. *Sci Transl Med* 7(292):292ra99.

201. Mandai K, et al. (1997) Afadin: A novel actin filament-binding protein with one PDZ domain localized at cadherin-based cell-to-cell adherens junction [published erratum appears in J Cell Biol 1997 Nov 17;139(4):1060]. *J Cell Biol* 139(2):517–528.

202. Majima T, et al. (2009) Involvement of afadin in the formation and remodeling of synapses in the hippocampus. *Biochem Biophys Res Commun* 385(4):539–544.

203. Zhadanov AB, et al. (1999) Absence of the tight junctional protein AF-6 disrupts epithelial cell-cell junctions and cell polarity during mouse development. *Curr Biol* 9(16):880–888.

204. Miyata M, et al. (2009) Localization of nectin-free afadin at the leading edge and its involvement in directional cell movement induced by platelet-derived growth factor. *J Cell Sci* 122(23):4319–4329.

205. Tanaka-Okamoto M, et al. (2011) Involvement of afadin in barrier function and homeostasis of mouse intestinal epithelia. *J Cell Sci* 124(13):2231–2240.

206. Elloul S, Kedrin D, Knoblauch NW, Beck AH, Toker A (2013) The Adherens Junction Protein Afadin Is an AKT Substrate that Regulates Breast Cancer Cell Migration. *Mol Cancer Res* 12(3):464–476.

207. Takai Y (2002) Nectin and afadin: novel organizers of intercellular junctions. *J Cell Sci* 116(1):17–27.

208. Choi W, et al. (2016) Remodeling the zonula adherens in response to tension and the role of afadin in this response. *J Cell Biol* 213(2):243–260.

209. Zankov DP, Shimizu A, Tanaka-Okamoto M, Miyoshi J, Ogita H (2017) Protective effects of intercalated disk protein afadin on chronic pressure overload-induced myocardial damage. *Sci Rep* 7(January):1–3.

210. Vite A, Radice GL (2014) N-cadherin/catenin complex as a master regulator of intercalated disc function. *Cell Commun Adhes* 21(3):169–79.

211. Ehler E (2018) Actin-associated proteins and cardiomyopathy—the 'unknown' beyond troponin and tropomyosin. *Biophys Rev* 10(4):1121–1128.

212. Halbleib JM, Nelson WJ (2006) Cadherins in development: Cell adhesion, sorting, and tissue morphogenesis. *Genes Dev*. doi:10.1101/gad.1486806.

213. Li J, et al. (2012) Loss of T-catenin alters the hybrid adhering junctions in the heart and leads to dilated cardiomyopathy and ventricular arrhythmia following acute ischemia. *J Cell Sci* 125:1058–1067.

214. Li D, Zhang W, Liu Y, Haneline LS, Shou W (2012) Lack of plakoglobin in epidermis leads to keratoderma. *J Biol Chem*. doi:10.1074/jbc.M111.299669.

215. Garcia-gras E, et al. (2012) Suppression of canonical Wnt / b -catenin signaling by nuclear plakoglobin recapitulates phenotype of arrhythmogenic right ventricular cardiomyopathy Find the latest version : Suppression of canonical Wnt / b -catenin signaling by nuclear plakoglobin reca. doi:10.1172/JCI27751.2012.

216. Garcia MA, Nelson WJ, Chavez N (2017) Cell – Cell Junctions Organize Structural and Signaling Networks. *Cold Spring Harb Perspect Biol* 10(4):1–28.

217. Padmanabhan A, Rao MV, Wu Y, Zaidel-Bar R (2015) Jack of all trades: Functional modularity in the adherens junction. *Curr Opin Cell Biol* 36:32–40.

218. Hoffman BD, Yap AS (2015) Towards a Dynamic Understanding of Cadherin-Based Mechanobiology. *Trends Cell Biol* 25(12):803–814.

219. Goncharova EJ, Kam Z, Geiger B (1992) The involvement of adherens junction components in myofibrillogenesis in cultured cardiac myocytes. *Development* 114:173–183.

220. Ehler E, Moore-Morris T, Lange S (2013) Isolation and culture of neonatal mouse cardiomyocytes. *J Vis Exp* 15(79):1–10.

221. Choi HJ, Gross JC, Pokutta S, Weis WI (2009) Interactions of plakoglobin and β-catenin with desmosomal cadherins: Basis of selective exclusion of α- and β-catenin from desmosomes. *J Biol Chem*. doi:10.1074/jbc.M109.047928.

222. Borrmann CM, et al. (2006) The area composita of adhering junctions connecting heart muscle cells of vertebrates. II. Colocalizations of desmosomal and fascia adhaerens molecules in the intercalated disk. *Eur J Cell Biol*. doi:10.1016/j.ejcb.2006.02.009.

223. Svitkina TM (2017) Platinum replica electron microscopy: Imaging the cytoskeleton globally and locally. *Int J Biochem Cell Biol*. doi:10.1016/j.biocel.2017.03.009.

224. Bennett PM (2006) The Transitional Junction: A New Functional Subcellular Domain at the Intercalated Disc. *Mol Biol Cell* 17(4):2091–2100.

225. Mueller F, Morisaki T, Mazza D, McNally JG (2012) Minimizing the impact of photoswitching of fluorescent proteins on FRAP analysis. *Biophys J*. doi:10.1016/j.bpj.2012.02.029.

226. Katsamba P, et al. (2009) Linking molecular affinity and cellular specificity in cadherin-mediated adhesion. *Proc Natl Acad Sci*. doi:10.1073/pnas.0905349106.

227. Hazan RB, Kang L, Roe S, Borgen PI, Rimm DL (1997) Vinculin is associated with the E-cadherin adhesion complex. *J Biol Chem*. doi:10.1074/jbc.272.51.32448.

228. Tachibana K, et al. (2000) Two cell adhesion molecules, nectin and cadherin, interact through their cytoplasmic domain-associated proteins. *J Cell Biol*. doi:10.1083/jcb.150.5.1161.

229. Weiss EE, Kroemker M, Rüdiger AH, Jockusch BM, Rüdiger M (1998) Vinculin is part of the cadherin-catenin junctional complex: Complex formation between α-catenin and vinculin. *J Cell Biol*. doi:10.1083/jcb.141.3.755.

230. Sawyer JK, Harris NJ, Slep KC, Gaul U, Peifer M (2009) The Drosophila afadin homologue Canoe regulates linkage of the actin cytoskeleton to adherens junctions during apical constriction. *J Cell Biol*. doi:10.1083/jcb.200904001.

231. Yonemura S, Wada Y, Watanabe T, Nagafuchi A, Shibata M (2010) alpha-Catenin as a tension transducer that induces adherens junction development. *Nat Cell Biol* 12:533–542.

232. Tompkins JD, et al. (2016) Mapping Human Pluripotent-to-Cardiomyocyte Differentiation: Methylomes, Transcriptomes, and Exon DNA Methylation "Memories." *EBioMedicine*. doi:10.1016/j.ebiom.2016.01.021.

233. Li B, et al. (2017) A Comprehensive Mouse Transcriptomic BodyMap across 17 Tissues by RNA-seq. *Sci Rep*. doi:10.1038/s41598-017-04520-z.

234. Estigoy CB, et al. (2009) Intercalated discs: Multiple proteins perform multiple functions in non-failing and failing human hearts. *Biophys Rev* 1(1):43–49.

235. Bass-Zubek AE, Godsel LM, Delmar M, Green KJ (2009) Plakophilins: multifunctional scaffolds for adhesion and signaling. *Curr Opin Cell Biol*. doi:10.1016/j.ceb.2009.07.002.

236. Chen CL, Perrimon N (2017) Proximity-dependent labeling methods for proteomic profiling in living cells. *Wiley Interdiscip Rev Dev Biol*. doi:10.1002/wdev.272.

237. Oh SW (2003) Archvillin, a muscle-specific isoform of supervillin, is an early expressed component of the costameric membrane skeleton. *J Cell Sci*. doi:10.1242/jcs.00422.

238. Weins A, et al. (2001) Differentiation- and stress-dependent nuclear cytoplasmic redistribution of myopodin, a novel actin-bundling protein. *J Cell Biol*. doi:10.1083/jcb.200012039.

239. Barton LJ, Soshnev AA, Geyer PK (2015) Networking in the nucleus: A spotlight on LEM-domain proteins. *Curr Opin Cell Biol*. doi:10.1016/j.ceb.2015.03.005.

240. Cartegni L (1997) Heart-specific localization of emerin: new insights into Emery-Dreifuss muscular dystrophy. *Hum Mol Genet*. doi:10.1093/hmg/6.13.2257.

241. Hishiya A, Kitazawa T, Takayama S (2010) BAG3 and Hsc70 interact with actin capping protein CapZ to maintain myofibrillar integrity under mechanical stress. *Circ Res*. doi:10.1161/CIRCRESAHA.110.225649.

242. Faulkner G, et al. (1999) ZASP: A new Z-band alternatively spliced PDZ-motif protein. *J Cell Biol*. doi:10.1083/jcb.146.2.465.

243. Moncman CL, Wang K (1995) Nebulette: A 107 kD nebulin-like protein in cardiac muscle. *Cell Motil Cytoskeleton*. doi:10.1002/cm.970320305.

244. Chen J, Zheng M, Cheng H, Banerjee I, Chen J (2010) ALP / Enigma PDZ-LIM domain proteins in the heart Review ALP / Enigma PDZ – LIM Domain Proteins in the Heart. 36(APRIL):96–102.

245. Frank D, Kuhn C, Katus HA, Frey N (2006) The sarcomeric Z-disc: A nodal point in signalling and disease. *J Mol Med*. doi:10.1007/s00109-005-0033-1.

246. Herzog W (2018) The multiple roles of titin in muscle contraction and force production. *Biophys Rev*. doi:10.1007/s12551-017-0395-y.

247. Frank D, Frey N (2011) Cardiac Z-disc signaling network. *J Biol Chem*. doi:10.1074/jbc.R110.174268.

248. Angst BD, et al. (1997) Dissociated spatial patterning of gap junctions and cell adhesion junctions during postnatal differentiation of ventricular myocardium. *Circ Res*. doi:10.1161/01.RES.80.1.88.

249. Nakata S, et al. (2007) Regulation of platelet-derived growth factor receptor activation by afadin through SHP-2: Implications for cellular morphology. *J Biol Chem*. doi:10.1074/jbc.M707461200.

250. Zuleger N, et al. (2011) System analysis shows distinct mechanisms and common principles of nuclear envelope protein dynamics. *J Cell Biol*. doi:10.1083/jcb.201009068.

251. Perrin BJ, Amann KJ, Huttenlocher A (2005) Proteolysis of Cortactin by Calpain Regulates Membrane Protrusion during Cell Migration. *Mol Biol Cell*. doi:10.1091/mbc.e05-06-0488.

252. Wulfkuhle JD, et al. (1999) Domain analysis of supervillin, an F-actin bundling plasma membrane protein with functional nuclear localization signals [In Process Citation]. *J Cell Sci*.

253. Geraldo S, Khanzada UK, Parsons M, Chilton JK, Gordon-Weeks PR (2008) Targeting of the F-actin-binding protein drebrin by the microtubule plus-tip protein EB3 is required for neuritogenesis. *Nat Cell Biol*. doi:10.1038/ncb1778.

254. Wang S, Tukachinsky H, Romano FB, Rapoport TA (2016) Cooperation of the ER-shaping proteins atlastin, lunapark, and reticulons to generate a tubular membrane network. *Elife*. doi:10.7554/elife.18605.

255. Fan W, et al. (2010) Keap1 facilitates p62-mediated ubiquitin aggregate clearance via autophagy. *Autophagy*. doi:10.4161/auto.6.5.12189.

256. Kim E, et al. (2016) Systematic functional interrogation of rare cancer variants identifies oncogenic alleles. *Cancer Discov*. doi:10.1158/2159-8290.CD-16-0160.

257. He TC, et al. (1998) A simplified system for generating recombinant adenoviruses. *Proc Natl Acad Sci U S A*.

258. Zhang M, et al. (2012) Rational design of true monomeric and bright photoactivatable fluorescent proteins. *Nat Methods*. doi:10.1038/nmeth.2021.

259. Svitkina TM, Borisy GG (1998) Correlative Light and Electron Microscopy of the Cytoskeleton. *Cell Biology, Four-Volume Set* doi:10.1016/B978-012164730-8/50156-8.

260. Luo J, et al. (2007) A protocol for rapid generation of recombinant adenoviruses using the AdEasy system. *Nat Protoc*. doi:10.1038/nprot.2007.135.

261. Braganza A, et al. (2017) UBE3B is a calmodulin-regulated, mitochondrion-associated E3 ubiquitin ligase. *J Biol Chem*. doi:10.1074/jbc.M116.766824.

262. Cox J, Mann M (2008) MaxQuant enables high peptide identification rates, individualized p.p.b.-range mass accuracies and proteome-wide protein quantification. *Nat Biotechnol*. doi:10.1038/nbt.1511.

263. Tyanova S, Temu T, Cox J (2016) The MaxQuant computational platform for mass spectrometry-based shotgun proteomics. *Nat Protoc*. doi:10.1038/nprot.2016.136.

264. Apweiler R, et al. (2011) Ongoing and future developments at the Universal Protein Resource. *Nucleic Acids Res*. doi:10.1093/nar/gkq1020.

265. Schwanhüusser B, et al. (2011) Global quantification of mammalian gene expression control. *Nature*. doi:10.1038/nature10098.

266. Hulsen T, de Vlieg J, Alkema W (2008) BioVenn - A web application for the comparison and visualization of biological lists using area-proportional Venn diagrams. *BMC Genomics*. doi:10.1186/1471-2164-9-488.

267. Fagerberg L, et al. (2014) Analysis of the human tissue-specific expression by genome-wide integration of transcriptomics and antibody-based proteomics. *Mol Cell Proteomics*. doi:10.1074/mcp.M113.035600.

268. Li Y, Lin B, Yang L (2015) Comparative transcriptomic analysis of multiple cardiovascular fates from embryonic stem cells predicts novel regulators in human cardiogenesis. *Sci Rep*. doi:10.1038/srep09758.

269. Matsuzawa K, Himoto T, Mochizuki Y, Ikenouchi J (2018) α-Catenin Controls the Anisotropy of Force Distribution at Cell-Cell Junctions during Collective Cell Migration. *Cell Rep*. doi:10.1016/j.celrep.2018.05.070.

270. Yap AS, Duszyc K, Viasnoff V (2018) Mechanosensing and mechanotransduction at cell –cell junctions. *Cold Spring Harb Perspect Biol* 10(8). doi:10.1101/cshperspect.a028761.

271. Yonemura S (2017) Actin filament association at adherens junctions. *J Med Investig* 64(1.2):14–19.

272. Kale GR, et al. (2018) Distinct contributions of tensile and shear stress on E-cadherin levels during morphogenesis. *Nat Commun* 9(1):5021.

273. Geiger B, Avnur Z, Volberg T, Volk T (1985) Molecular domains of adherens junctions. *cell contact*:461–489.

274. Satomi-Kobayashi S, et al. (2009) Deficiency of nectin-2 leads to cardiac fibrosis and dysfunction under chronic pressure overload. *Hypertension* 54(4):825–831.

275. Hong S, Troyanovsky RB, Troyanovsky SM (2013) Binding to F-actin guides cadherin cluster assembly, stability, and movement. *J Cell Biol*. doi:10.1083/jcb.201211054.

276. Aguilar F, et al. (2011) Mammalian enabled (Mena) is a critical regulator of cardiac function. *Am J Physiol Circ Physiol* 300(5):1–12.

277. Kroemker M, Rüdiger AH, Jockusch BM, Rüdiger M (1994) Intramolecular interactions in vinculin control α-actinin binding to the vinculin head. *FEBS Lett* 355(3):259–262.

278. Higashi T, Miller AL (2017) Tricellular junctions: how to build junctions at the TRICkiest points of epithelial cells. *Mol Biol Cell*. doi:10.1091/mbc.e16-10-0697.

279. Bays JL, DeMali KA (2017) Vinculin in cell–cell and cell–matrix adhesions. *Cell Mol Life Sci* 74(16):2999–3009.

280. Biernacka A, Frangogiannis NG (2011) Aging and Cardiac Fibrosis. *Aging Dis* 2(2):158–173.

281. Maiers JL, Peng X, Fanning AS, DeMali KA (2013) ZO-1 recruitment to -catenin - a novel mechanism for coupling the assembly of tight junctions to adherens junctions. *J Cell Sci* 126(17):3904–3915.

282. Tu C, Zoldan J (2018) Moving iPSC-Derived Cardiomyocytes Forward to Treat Myocardial Infarction. *Cell Stem Cell* 23(3):322–323.

283. Yester JW, Kühn B (2017) Mechanisms of Cardiomyocyte Proliferation and Differentiation in Development and Regeneration. *Curr Cardiol Rep* 19(2). doi:10.1007/s11886-017-0826-1.

284. Ronaldson-bouchard K, et al. (2018) Grown From Pluripotent Stem Cells.

285. Liu Y-W, et al. (2018) Human embryonic stem cell-derived cardiomyocytes restore function in infarcted hearts of non-human primates. *Nat Biotechnol* 36(7):597–605.

286. Shiba Y, et al. (2016) Allogeneic transplantation of iPS cell-derived cardiomyocytes regenerates primate hearts. *Nature* 538(7625):388–391.

287. Yang X, Pabon L, Murry CE (2014) Engineering adolescence: Maturation of human pluripotent stem cell-derived cardiomyocytes. *Circ Res* 114(3):511–523.

288. Chong JJH, et al. (2014) Human embryonic-stem-cell-derived cardiomyocytes regenerate non-human primate hearts. *Nature* 510(7504):273–277.